NASA TECHNICAL NOTE

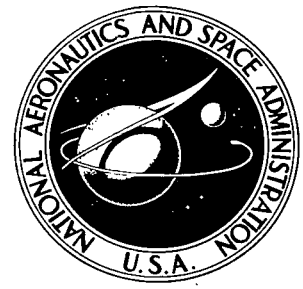


NASA TN D-8022 c.1


NASA TN D-8022

# COMPUTED LATERAL RATE AND ACCELERATION POWER SPECTRAL RESPONSE OF CONVENTIONAL AND STOL AIRPLANES TO ATMOSPHERIC TURBULENCE



*Jacob H. Lichtenstein*

*Langley Research Center*
*Hampton, Va. 23665*

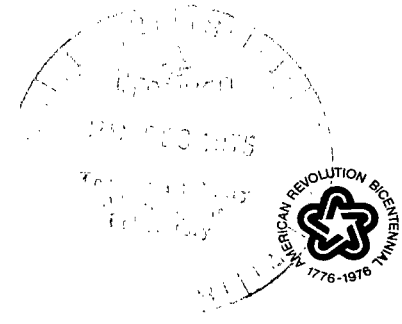


NATIONAL AERONAUTICS AND SPACE ADMINISTRATION • WASHINGTON, D. C. • DECEMBER 1975

| 1 Report No. | 2. Government Accession No. | 3. Recipient's Catalog No. |
|---|---|---|
| NASA TN D-8022 | | |

4. Title and Subtitle
COMPUTED LATERAL RATE AND ACCELERATION POWER SPECTRAL RESPONSE OF CONVENTIONAL AND STOL AIRPLANES TO ATMOSPHERIC TURBULENCE

5. Report Date: December 1975

6. Performing Organization Code:

7. Author(s)
Jacob H. Lichtenstein

8. Performing Organization Report No.: L-10018

9. Performing Organization Name and Address
NASA Langley Research Center
Hampton, Va. 23665

10. Work Unit No.: 505-06-93-03

11. Contract or Grant No.:

12. Sponsoring Agency Name and Address
National Aeronautics and Space Administration
Washington, D.C. 20546

13. Type of Report and Period Covered: Technical Note

14. Sponsoring Agency Code:

15. Supplementary Notes

16. Abstract

Power-spectral-density calculations were made of the lateral responses to atmospheric turbulence for several conventional and short take-off and landing (STOL) airplanes. The turbulence was modeled as three orthogonal velocity components, which were uncorrelated, and each was represented with a one-dimensional power spectrum. Power spectral densities were computed for displacements, rates, and accelerations in roll, yaw, and sideslip. In addition, the power spectral density of the transverse acceleration was computed. Evaluation of ride quality based on a specific ride quality criterion was also made for these airplanes.

The results show that the STOL airplanes generally had larger values for the rate and acceleration power spectra (and, consequently, larger corresponding root-mean-square values) than the conventional airplanes. The ride quality criterion gave poorer ratings to the STOL airplanes than to the conventional airplanes. This result indicates that the STOL airplanes would have a less comfortable ride than the conventional airplanes.

17. Key Words (Suggested by Author(s))
Power-spectral-density response of airplanes
Airplane acceleration response to gusts
STOL airplane acceleration response

18. Distribution Statement
Unclassified – Unlimited

Subject Category 02

| 19. Security Classif. (of this report) | 20. Security Classif. (of this page) | 21. No. of Pages | 22. Price* |
|---|---|---|---|
| Unclassified | Unclassified | 122 | $5.25 |

*For sale by the National Technical Information Service, Springfield, Virginia 22161

# COMPUTED LATERAL RATE AND ACCELERATION POWER SPECTRAL RESPONSE OF CONVENTIONAL AND STOL AIRPLANES TO ATMOSPHERIC TURBULENCE

Jacob H. Lichtenstein
Langley Research Center

## SUMMARY

Power-spectral-density calculations were made of the lateral responses to atmospheric turbulence for several conventional and short take-off and landing (STOL) airplanes. The turbulence was modeled as three orthogonal velocity components, which were uncorrelated, and each was represented with a one-dimensional power spectrum. Power spectral densities were computed for displacements, rates, and accelerations in roll, yaw, and sideslip. In addition, the power spectral density of the transverse acceleration was computed. Evaluation of ride quality based on a specific ride quality criterion was also made for these airplanes.

The results show that the STOL airplanes generally had larger values for the rate and acceleration power spectra (and, consequently, larger corresponding root-mean-square values) than the conventional airplanes. The ride quality criterion gave poorer ratings to the STOL airplanes than to the conventional airplanes. This result indicates that the STOL airplanes would have a less comfortable ride than the conventional airplanes.

## INTRODUCTION

One present technique of achieving the short take-off and landing (STOL) operation is to utilize a relatively light wing loading for the vehicle. Unfortunately, the motion and acceleration response of an airplane to atmospheric turbulence is inversely related to its wing loading. The large response of such an airplane to atmospheric turbulence could result in poor riding qualities. An evaluation report (ref. 1) on the suitability of a typical STOL type airplane for airline operation includes a discussion of its unsatisfactory riding qualities in rough air, particularly in the lateral-directional mode.

The subject of riding qualities of airplanes has been investigated, and a synopsis of the current knowledge of the subject can be found in reference 2. At present, few generally accepted criteria for defining good or acceptable riding qualities are available. Moreover, the specific airplane characteristics which contribute to good riding qualities are not clearly understood. It is apparent, however, that the motion of the airplane in response to atmospheric turbulence is one of the contributing factors.

Because atmospheric turbulence is most appropriately treated analytically as a random quantity, airplane motion resulting from turbulence excitation is also random and can be described only in a statistical manner. An overall discussion of the dynamic response of airplanes to atmospheric turbulence is given in reference 3. Three descriptions of the response are the response power spectrum, the response root-mean-square (rms) value, and the expected number of exceedances of a given response level. Of these, the output power spectrum yields information most directly related to configuration differences. A correlation of the frequencies at which maximum response occurs with those that cause the most discomfort in airplane passengers may indicate areas in which the airplane dynamic behavior should be altered.

The power spectral densities (psd) of the lateral angular response of a group of 12 airplanes of various configurations, including potential STOL vehicles, computed by the method presented in reference 4 have been presented in reference 5. In the present paper, the same method is used to extend the study to obtain the power-spectral-density functions of the lateral response for angular velocities and accelerations and the transverse linear accelerations for the same airplanes. The gust field was represented by three orthogonal velocity components, which are uncorrelated, and each is represented with a one-dimensional Dryden power spectrum. The power spectral densities of the transverse acceleration were obtained for several locations forward of, rearward of, above, and below the center of gravity of each airplane. The root-mean-square values of the responses were obtained from the power spectra and were used in calculating a ride quality index for each airplane by using a criterion as presented in reference 6.

## SYMBOLS

Values are given in both SI and U.S. Customary Units. The measurements and calculations were made in U.S. Customary Units.

$A$ aspect ratio

$a_t$ transverse acceleration, g units or $m/sec^2$ $(ft/sec^2)$

$b$ wing span, m (ft)

$C_{D,o}$ drag coefficient at zero lift, $\frac{Drag}{qS}$

$C_L$ lift coefficient, $\frac{Lift}{qS}$

$C_l$ rolling-moment coefficient, $\frac{\text{Rolling moment}}{qSb}$

$C_n$ yawing-moment coefficient, $\frac{\text{Yawing moment}}{qSb}$

$C_Y$ side-force coefficient, $\frac{\text{Side force}}{qS}$

D nondimensional operator, $\frac{b}{U}\frac{d}{dt}$

G matrix containing stability derivatives relating airplane moments and forces to gust velocities

g acceleration due to gravity, $m/sec^2$ $(ft/sec^2)$

h altitude, m (ft)

$h_z$ height of center of pressure of vertical tail above X-axis, m (ft)

i $= \sqrt{-1}$

$K_X$ nondimensional radius of gyration about X-axis, $k_x/b$

$K_Z$ nondimensional radius of gyration about Z-axis, $k_z/b$

$K_{XZ}$ nondimensional product of gyration, $k_{xz}/b^2$

$k_X, k_Z$ radii of gyration, m (ft)

$k_{XZ}$ product of gyration, $m^2$ $(ft^2)$

L scale of turbulence, m (ft)

$l_T$ tail length measured from center of gravity to center of pressure of vertical tail, m (ft)

m mass of airplane, kg (slugs)

| | |
|---|---|
| $p$ | rolling velocity, $\dot{\varphi}$, rad/sec |
| $p_g$ | gust rolling velocity $\left(D\varphi_g \text{ of ref. 4}\right)$, rad/sec |
| $q$ | dynamic pressure, $\frac{1}{2}\rho U^2$, $N/m^2$ $\left(lb/ft^2\right)$ |
| $R_c$ | computed ride quality index |
| $r$ | yawing velocity, $\dot{\psi}$, rad/sec |
| $r_g$ | gust yawing velocity $\left(D\psi_g \text{ of ref. 4}\right)$, rad/sec |
| $S$ | wing area, $m^2$ $\left(ft^2\right)$ |
| $s$ | profile height (refer to sketch in section entitled "Aircraft Parameters"), m (ft) |
| $t$ | time, sec |
| $U$ | relative velocity between airplane and general air mass, m/sec (ft/sec) |
| $u$ | velocity along X-axis, m/sec (ft/sec) |
| $\overline{V_g^2}$ | mean square of gust-velocity components (see eq. (19a)) |
| $v$ | velocity along Y-axis, m/sec (ft/sec) |
| $W$ | weight of airplane, N (lb) |
| $w$ | velocity along Z-axis, m/sec (ft/sec) |
| X,Y,Z | three orthogonal stability axes of airplane |
| x,y,z | coordinates with reference to X-, Y-, and Z-axes, m (ft) |
| $\alpha$ | angle of attack, deg (rad) |
| $\alpha_0$ | trim (steady-state) angle of attack, deg (rad) |

$\beta$ angle of sideslip, rad

$\Gamma$ dihedral angle, deg

$\gamma$ flight-path angle, rad

$\Delta$ matrix of airplane equations of motion in still air (see ref. 1)

$\zeta$ damping ratio for Dutch roll mode

$\mu$ relative mass parameter, $\frac{m}{\rho Sb}$

$\rho$ density of atmosphere, $kg/m^3$ $(slugs/ft^3)$

$\sigma$ sidewash angle, rad

$\sigma_R$ root-mean-square value of quantity R

$\Phi$ power-spectral-density function

$\Phi_R$ power-spectral-density function of quantity R

$\varphi$ angle of roll, rad

$\psi$ angle of yaw, rad

$\omega$ circular frequency, rad/sec

$\omega_n$ undamped natural frequency of Dutch roll mode, rad/sec

$| \; |$ absolute value of quantity or determinant of matrix

$[ \; ]$ rectangular matrix

$\{ \; \}$ row or column matrix

Stability derivatives of airplane are indicated by subscript notation; for example,

$$C_{l_r} = \frac{\partial C_l}{\partial\left(\frac{rb}{2U}\right)} \qquad C_{n_p} = \frac{\partial C_n}{\partial\left(\frac{pb}{2U}\right)} \qquad C_{Y_\beta} = \frac{\partial C_Y}{\partial\left(\frac{v}{U}\right)}$$

Subscripts:

| | |
|---|---|
| F | fuselage |
| g | gust |
| T | vertical tail |
| W | wing |
| 0 | general air mass |

Bar over a quantity denotes a mean value.

Dot over a quantity denotes differentiation with respect to time.

## MATHEMATICAL DEVELOPMENT

### Response Power Spectra

The governing equations for the power spectra of the airplane angular displacements are developed in detail in reference 4 and outlined herein. This development was used to calculate the power spectra for the angular velocities and accelerations. The angular velocities and accelerations, in turn, are used in developing the term for the transverse acceleration.

The airplanes considered in this investigation are assumed to be rigid bodies with fixed control surfaces and no auxiliary damping devices, and to be flying in straight and level flight. Quasi-steady aerodynamic forces are employed. The gust field of the atmosphere is modeled as three orthogonal velocity components, which are uncorrelated, and each is represented with a one-dimensional power spectrum. Variations in the lateral gust velocity along the spanwise direction are assumed to be negligible. The airplane is executing small motions in sideslip, yaw, and roll, as described by the linear equations of motion normally employed in

stability analyses. Expressions for the response power spectra, which are numerically evaluated for the various airplane configurations given in this paper, are described in the following discussion.

The lateral equations of motion for an airplane are given by

$$\left.\begin{aligned} &2\mu K_X^2 D^2\varphi_0 - \tfrac{1}{2}C_{l_p} D\varphi - 2\mu K_{XZ} D^2\psi_0 - \tfrac{1}{2}C_{l_r} D\psi - C_{l_\beta}\beta = 0 \\ &-2\mu K_{XZ} D^2\varphi_0 - \tfrac{1}{2}C_{n_p} D\varphi + 2\mu K_Z^2 D^2\psi_0 - \tfrac{1}{2}C_{n_r} D\psi - C_{n_\psi}\psi - C_{n_\beta}\beta = 0 \\ &-\tfrac{1}{2}C_{Y_p} D\varphi - C_L\varphi_0 + 2\mu D\psi_0 - \tfrac{1}{2}C_{Y_r} D\psi - C_L \tan\gamma\psi_0 + 2\mu D\beta_0 - C_{Y_\beta}\beta = 0 \end{aligned}\right\} \quad (1)$$

where the subscript 0 in the inertial and weight terms is used to denote angular displacement with respect to an absolute system of axes fixed in the general air mass. The reason for including the term $C_{n_\psi}$ in equation (1) is discussed later. In calculations of the motion of an airplane in still air, the angular displacements and velocities appearing in the aerodynamic terms are identical with these zero-subscript values. When flying in turbulent air, however, the airplane is subjected to the motion of local air masses, generally referred to as gusts. Both the relative linear and angular velocities of the airplane with respect to the local air mass may be considered as made up of two parts

$$\left.\begin{aligned} D\varphi &= D\varphi_0 + p_g \\ D\psi &= D\psi_0 + r_g \\ \beta &= \beta_0 + \beta_g \end{aligned}\right\} \quad (2)$$

where the terms $p_g$ and $r_g$ are the same as $D\varphi_g$ and $D\psi_g$, respectively, in reference 4.

Substitution of equation (2) into equation (1) and transposition of the terms resulting from gust disturbances to the right-hand side of the equation gives the result written in matrix form

$$[\Delta]\begin{Bmatrix}\varphi_0\\ \psi_0\\ \beta_0\end{Bmatrix} = [G]\begin{Bmatrix}p_g\\ r_g\\ \beta_g\end{Bmatrix} \quad (3)$$

where the equation $|[\Delta]| = 0$ is the familiar still-air rigid-airplane characteristic equation and the matrix G gives the relationship between the aerodynamic moments and forces resulting from the gust velocities.

The frequency response of the airplane is obtained by taking the Fourier transform of equation (3) and is given by

$$\begin{Bmatrix} \varphi_0(\omega) \\ \psi_0(\omega) \\ \beta_0(\omega) \end{Bmatrix} = [\Delta(\omega)]^{-1}[G(\omega)] \begin{Bmatrix} p_g(\omega) \\ r_g(\omega) \\ \beta_g(\omega) \end{Bmatrix} \tag{4}$$

Equation (4) is meaningful only if the airplane is stable. In order to calculate the frequency response of the airplanes for a stable condition, the term $C_{n_\psi}$ was introduced in the equations. This term could represent a yawing moment introduced by the pilot to correct heading changes. When this term was present, the roots of the characteristic equation of the airplanes were generally stable. It could be shown that as the value of $C_{n_\psi}$ was reduced to negligibly small values, the power spectra approached those values which were obtained if $C_{n_\psi} = 0$ in the frequency range presented. This procedure demonstrates that the results are valid for the condition with $C_{n_\psi} = 0$, even though in this case, the equations have a zero root, thereby indicating neutral stability. It should be mentioned that if instabilities occur in other modes or investigations which require frequency response analyses, a similar approach of inserting additional terms to compensate for the instabilities should be used. The frequency-dependent forms of $[\Delta]$ and $[G]$ are given by

$$[\Delta(\omega)] = \begin{bmatrix} -2\mu K_X^2 \frac{b^2}{U^2}\omega^2 - \frac{1}{2}C_{l_p} i\omega & 2\mu K_{XZ}\frac{b^2}{U^2}\omega^2 - \frac{1}{2}C_{l_r} i\omega & -C_{l_\beta} \\ 2\mu K_{XZ}\frac{b^2}{U^2}\omega^2 - \frac{1}{2}C_{n_p} i\omega & -2\mu K_Z^2\frac{b^2}{U^2}\omega^2 - \frac{1}{2}C_{n_r} i\omega & -C_{n_\beta} \\ -\frac{1}{2}C_{Y_p} i\omega - C_L & \left(2\mu - \frac{1}{2}C_{Y_r}\right)i\omega - C_L \tan\gamma & 2\mu i\omega - C_{Y_\beta} \end{bmatrix} \tag{5}$$

and

$$[G(\omega)] = \begin{bmatrix} \left(\frac{1}{2}C_{l_p}\right)_W & \left(\frac{1}{2}C_{l_r}\right)_W & \left(C_{l_\beta}(\omega)\right)_{WT} \\ \left(\frac{1}{2}C_{n_p}\right)_W & \left(\frac{1}{2}C_{n_r}\right)_W & \left(C_{n_\beta}(\omega)\right)_{FT} \\ 0 & 0 & \left(C_{Y_\beta}(\omega)\right)_{FT} \end{bmatrix} \tag{6}$$

The effects of the distribution of the side gusts along the length of the airplane are accounted for in the frequency-dependent coefficients $C_{l_\beta}(\omega)$, $C_{n_\beta}(\omega)$, and $C_{Y_\beta}(\omega)$. (See ref. 4.)

The product $[\Delta(\omega)]^{-1}[G(\omega)]$ is the matrix of the frequency-response functions which relates the airplane response to the gust velocities. Equation (4) can be expressed as

$$\begin{Bmatrix} \varphi_0(\omega) \\ \psi_0(\omega) \\ \beta_0(\omega) \end{Bmatrix} = \begin{bmatrix} \frac{\varphi_0}{p_g}(\omega) & \frac{\varphi_0}{r_g}(\omega) & \frac{\varphi_0}{\beta_g}(\omega) \\ \frac{\psi_0}{p_g}(\omega) & \frac{\psi_0}{r_g}(\omega) & \frac{\psi_0}{\beta_g}(\omega) \\ \frac{\beta_0}{p_g}(\omega) & \frac{\beta_0}{r_g}(\omega) & \frac{\beta_0}{\beta_g}(\omega) \end{bmatrix} \begin{Bmatrix} p_g(\omega) \\ r_g(\omega) \\ \beta_g(\omega) \end{Bmatrix} \tag{7}$$

In the development, it is assumed that the cross-power spectra terms of the gust-velocity input are negligible (see ref. 4) so that the final equations for the power spectra are of the form (see ref. 4)

$$\begin{Bmatrix} \Phi_{\varphi_0}(\omega) \\ \Phi_{\psi_0}(\omega) \\ \Phi_{\beta_0}(\omega) \end{Bmatrix} = \begin{bmatrix} \left|\frac{\varphi_0}{p_g}(\omega)\right|^2 & \left|\frac{\varphi_0}{r_g}(\omega)\right|^2 & \left|\frac{\varphi_0}{\beta_g}(\omega)\right|^2 \\ \left|\frac{\psi_0}{p_g}(\omega)\right|^2 & \left|\frac{\psi_0}{r_g}(\omega)\right|^2 & \left|\frac{\psi_0}{\beta_g}(\omega)\right|^2 \\ \left|\frac{\beta_0}{p_g}(\omega)\right|^2 & \left|\frac{\beta_0}{r_g}(\omega)\right|^2 & \left|\frac{\beta_0}{\beta_g}(\omega)\right|^2 \end{bmatrix} \begin{Bmatrix} \Phi_{p_g}(\omega) \\ \Phi_{r_g}(\omega) \\ \Phi_{\beta_g}(\omega) \end{Bmatrix} = [T(\omega)] \begin{Bmatrix} \Phi_{p_g}(\omega) \\ \Phi_{r_g}(\omega) \\ \Phi_{\beta_g}(\omega) \end{Bmatrix} \tag{8}$$

where $[T(\omega)]$ is used symbolically to represent the first matrix after the equal sign.

All numerical results presented in this paper were obtained through the application of equation (8) and the appropriate form for the input gust spectrum.

Angular velocities and accelerations.- The angular velocities and accelerations are given by

$$\begin{Bmatrix} \dot{\varphi}_0 \\ \dot{\psi}_0 \\ \dot{\beta}_0 \end{Bmatrix} = \frac{d}{dt} \begin{Bmatrix} \varphi_0 \\ \psi_0 \\ \beta_0 \end{Bmatrix} \tag{9}$$

and

$$\begin{Bmatrix} \ddot{\varphi}_0 \\ \ddot{\psi}_0 \\ \ddot{\beta}_0 \end{Bmatrix} = \frac{d^2}{dt^2} \begin{Bmatrix} \varphi_0 \\ \psi_0 \\ \beta_0 \end{Bmatrix} \tag{10}$$

Equations (9) and (10) can be transformed into the frequency domain by substituting $i\omega$ for $d/dt$, and the power spectral densities of the angular velocities and accelerations obtained from them are given by

$$\begin{Bmatrix} \Phi_{\dot{\varphi}_0}(\omega) \\ \Phi_{\dot{\psi}_0}(\omega) \\ \Phi_{\dot{\beta}_0}(\omega) \end{Bmatrix} = \omega^2[T(\omega)] \begin{Bmatrix} \Phi_{p_g}(\omega) \\ \Phi_{r_g}(\omega) \\ \Phi_{\beta_g}(\omega) \end{Bmatrix} \tag{11}$$

and

$$\begin{Bmatrix} \Phi_{\ddot{\varphi}_0}(\omega) \\ \Phi_{\ddot{\psi}_0}(\omega) \\ \Phi_{\ddot{\beta}_0}(\omega) \end{Bmatrix} = \omega^4[T(\omega)] \begin{Bmatrix} \Phi_{p_g}(\omega) \\ \Phi_{r_g}(\omega) \\ \Phi_{\beta_g}(\omega) \end{Bmatrix} \tag{12}$$

Transverse accelerations.- The transverse acceleration $a_t$ consists of the acceleration at the center of gravity plus terms to account for effects of angular accelerations at points displaced from the center of gravity along the X- and Z-axes. It was assumed that the effect of possible displacement of airplane passengers along the Y-axis would be negligible. The transverse acceleration is given by

$$a_t = U\dot{\beta}_0 + U\dot{\psi}_0 - g\varphi_0 + x\ddot{\psi}_0 - z\ddot{\varphi}_0 \tag{13}$$

Here the quantity $U\dot{\beta}_0 + U\dot{\psi}_0 - g\varphi_0$ is the acceleration of the center of gravity of the airplane.

The Fourier transform of equation (13) is

$$a_t = \left\{\left(z\omega^2 - g\right),\left(iU\omega - x\omega^2\right),\left(iU\omega\right)\right\} \begin{Bmatrix} \varphi_0(\omega) \\ \psi_0(\omega) \\ \beta_0(\omega) \end{Bmatrix} \tag{14}$$

Substitution of equation (7) for the column matrix in equation (14) yields the transverse acceleration

$$a_t = \left\{a_{11}(\omega), a_{12}(\omega), a_{13}(\omega)\right\} \begin{Bmatrix} p_g(\omega) \\ r_g(\omega) \\ \beta_g(\omega) \end{Bmatrix} \tag{15}$$

where

$$a_{11} = iU\omega\left(\frac{\psi_0}{p_g}(\omega) + \frac{\beta_0}{p_g}(\omega)\right) + \omega^2\left(z\,\frac{\varphi_0}{p_g}(\omega) - x\,\frac{\psi_0}{p_g}(\omega)\right) - g\,\frac{\varphi_0}{p_g}(\omega)$$

$$a_{12} = iU\omega\left(\frac{\psi_0}{r_g}(\omega) + \frac{\beta_0}{r_g}(\omega)\right) + \omega^2\left(z\,\frac{\varphi_0}{r_g}(\omega) - x\,\frac{\psi_0}{r_g}(\omega)\right) - g\,\frac{\varphi_0}{r_g}(\omega)$$

$$a_{13} = iU\omega\left(\frac{\psi_0}{\beta_g}(\omega) + \frac{\beta_0}{\beta_g}(\omega)\right) + \omega^2\left(z\,\frac{\varphi_0}{\beta_g}(\omega) - x\,\frac{\psi_0}{\beta_g}(\omega)\right) - g\,\frac{\varphi_0}{\beta_g}(\omega)$$

The power spectral density of the transverse acceleration can be expressed as

$$\Phi_{a_t}(\omega) = \left\{\left|a_{11}(\omega)\right|^2, \left|a_{12}(\omega)\right|^2, \left|a_{13}(\omega)\right|^2\right\} \begin{Bmatrix} \Phi_{p_g}(\omega) \\ \Phi_{r_g}(\omega) \\ \Phi_{\beta_g}(\omega) \end{Bmatrix} \tag{16}$$

## Gust-Velocity Power Spectrum

For the purpose of this paper, the Dryden spectrum was chosen rather than the von Kármán because of its simpler mathematical form. The Dryden formulations of the power spectra for the lateral gust-velocity components are expressed as

$$\frac{\Phi_{v_g}}{v_g^2} = \frac{\Phi_{w_g}}{w_g^2} = \frac{L}{\pi U}\,\frac{1 + 3(k')^2}{\left[1 + (k')^2\right]^2} \tag{17}$$

The power spectrum of the longitudinal gust velocity is expressed as

$$\frac{\Phi_{u_g}}{\overline{u_g^2}} = \frac{2L}{\pi U} \frac{1}{1 + (k')^2} \tag{18}$$

where $k' = \frac{\omega L}{U}$.

As a result of the assumptions of homogeneity and isotropy, the mean-square values of the three components of the gust velocities are equal; thus

$$\overline{u_g^2} = \overline{w_g^2} = \overline{v_g^2} = \overline{V_g^2} \tag{19a}$$

By using the relationship $\beta_g = v_g/U$ and equation (17), the resulting gust spectra relationships are

$$\Phi_{v_g}(\omega) = \Phi_{w_g}(\omega) = U^2 \Phi_{\beta_g}(\omega) \tag{19b}$$

As a consequence of equations (19a) and (19b) the power spectra of the lateral and vertical gust velocities may be specified in terms of a single quantity, the side gust spectrum $\Phi_{\beta_g}$, which is given by

$$\Phi_{\beta_g} = \frac{\overline{V_g^2}}{U^2} \frac{L}{\pi U} \frac{1 + 3(k')^2}{\left[1 + (k')^2\right]^2} \tag{20}$$

In the analysis performed in reference 4 the airplane response spectra were developed in terms of the rolling gust spectrum $\Phi_{p_g}$, yawing gust spectrum $\Phi_{r_g}$, and side gust spectrum $\Phi_{\beta_g}$. Because the development in this paper follows the same method as that in reference 4, the same gust spectra are used as input to the airplanes.

A description of how the linear gust velocity spectra $\left(\Phi_{u_g}, \Phi_{v_g}, \Phi_{w_g}\right)$ are related to $\Phi_{p_g}$, $\Phi_{r_g}$, and $\Phi_{\beta_g}$ is given in reference 4. The effective rolling gust velocity $p_g$ is derived from the spanwise gradient of the vertical gust distributions $v_g$. The effective yawing gust $r_g$ is derived from the spanwise gradient of the longitudinal gust velocities $u_g$. These relationships are incorporated in the terms $\left|\frac{p_g}{\beta_g}\right|^2$ and $\left|\frac{r_g}{\beta_g}\right|^2$, which

are the ratios of the rolling and yawing gust spectra to the side gust spectrum. Therefore the power spectra of the gusts can be expressed as

$$\begin{Bmatrix} \Phi_{p_g} \\ \Phi_{r_g} \\ \Phi_{\beta_g} \end{Bmatrix} = \begin{Bmatrix} \left|\frac{p_g}{\beta_g}\right|^2 \\ \left|\frac{r_g}{\beta_g}\right|^2 \\ 1 \end{Bmatrix} \Phi_{\beta_g} \tag{21}$$

Response Power Spectra as Functions of Side Gust Power Spectra

Substitution of the gust power spectrum equation (21) into the response power spectrum equation (8) results in an equation for the response power spectra as a function of the side gust power spectra. The resulting equation for the power spectral density of the angle response is given by

$$\begin{Bmatrix} \Phi_{\varphi_0}(\omega) \\ \Phi_{\psi_0}(\omega) \\ \Phi_{\beta_0}(\omega) \end{Bmatrix} = \begin{bmatrix} \left|\frac{\varphi_0}{p_g}(\omega)\right|^2 & \left|\frac{\varphi_0}{r_g}(\omega)\right|^2 & \left|\frac{\varphi_0}{\beta_g}(\omega)\right|^2 \\ \left|\frac{\psi_0}{p_g}(\omega)\right|^2 & \left|\frac{\psi_0}{r_g}(\omega)\right|^2 & \left|\frac{\psi_0}{\beta_g}(\omega)\right|^2 \\ \left|\frac{\beta_0}{p_g}(\omega)\right|^2 & \left|\frac{\beta_0}{r_g}(\omega)\right|^2 & \left|\frac{\beta_0}{\beta_g}(\omega)\right|^2 \end{bmatrix} \begin{Bmatrix} \left|\frac{p_g}{\beta_g}(\omega)\right|^2 \\ \left|\frac{r_g}{\beta_g}(\omega)\right|^2 \\ 1 \end{Bmatrix} \Phi_{\beta_g}(\omega) \tag{22}$$

Substitution of equation (21) into equation (11) for the power spectral density of the angular rate results in

$$\begin{Bmatrix} \Phi_{\dot{\varphi}_0}(\omega) \\ \Phi_{\dot{\psi}_0}(\omega) \\ \Phi_{\dot{\beta}_0}(\omega) \end{Bmatrix} = \omega^2[T(\omega)] \begin{Bmatrix} \left|\frac{p_g}{\beta_g}(\omega)\right|^2 \\ \left|\frac{r_g}{\beta_g}(\omega)\right|^2 \\ 1 \end{Bmatrix} \Phi_{\beta_g}(\omega) \tag{23}$$

When the substitution of equation (21) into equation (12) for the power spectral density of the angular acceleration is made, the resulting equation is

$$\begin{Bmatrix} \Phi_{\ddot{\varphi}_0}(\omega) \\ \Phi_{\ddot{\psi}_0}(\omega) \\ \Phi_{\ddot{\beta}_0}(\omega) \end{Bmatrix} = \omega^4[T(\omega)] \begin{Bmatrix} \left|\frac{p_g}{\beta_g}(\omega)\right|^2 \\ \left|\frac{r_g}{\beta_g}(\omega)\right|^2 \\ 1 \end{Bmatrix} \Phi_{\beta_g}(\omega) \tag{24}$$

Similarly, the substitution of equation (21) into the equation for the power spectral density of the transverse acceleration (eq. (16)) yields an expression for the power spectral density in terms of the side gust

$$\Phi_{a_t}(\omega) = \left\{ \left|a_{11}(\omega)\right|^2, \left|a_{12}(\omega)\right|^2, \left|a_{13}(\omega)\right|^2 \right\} \begin{Bmatrix} \left|\frac{p_g}{\beta_g}(\omega)\right|^2 \\ \left|\frac{r_g}{\beta_g}(\omega)\right|^2 \\ 1 \end{Bmatrix} \Phi_{\beta_g}(\omega) \tag{25}$$

Root-Mean-Square Values

In addition to the power spectra discussed previously, the root-mean-square (rms) values of the various responses were computed from the power spectra. The root-mean-square values are indicative of the total power in the system as a result of the disturbances in the frequency band that is being considered.

The root-mean-square value of a quantity R as used in this study is given by

$$\sigma_R = \left( \int_{0.622}^{50.222} \Phi_R(\omega) d\omega \right)^{1/2} \tag{26}$$

The integration was truncated at the limits shown. The upper end was cut off at about 8 Hz (50.222 rad/sec) and was considered adequate because the data at higher frequencies generally

were several orders of magnitude lower than those in the region of primary interest (about 1 Hz), and thus their contribution to the root-mean-square value would be negligible. The lower end was cut off at about 0.1 Hz (0.622 rad/sec). This value was considered a practical limit because any motion with a period of 10 seconds or longer probably would be subconsciously corrected by the pilot before it would fully develop.

## Ride Quality Evaluation

A ride quality response rating mode was developed empirically in reference 6. The computed ride quality index from this model is a measure of the ride quality of the airplane and is given by

$$R_c = 1 + \log_{10}\bar{S}_{max} + 0.000176\left(\log_{10}\bar{S}_{max}\right)^4\left[\sum_{i=1}^{3}\left(\log_{10}\bar{S}_i\right)^4 - \left(\log_{10}\bar{S}_{max}\right)^4\right] \quad (27)$$

where $R_c$ is the computed ride quality index. The terms $\bar{S}_i$ are defined as the effective stimuli and are given by $\bar{S}_i = \left(\frac{S_i}{S_{T_i}}\right)^{K_i}$, and $\bar{S}_{max}$ is the largest of the $\bar{S}_i$ terms. The $S_i$ terms are the root-mean-square values of the various turbulence responses (i.e., $\dot{\varphi}$, $\dot{\psi}$, and $a_t$). The terms $S_{T_i}$ are the human perception threshold for the response being considered. The values for the constants $K_i$ and $S_{T_i}$ are listed in the following table:

| i | Response | $K_i$ | $S_{T_i}$ |
|---|---|---|---|
| 1 | Roll rate | 0.650 | 0.000166 |
| 2 | Yaw rate | 1.194 | .000763 |
| 3 | Transverse acceleration | 1.140 | .001220 |

In order to obtain values for the computed index the root-mean-square value from the transverse acceleration and rate power spectra must be used. This index is the type that obtains one rating number for each airplane encompassing the total frequency spectrum. It does not account or allow for the variation in sensitivity of the subject with frequency.

Interpretation of the computed ride quality indices in terms of riding quality rating and the percentage of passengers with no doubts about flying again are given in the following table:

| Computed ride quality index | Ride quality rating | Passengers with no doubts about flying again, % |
|---|---|---|
| 1 | Very comfortable | 100 |
| 2 | Comfortable | 95 |
| 3 | Acceptable | 80 |
| 4 | Uncomfortable | 40 |
| 5 | Very uncomfortable | 20 |

## AIRPLANE PARAMETERS

A listing of the airplanes, pertinent geometric and aerodynamic characteristics, and flight conditions are given in table I. The flight conditions considered are representative of either the cruise condition or a low-altitude holding-pattern condition. The roots of the characteristic equation of each airplane are presented in table II.

Because the airplanes investigated in this paper are the same ones discussed in reference 5, the airplane grouping is also the same. The airplanes are grouped in the following manner: The three conventional airplanes are designated C-A, C-B, and C-C; the five large STOL airplanes are designated LS-A, LS-B, LS-C, LS-D, and LS-E; and the four relatively small STOL airplanes are designated SS-A, SS-B, SS-C, and SS-D.

The first group represents conventional type of airplanes. The stability derivatives for the first of the conventional airplanes, C-A, were obtained by using the method presented in reference 7; the derivatives for the second airplane, C-B, are for the same airplane, but in this case the stability derivatives were obtained by the Datcom method presented in reference 8; the third airplane, C-C, represents an enlarged version of the same airplane, and the derivatives were obtained by a combination of the methods used for airplanes C-A and C-B.

The next group consists of airplanes currently representative of large STOL vehicles. There are two versions of the first airplane, designated LS-A and LS-B. The first was represented with stability derivatives obtained in a manner similar to the conventional airplane, C-B; the second used aerodynamic derivatives obtained during a riding qualities investigation conducted on an NASA moving-base simulation of the airplane. The derivatives were developed by modifying the initial derivatives used in the simulator until the pilots judged that the flight characteristics of the simulator closely matched those of the actual airplane. The derivatives are used in the present paper so as to compare the responses of the same airplane described with data obtained by two alternate procedures. The stability derivatives for airplanes LS-C, LS-D, and LS-E were obtained by the Datcom procedures with

the wing-alone derivatives being computed by the method given in reference 9. Airplanes LS-D and LS-E are the same airplane but flying at different velocities representing Mach numbers of 0.36 and 0.75, respectively.

The last group consists of small STOL airplanes. The first three sets of airplane parameters (SS-A, SS-B, and SS-C) are for the same airplane but with different inertias and flight altitudes. The aerodynamic derivatives were the same for the three airplanes and were obtained by the Datcom method. Two versions, SS-A and SS-B (original and modified inertias), differed only in their moments of inertias; the third version, SS-C, was computed for a different flight altitude which was comparable with most of the other airplanes. The aerodynamic derivatives for airplane SS-D were obtained from reference 10.

The development of the frequency-dependent expressions for $C_{l_\beta}(\omega)$, $C_{n_\beta}(\omega)$, and $C_{Y_\beta}(\omega)$ are given in appendix C of reference 4. These derivatives were computed by using the s- and x-dimensions given in table I. The s- and x-dimensions are illustrated in the following sketch:

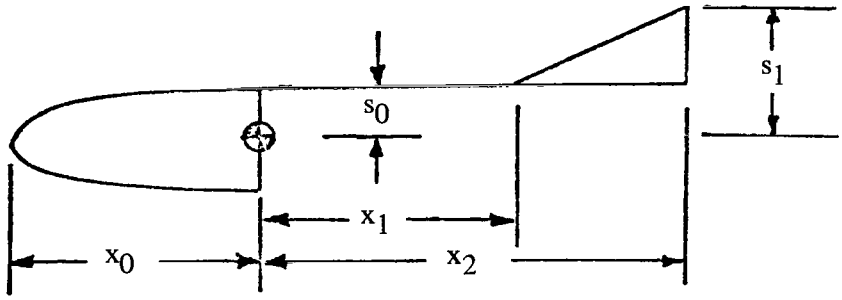


## PROCEDURE

The power spectral densities of the responses for the lateral angular displacements $(\varphi_0, \psi_0, \beta_0)$, velocities $(\dot{\varphi}_0, \dot{\psi}_0, \dot{\beta}_0)$, and accelerations $(\ddot{\varphi}_0, \ddot{\psi}_0, \ddot{\beta}_0)$ as given by equations (22), (23), and (24), respectively, and for the transverse acceleration obtained from equation (25) were computed for 12 airplanes. The data presented for the power spectra were normalized with respect to a unit 1 m/sec root-mean-square gust velocity $\left(\overline{V_g^2} = 1 \text{ m/sec}\right)$ The scale length of the turbulence L was 335.28 m (1100 ft). Reference 11 has shown that people are most sensitive to and least tolerant of linear accelerations in the transverse direction. For this reason, the transverse acceleration $a_t$ has been chosen for presentation in this paper. The transverse accelerations were computed for 13 different locations in each of the 12 airplanes, generally covering the spread in seating positions. The positions

considered were the center of gravity, four positions forward and four rearward of the center of gravity, and two above and two below the center of gravity. The longitudinal spread in the seating locations for the various airplanes is presented in table III. The distance to permissible seating locations to the side of the center was considered too small to have an appreciable effect on the transverse acceleration. The computed ride quality index given by equation (27) was computed for three locations on each airplane: the pilot's position, the center of gravity, and the rear passenger position.

## PRESENTATION OF RESULTS

The computed power spectral densities for the 12 airplanes are presented in figures 1 to 12. Each figure consists of five parts. Part (a) shows the lateral angular power spectral densities for the roll angle, yaw angle, and sideslip angle; part (b) shows the power spectral densities for the angular rates; part (c) shows the power spectral densities for the angular accelerations; parts (d), (e), and (f) show the power spectral densities of the transverse acceleration for the various locations in the airplane. The airplanes were divided into three groups: the conventional airplanes, C-A, C-B, C-C (figs. 1 to 3); the large STOL airplanes, LS-A, LS-B, LS-C, LS-D, LS-E (figs. 4 to 8); and the small STOL airplanes, SS-A, SS-B, SS-C, SS-D (figs. 9 to 12).

A comparison of the power spectral densities of the transverse acceleration for the airplanes in each group (conventional, large STOL, and small STOL) at three longitudinal positions (pilot's position, center of gravity, and rear passenger position) is shown in figures 13, 14, and 15. A comparison of the power spectral densities for transverse accelerations for four airplanes from the three groups (conventional, large STOL, and small STOL) is presented in figure 16. The data are presented for the pilot's position, center of gravity, and rear passenger position in each airplane. Figure 17 shows the variation of the power spectral densities of the transverse acceleration as a function of longitudinal location for the three groups of airplanes at a frequency of 0.45 Hz. In figure 18 the same variation is shown for airplanes representative of each group (C-A, LS-B, SS-C, and SS-D) for four frequencies varying from 0.2 Hz to 2.42 Hz. The data presented in figure 19 show the location of the minimum point of the data in figure 18 as a function of frequency.

The root-mean-square values for the angular displacements, angular rates, angular accelerations, and transverse accelerations are presented in table IV. The ride quality indices obtained for the pilot's position, center of gravity, and rear passenger position are presented in table V for each airplane.

## DISCUSSION

### Airplane Comparisons

Part (a) of figures 1 to 12 is the same as that presented in reference 5 and is reproduced herein for completeness.

Conventional airplanes.- As mentioned previously, airplanes C-A and C-B are the same airplanes for which the stability derivatives were computed by two different methods. Comparison of each power-spectral-density curve in figures 1 and 2 shows that there is little difference between them. As pointed out in reference 5, the difference in results is due mainly to the difference in the derivatives $C_{n_r}$ and $C_{n_\beta}$. The root-mean-square values presented in table IV show that generally airplanes C-A and C-B had similar values. Because both methods of obtaining the stability derivatives are valid, the results indicate that differences in the power spectra and root-mean-square values of the magnitude shown herein are indicative of the spread that could be obtained for a given airplane. Thus differences of this magnitude between two airplanes should not be considered particularly significant.

Airplane C-C is an enlarged version of airplanes C-A and C-B, and, consequently, the stability derivatives are very similar to those for airplane C-A. However, the power spectra and root-mean-square values are lower for airplane C-C than for the other two as can be seen by comparing the power spectral densities in figure 3 with those in figures 1 and 2 and the root-mean-square values in table IV. This comparison is also valid for the power spectral densities of the transverse acceleration $\left(\Phi_{a_t}\right)$ shown in figure 13. At the low frequencies the value for airplane C-C is lowest of the three, and above about $\omega = 2$ rad/sec, even though its stability derivatives are similar to airplane C-A, its $\Phi_{a_t}$ is still somewhat lower. This difference is due to the different flight conditions for the two airplanes; airplane C-C is flying at 7620 m (25 000 ft) and 241.4 m/sec (792 ft/sec), whereas airplanes C-A and C-B are flying at 1524 m (5000 ft) and 134.8 m/sec (442.2 ft/sec). The relatively small difference in relative mass parameter is not an important factor.

Large STOL.- In a manner similar to that for the conventional airplanes, the same airplane with two sets of aerodynamic coefficients, LS-A and LS-B, has been analyzed. A comparison of the results, both the power spectra in figures 4 and 5 and the root-mean-square values in table IV, shows that the second version of the airplane, LS-B, had larger values for both, and the response peaked at a lower frequency (2.49 rad/sec vs 3.24 rad/sec). This difference would indicate a larger amplitude of the motion but at a lower frequency for airplane LS-B. In figure 14 the $\Phi_{a_t}$ values for the two airplanes are compared directly and the effects of the two sets of derivatives are similar in that LS-B had larger values. The values for $\omega_n$ and $\zeta$ in table II show less damping and a lower natural frequency for

airplane LS-B than for airplane LS-A. These differences are due mainly to the different values of $C_{n_r}$ and $C_{n_\beta}$ for the two versions and indicate that accurate stability derivatives are necessary to obtain a truly representative result.

Airplane LS-C is included in this group because it had been considered as a STOL design. The shape of the power-spectral-density curves was different from that of the other airplanes in this group; it had a broader response peak and at a much lower frequency. The $a_t$ root-mean-square values for airplane LS-C in table IV are large compared with the values for the other airplanes in this group, thereby indicating that it may be a relatively poor riding airplane. These results probably are due to the large value of $C_{n_r}$ and low value of $C_{n_\beta}$. The large value of $C_{n_r}$ is responsible for the high Dutch roll damping (flatter peak) and the low value of $C_{n_\beta}$ results in a lower Dutch roll frequency.

Airplanes LS-D and LS-E are the same airplane but flying at two different velocities, 121.92 m/sec and 250.85 m/sec, respectively. The difference in the results is due entirely to the different flight conditions. For the high-speed condition, both the natural frequency and damping (table II) are higher, and, as a result, the peak amplitude and the angular displacement power-spectral-density curves are less and occur at a higher frequency (4.5 rad/sec vs 2.26 rad/sec). As a result of the higher natural frequency the high-speed condition airplane (LS-E) has more power in the higher frequencies. Similar effects can be seen from the comparison of $\Phi_{a_t}$ made in figure 14.

Small STOL.- Airplanes SS-A and SS-B also are the same, differing only in the weight and moments of inertia. The moments of inertias were larger by about 100 percent for airplane SS-B. This decreased the value for $\omega_n$ (table II), as expected, but had a relatively minor effect on the power spectra. It resulted in lower values for the angular rate and angular acceleration power spectral densities at frequencies above about 0.4 Hz (compare figs. 10(b) and 10(c) with figs. 9(b) and 9(c)). However, the transverse acceleration was slightly higher throughout the frequency range (fig. 15). Airplane SS-C is the same airplane as SS-B but is flying at a slightly lower altitude (1524 m compared with 2591 m) which resulted essentially in a decreased relative mass factor (4.88 compared with 5.50). This difference had no appreciable effect on the angular rate and acceleration power spectral densities but caused a slight increase in the transverse acceleration power spectral density. Airplane SS-D is a larger and heavier airplane than the previous SS airplanes and all the power spectra for this airplane are considerably lower than the others.

Groups.- The data in figure 16 present $\Phi_{a_t}$ for airplanes representative of each group (C-A, LS-B, SS-C, and SS-D) for three longitudinal locations along the fuselage. The pilot and rear passenger positions are not the same for the various airplanes (see table III). Nevertheless, it can be seen from the curves in figures 16(a) to 16(c) that the conventional airplane had lower values across almost the entire frequency range. The lightest STOL (SS-C) had the highest values, whereas the results for the large STOL (LS-B) and the largest of the

small STOL airplanes (SS-D) were between the other two. Actually, airplanes LS-B and SS-D had very similar results. Although their stability coefficients were appreciably different, the combination was such that the values for $\omega_n$ and $\zeta$ for the two airplanes were very close and probably played a significant factor in the results turning out so similar.

The variation of $\Phi_{a_t}$ with location along the longitudinal axis is shown in figure 17 for the various groups of airplanes at a frequency of 0.45 Hz. This frequency was chosen because the data presented in reference 11 showed that people were most sensitive to transverse accelerations at about 0.45 Hz. The data in figure 17 show that generally all the airplanes follow a similar pattern with a minimum point approximately 0.2x/b forward of the center of gravity.

The results for the conventional airplanes presented in figure 17(a) show that for the two versions of the same airplane, C-A and C-B, the curves are similar but the power-spectral-density curve for C-B was higher than for C-A. This spread indicates how well the power spectral density computed from a given set of parameters is likely to represent the airplane. The variation of $\Phi_{a_t}$ for airplane C-C is less dependent on location than the variation of $\Phi_{a_t}$ for the other conventional airplanes because it is a larger and heavier airplane.

The results in figure 17(b) for the large STOL airplanes show the effect of Mach number on the variation of $\Phi_{a_t}$ with location (airplanes LS-D and LS-E, Mach numbers 0.36 and 0.75, respectively). Although the curves for the two airplanes were not particularly separated from each other, the variation for the higher Mach number showed less variation with the minimum point farther forward. The results for airplane LS-C again were unusual in that it was the only airplane that exhibited no minimum point at this frequency (0.45 Hz).

The information in figure 17(c) for the small STOL airplanes shows the effect of moment-of-inertia changes. Airplane SS-B has higher values for $\Phi_{a_t}$, and its minimum point is farther forward than that for airplane SS-A.

Figure 18 shows how the variation of $\Phi_{a_t}$ with longitudinal location changes with the frequency of the motion. Curves for the same representative airplanes (C-A, LS-B, SS-C, and SS-D) are presented for four frequencies from 0.2 Hz to 2.42 Hz. The pattern of the variation is similar for all four airplanes. However the minimum point has a noticeable shift rearward as the frequency increases. This change in minimum point is specifically shown in figure 19. The change is rapid at low frequencies, but above 0.8 to 1.0 Hz there is little change. The curves should approach the center-of-gravity location at the higher frequencies. This information could have some bearing on the location of components within an airplane; for example, components that may be sensitive to the transverse acceleration at certain frequencies should be located in the vicinity of the minimum point for those frequencies, whereas insensitive components can be located elsewhere.

### Ride Quality Evaluation

The ride quality indices were computed for each airplane and are presented in table V. Because the airplanes were considered rigid bodies with no auxiliary damping devices, the computed ride quality indices may be higher than those for operational airplanes in flight. Therefore, the indices can be considered to represent relative values only; that is, an airplane with a lower index would be a more comfortable flying airplane than one with a higher index. The data show that all conventional but only two versions of STOL airplanes have a better than uncomfortable rating. The rest of the large STOL airplanes have ratings between uncomfortable and very uncomfortable. The small STOL airplanes generally are in the very uncomfortable range. This means that flight in STOL airplanes probably would generate an adverse opinion in about 60 percent of the passengers. A brief check on the terms comprising the criterion showed, at least for the airplanes considered in this paper, that the yaw-rate term ($\dot{\psi}$) contributed most to the value of the index.

## CONCLUDING REMARKS

An analytical investigation was made in which the power spectra of the lateral angular rates, angular accelerations, and transverse accelerations were computed for 12 airplanes. These airplanes were divided into three classifications: conventional, large short take-off and landing (STOL), and small STOL. The atmospheric turbulence was represented by three orthogonal velocity components, which were uncorrelated, and each was represented with a one-dimensional Dryden power spectrum.

Two methods of determining the stability derivatives for the same airplane were found to result in somewhat different power spectra. This comparison highlights the necessity of utilizing the best methods available to insure the most representative power spectra for the airplane. For the airplanes considered in this study, the conventional airplanes generally had the lowest root-mean-square values for the power spectra, the large STOL airplanes had values somewhat higher than the conventional, and the small STOL airplanes had the highest values.

The power spectra result pattern generally carried over to the ride quality results in that the conventional airplanes had the most favorable index, the large STOL airplanes had a less favorable index, and the small STOL airplanes had the worst index of the three.

Langley Research Center
National Aeronautics and Space Administration
Hampton, Va. 23665
August 20, 1975

## REFERENCES


1. Inter-Metropolitan STOL Evaluation (Phase X). Develop. Engineer. Rep. 50, American Airlines, Jan. 1970.
2. Symposium on Vehicle Ride Quality. NASA TM X-2620, 1972.
3. Houbolt, John C.; Steiner, Roy; and Pratt, Kermit G.: Dynamic Response of Airplanes to Atmospheric Turbulence Including Flight Data on Input and Response. NASA TR R-199, 1964.
4. Eggleston, John M.; and Phillips, William H.: The Lateral Response of Airplanes to Random Atmospheric Turbulence. NASA TR R-74, 1960. (Supersedes NACA TN 3954 by Eggleston and TN 4196 by Eggleston and Phillips.)
5. Lichtenstein, Jacob H.: Computed Lateral Power Spectral Density Response of Conventional and STOL Airplanes to Random Atmospheric Turbulence. NASA TN D-7444, 1974.
6. Stone, Ralph W., Jr.: An Elementary Psychophysical Model To Predict Ride Comfort in the Combined Stress of Multiple Degrees of Freedom. Vibration and Combined Stresses in Advanced Systems, AGARD-CP-145, Mar. 1975, pp. B22-1 – B22-7.
7. Lina, Lindsay J.; and Canavos, George C.: Influence of Angle of Glide Slope on the Accuracy of Performing Instrument Approaches in a Simulator. NASA TN D-4835, 1968.
8. USAF Stability and Control Datcom. Contracts AF 33(616)-6460, AF 33(615)-1605, F33615-67-C-1156, F33615-68-C-1260, and F33615-70-C-1087, McDonnell Douglas Corp., Oct. 1960. (Revised Sept. 1970.)
9. Queijo, M. J.: Theory for Computing Span Loads and Stability Derivatives Due to Sideslip, Yawing, and Rolling for Wings in Subsonic Compressible Flow. NASA TN D-4929, 1968.
10. STOL Airplane Characteristics Documentation for a 12,500 Pound Turbo-Prop Airplane. DHC Rep. 71-6, De Havilland Aircraft of Canada, Ltd., Sept. 16, 1971.
11. Stone, Ralph W., Jr.: Ride-Quality Overview. Symposium on Vehicle Ride Quality, NASA TM X-2620, 1972.

TABLE I.- FLIGHT CONDITIONS, PHYSICAL DIMENSIONS, AND STABILITY DERIVATIVES OF AIRPLANES CONSIDERED IN INVESTIGATION

| Quantity | Conventional | | | Large STOL | | | | | Small STOL | | | |
|---|---|---|---|---|---|---|---|---|---|---|---|---|
| | A | B | C | A | B | C | D | E | A | B | C | D |
| Flight conditions, mass and inertia parameters | | | | | | | | | | | | |
| h, m | 1 524 | 1 524 | 7 620 | 1 524 | 1 524 | 1 524 | 1 524 | 1 524 | 2 591 | 2 591 | 1 524 | 1 524 |
| (ft) | (5 000) | (5 000) | (25 000) | (5 000) | (5 000) | (5 000) | (5 000) | (5 000) | (8 500) | (8 500) | (5 000) | (5 000) |
| U, m/sec | 134.78 | 134.78 | 241.40 | 120.70 | 120.70 | 121.92 | 121.92 | 250.85 | 73.76 | 73.76 | 73.76 | 77.18 |
| (ft/sec) | (442.2) | (442.2) | (792) | (396) | (396) | (400) | (400) | (823) | (242) | (242) | (242) | (253.2) |
| m, kg | 27 751 | 27 751 | 38 029 | 22 226 | 20 412 | 16 982 | 24 993 | 24 993 | 1 542 | 1 315 | 1 315 | 5 216 |
| (slugs) | (1901.8) | (1901.8) | (2606.2) | (1523.2) | (1398.8) | (1163.8) | (1712.8) | (1712.8) | (105.7) | (90.1) | (90.1) | (357.5) |
| W, N | 272 142 | 272 142 | 372 939 | 217 963 | 200 170 | 166 537 | 245 097 | 245 097 | 15 124 | 12 899 | 12 899 | 51 155 |
| (lb) | (61 180) | (61 180) | (83 840) | (49 000) | (45 000) | (37 439) | (55 100) | (55 100) | (3 400) | (2 900) | (2 900) | (11 500) |
| m/S, $kg/m^2$ | 319.7 | 319.7 | 409.4 | 269.1 | 243.6 | 342.0 | 319.2 | 319.2 | 71.9 | 61.3 | 61.3 | 133.7 |
| $(slugs/ft^2)$ | (2.036) | (2.036) | (2.606) | (1.713) | (1.551) | (2.178) | (2.032) | (2.032) | (0.458) | (0.390) | (0.390) | (0.851) |
| W/S, $N/m^2$ | 3135.3 | 3135.3 | 4014.4 | 2639.1 | 2388.7 | 3354.2 | 3129.8 | 3129.8 | 704.8 | 601.1 | 601.1 | 1311.0 |
| $(lb/ft^2)$ | (65.48) | (65.48) | (83.84) | (55.12) | (49.89) | (70.02) | (65.36) | (65.36) | (14.72) | (12.55) | (12.55) | (27.38) |
| $\mu$ | 11.163 | 11.163 | 26.2 | 10.99 | 9.99 | 15.746 | 12.721 | 12.72 | 6.477 | 5.50 | 4.88 | 6.397 |
| $C_L$ | .33 | .33 | .251 | .343 | .343 | .429 | .4 | .0946 | .2765 | .2358 | .2094 | .4174 |
| $\tan\gamma$ | 0 | 0 | 0 | 0 | 0 | 0 | 0 | 0 | 0 | 0 | 0 | 0 |
| $\alpha_0$, rad | .031 | .0318 | .0310 | −.0349 | −.0349 | .1101 | .086 | .01 | .0614 | .0524 | .0465 | .0227 |
| $K_X^2$ | 0.0137 | 0.0137 | 0.0128 | 0.0325 | 0.0315 | 0.0327 | 0.0234 | 0.0234 | 0.0075 | 0.0175 | 0.0175 | 0.0103 |
| $K_Z^2$ | .0656 | .0656 | .0700 | .0578 | .0604 | .0504 | .0443 | .0443 | .0156 | .0328 | .0328 | .0247 |
| $K_{XZ}$ | .00468 | .00468 | .0043 | −.004 | .00022 | .0045 | .00195 | .00195 | −.00103 | .00241 | .00241 | .00085 |

TABLE I.- Continued

| Quantity | Conventional | | | Large STOL | | | | | Small STOL | | | |
|---|---|---|---|---|---|---|---|---|---|---|---|---|
| | A | B | C | A | B | C | D | E | A | B | C | D |
| | | | | | | Dimensions | | | | | | |
| b, m | 27.13 | 27.13 | 28.47 | 23.20 | 23.16 | 20.57 | 23.77 | 23.77 | 11.89 | 11.89 | 11.89 | 19.81 |
| (ft) | (89) | (89) | (93.4) | (76.1) | (76.0) | (67.5) | (78) | (78) | (39) | (39) | (39) | (65) |
| S, $m^2$ | 86.80 | 86.80 | 92.90 | 82.59 | 83.80 | 49.65 | 78.31 | 78.31 | 21.46 | 21.46 | 21.46 | 39.02 |
| ($ft^2$) | (934.3) | (934.3) | (1000) | (889) | (902) | (534.4) | (843) | (843) | (231) | (231) | (231) | (420) |
| $S_T$, $m^2$ | 18.09 | 19.56 | 19.46 | 20.35 | 20.35 | 12.08 | 16.62 | 16.62 | 2.40 | 2.40 | 2.40 | 9.20 |
| ($ft^2$) | (194.7) | (210.5) | (209.5) | (219) | (219) | (130.0) | (178.9) | (178.9) | (25.8) | (25.8) | (25.8) | (99) |
| A | 8.25 | 8.25 | 8.72 | 6.52 | 6.52 | 8.53 | 7.75 | 7.75 | 6.58 | 6.58 | 6.58 | 10 |
| $\Gamma$, deg | 3 | 3 | 3 | 4 | 4 | –2.12 | –3.5 | –3.5 | 0 | 0 | 0 | 3 |
| $h_z$, m | 3.712 | 3.712 | 4.243 | 3.000 | 3.000 | 2.990 | 3.575 | 3.575 | 2.179 | 2.179 | 2.179 | 1.829 |
| (ft) | (12.18) | (12.18) | (13.92) | (9.84) | (9.84) | (9.81) | (11.73) | (11.73) | (7.15) | (7.15) | (7.15) | (6.1) |
| $l_T$, m | 11.08 | 11.08 | 15.00 | 11.29 | 11.29 | 6.52 | 7.78 | 7.78 | 5.79 | 5.79 | 5.79 | 7.96 |
| (ft) | (36.34) | (36.34) | (49.20) | (37.05) | (37.05) | (21.40) | (25.53) | (25.53) | (19) | (19) | (19) | (26.1) |
| $x_0$, m | 14.48 | 14.48 | 17.53 | 7.39 | 7.39 | 6.72 | 11.04 | 11.04 | 2.33 | 2.33 | 2.33 | 5.94 |
| (ft) | (47.50) | (47.50) | (57.50) | (24.26) | (24.26) | (22.04) | (36.23) | (36.23) | (7.63) | (7.63) | (7.63) | (19.5) |
| $x_1$, m | 8.36 | 8.36 | 11.92 | 9.48 | 9.48 | 4.97 | 5.42 | 5.42 | 5.19 | 5.19 | 5.19 | 6.71 |
| (ft) | (27.43) | (27.43) | (39.10) | (31.09) | (31.09) | (16.31) | (17.77) | (17.77) | (17.04) | (17.04) | (17.04) | (22.0) |
| $x_2$, m | 15.94 | 15.94 | 18.36 | 14.81 | 14.81 | 8.69 | 9.61 | 9.61 | 6.72 | 6.72 | 6.72 | 9.97 |
| (ft) | (52.30) | (52.30) | (60.25) | (48.59) | (48.59) | (28.52) | (31.53) | (31.53) | (22.06) | (22.06) | (22.06) | (32.7) |
| $s_0$, m | 1.82 | 1.82 | 2.47 | 1.50 | 1.50 | 1.88 | 1.22 | 1.22 | 0.63 | 0.63 | 0.63 | 1.22 |
| (ft) | (5.96) | (5.96) | (8.10) | (4.92) | (4.92) | (6.18) | (4.01) | (4.01) | (2.07) | (2.07) | (2.07) | (4) |
| $s_1$, m | 5.63 | 5.63 | 6.39 | 6.22 | 6.22 | 6.50 | 6.11 | 6.11 | 2.86 | 2.86 | 2.86 | 4.11 |
| (ft) | (18.47) | (18.47) | (20.95) | (20.52) | (20.42) | (21.33) | (20.06) | (20.06) | (9.39) | (9.39) | (9.39) | (13.5) |

TABLE I.- Concluded

| Quantity | Conventional | | | Large STOL | | | | | Small STOL | | | |
|---|---|---|---|---|---|---|---|---|---|---|---|---|
| | A | B | C | A | B | C | D | E | A | B | C | D |
| Stability derivatives for airplane | | | | | | | | | | | | |
| $C_{l_p}$ | −0.4783 | −0.388 | −0.4783 | −0.443 | −0.4974 | −0.73 | −0.438 | −0.51 | −0.4875 | −0.4875 | −0.4875 | −0.548 |
| $C_{l_r}$ | .1623 | .168 | .1623 | .1965 | −.0671 | .20 | .1436 | .10 | .1034 | .1034 | .1034 | .107 |
| $C_{l_\beta}$ | −.1419 | −.1489 | −.1419 | −.1397 | −.0952 | −.175 | −.2443 | −.20 | −.0651 | −.0651 | −.0651 | −.113 |
| $C_{n_p}$ | 0.00322 | −0.0584 | 0.00322 | −0.0733 | −0.1519 | −0.050 | −0.092 | −0.05 | −0.0209 | −0.0209 | −0.0209 | 0.0132 |
| $C_{n_r}$ | −.2277 | −.2973 | −.328 | −.5833 | −.456 | −.73 | −.203 | −.20 | −.149 | −.149 | −.149 | −.1827 |
| $C_{n_\beta}$ | .1383 | .1709 | .1657 | .463 | .267 | .060 | .200 | .20 | .0605 | .0605 | .0605 | .1247 |
| $C_{Y_p}$ | 0.0568 | 0.039 | 0.0568 | −0.079 | −0.079 | 0.500 | 0.044 | 0.10 | −0.0637 | −0.0637 | −0.0637 | 0 |
| $C_{Y_r}$ | .5365 | .706 | .5365 | 1.17 | 1.17 | .400 | .70 | .70 | .2549 | .2549 | .2549 | 0 |
| $C_{Y_\beta}$ | −.899 | −1.16 | −1.081 | −1.486 | −1.35 | −1.65 | −1.146 | −1.146 | −.460 | −.460 | −.460 | −.8457 |
| $C_{L_\alpha}$, per rad | 5.872 | 5.872 | 5.872 | 6.55 | 6.55 | 3.896 | 4.68 | 4.68 | 4.5 | 4.5 | 4.5 | 5.79 |
| Wing or tail stability derivatives and parameters | | | | | | | | | | | | |
| $(C_{l_p})_W$ | −0.4676 | −0.4676 | −0.4676 | −0.42 | −0.42 | −0.5185 | −0.452 | −0.524 | −0.123 | −0.123 | −0.123 | −0.548 |
| $(C_{l_r})_W$ | .437 | .437 | .437 | .0803 | .0803 | .0627 | .067 | .0235 | .0419 | .0357 | .0317 | .107 |
| $(C_{l_\beta})_W$ | −.056 | −.072 | −.056 | −.0703 | −.0703 | −.0165 | −.0608 | −.0166 | −.0177 | −.0151 | −.0134 | −.0441 |
| $(C_{n_p})_W$ | −0.40 | −0.40 | −0.40 | −0.0382 | −0.0382 | −0.0553 | −0.0544 | −0.0129 | −0.0368 | −0.0314 | −0.0279 | 0.0132 |
| $(C_{n_r})_W$ | .023 | .023 | .023 | −.0061 | −.0061 | −.0074 | −.0074 | −.00436 | −.0240 | −.0241 | −.0237 | −.126 |
| $C_{D,o}$ | .018 | .0052 | .018 | .00656 | .00656 | .0071 | .01 | .01 | .0073 | .0073 | .0073 | .01 |
| $\alpha_W$, rad | .031 | .0318 | .0310 | −.0349 | −.0349 | .1101 | .086 | .01 | .0614 | .0524 | .0465 | .0227 |
| $(C_{Y_\beta})_T$ | −0.607 | −0.8512 | −0.607 | −1.185 | −1.185 | −0.647 | −0.537 | −0.537 | −0.575 | −0.575 | −0.575 | −0.6921 |
| $\sigma/\beta_T$ | .2 | .332 | .2 | .489 | .489 | .0068 | .3455 | .3455 | −.241 | −.241 | −.241 | .0849 |
| Source reference | 7 | 8 | 8 | 8 | (a) | 8 | 8 | 8 | 8 | 8 | 8 | 10 |

[a]Aerodynamic coefficients modified for use on a NASA moving-base simulator to give realistic handling qualities.

TABLE II.- COMPUTED ROOTS OF CHARACTERISTIC EQUATION, NATURAL FREQUENCY, AND DAMPING RATIO

| Airplane | Spiral-mode roots, 1/sec | Roll-mode roots, 1/sec | Dutch roll mode | | | |
|---|---|---|---|---|---|---|
| | | | Roots, 1/sec | | Damping ratio, $\zeta$ | Natural frequency of Dutch roll, $\omega_n$, rad/sec |
| | | | Real | Imaginary | | |
| C-A | $-9.987 \times 10^{-3}$ | -4.123 | -0.1723 | ±1.562 | 0.110 | 1.57 |
| C-B | -13.843 | -3.519 | -.2024 | ±1.802 | .112 | 1.81 |
| C-C | -9.463 | -3.313 | -.1318 | ±1.790 | .073 | 1.79 |
| LS-A | 3.408 | -1.683 | -.7676 | ±3.151 | .237 | 3.24 |
| LS-B | -36.342 | -2.257 | -.5501 | ±2.428 | .221 | 2.49 |
| LS-C | -215.052 | -2.343 | -.5985 | ±.916 | .547 | 1.09 |
| LS-D | -14.195 | -2.328 | -.1167 | ±2.262 | .052 | 2.26 |
| LS-E | -68.636 | -4.958 | -.4806 | ±4.474 | .107 | 4.50 |
| SS-A | -14.166 | -15.791 | -1.314 | ±3.303 | .370 | 3.55 |
| SS-B | -13.949 | -8.000 | -.6896 | ±2.580 | .258 | 2.67 |
| SS-C | -13.939 | -8.990 | -.7912 | ±2.730 | .278 | 2.84 |
| SS-D | -13.034 | -8.150 | -.6453 | ±2.423 | .257 | 2.51 |

TABLE III.- SEATING POSITIONS LIMITS FOR VARIOUS AIRPLANES

| Airplane | Fraction of span from center of gravity | |
|---|---|---|
| | Forward limit (pilot's position) | Rearward limit (rear passenger's position) |
| C-A | 0.56 | 0.21 |
| C-B | .56 | .21 |
| C-C | ≈.65 | .35 |
| LS-A | .28 | .24 |
| LS-B | .28 | .24 |
| LS-C | .25 | .26 |
| LS-D | .38 | .30 |
| LS-E | .38 | .30 |
| SS-A | .06 | .14 |
| SS-B | .06 | .14 |
| SS-C | .06 | .14 |
| SS-D | .15 | .18 |

TABLE IV.- ROOT-MEAN-SQUARE TURBULENCE RESPONSES OF DISPLACEMENT, RATE, ACCELERATION, AND TRANSVERSE ACCELERATION[a]

| Airplane | Displacement, $\frac{\text{rad}}{\text{m/sec}}$ | | | Rate, $\frac{\text{rad/sec}}{\text{m/sec}}$ | | | Acceleration, $\frac{\text{rad/sec}^2}{\text{m/sec}}$ | | | Transverse acceleration, $\frac{\text{g units}}{\text{m/sec}} \times 10^2$ | | |
|---|---|---|---|---|---|---|---|---|---|---|---|---|
| | $\sigma_{\varphi_0}$ | $\sigma_{\psi_0}$ | $\sigma_{\beta_0}$ | $\sigma_{\dot{\varphi}_0}$ | $\sigma_{\dot{\psi}_0}$ | $\sigma_{\dot{\beta}_0}$ | $\sigma_{\ddot{\varphi}_0}$ | $\sigma_{\ddot{\psi}_0}$ | $\sigma_{\ddot{\beta}_0}$ | $\sigma_{a_t}$ Pilot's position | $\sigma_{a_t}$ Center of gravity | $\sigma_{a_t}$ Rear passenger's position |
| C-A | 0.0262 | 0.0122 | 0.0135 | 0.0369 | 0.0181 | 0.0196 | 0.0821 | 0.0340 | 0.0355 | 0.890 | 1.120 | 1.661 |
| C-B | .0233 | .0103 | .0108 | .0376 | .0168 | .0177 | .0949 | .0351 | .0363 | .840 | 1.145 | 1.700 |
| C-C | .0193 | .0066 | .0069 | .0317 | .0114 | .0120 | .0769 | .0249 | .0253 | .700 | .956 | 1.630 |
| LS-A | .0157 | .0078 | .0068 | .0172 | .0153 | .0150 | .0498 | .0505 | .0506 | .40 | .677 | 1.530 |
| LS-B | .0155 | .0135 | .0124 | .0211 | .0234 | .0227 | .0584 | .0598 | .0589 | .705 | 1.402 | 2.354 |
| LS-C | .0815 | .0208 | .0277 | .0695 | .0230 | .0282 | .0750 | .0405 | .0443 | 2.910 | 3.348 | 3.850 |
| LS-D | .0330 | .0160 | .0171 | .0596 | .0344 | .0358 | .1326 | .0799 | .0825 | .420 | 1.421 | 3.300 |
| LS-E | .0197 | .0069 | .0072 | .0395 | .0256 | .0259 | .1648 | .1191 | .1196 | .850 | 2.273 | 4.950 |
| SS-A | .0540 | .0398 | .0457 | .0666 | .0874 | .0916 | .1892 | .3345 | .3410 | 1.41 | 1.825 | 3.250 |
| SS-B | .0578 | .0449 | .0507 | .0712 | .0885 | .0932 | .1509 | .2528 | .2594 | 2.11 | 2.532 | 3.610 |
| SS-C | .0567 | .0435 | .0491 | .0692 | .0880 | .0925 | .1525 | .2674 | .2737 | 2.308 | 2.730 | 3.893 |
| SS-D | .0185 | .0161 | .0180 | .0283 | .0299 | .0321 | .1174 | .0828 | .0864 | .478 | .919 | 1.769 |

[a]Values obtained by integrating normalized power spectrum from $\omega$ = 0.0622 rad/sec to 50.222 rad/sec.

TABLE V.- COMPUTED RIDE QUALITY INDEX

(a) Computed values of ride quality index

| Airplane | Range of computed ride quality index from pilot to c.g. to rear passenger locations |
|---|---|
| C-A | 3.72 to 3.73 to 3.74 |
| C-B | 3.66 to 3.66 to 3.67 |
| C-C | 3.31 to 3.31 to 3.32 |
| LS-A | 3.55 to 3.55 to 3.56 |
| LS-B | 3.94 to 3.95 to 3.98 |
| LS-C | 4.05 to 4.06 to 4.07 |
| LS-D | 4.37 to 4.39 to 4.48 |
| LS-E | 4.06 to 4.10 to 4.19 |
| SS-A | 5.46 to 5.51 to 5.68 |
| SS-B | 5.57 to 5.62 to 5.76 |
| SS-C | 5.58 to 5.63 to 5.77 |
| SS-D | 4.18 to 4.17 to 4.21 |

(b) Interpretation of ride quality index

| Computed index | Ride quality rating | Passengers with no doubts about flying again, % |
|---|---|---|
| 1 | Very comfortable | 100 |
| 2 | Comfortable | 95 |
| 3 | Acceptable | 80 |
| 4 | Uncomfortable | 40 |
| 5 and higher | Very uncomfortable | 20 |

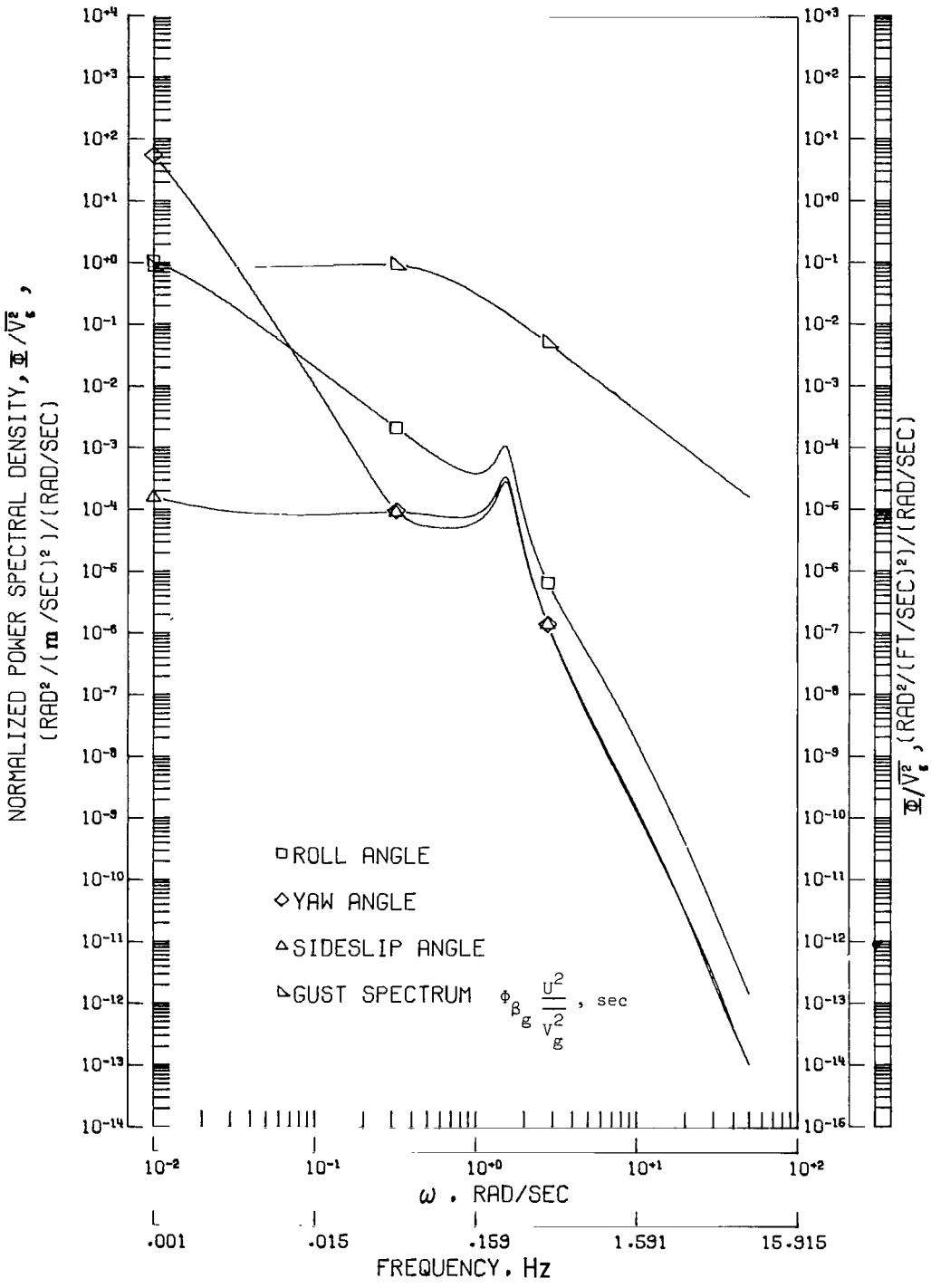


(a) Normalized power spectral density response for each lateral angular displacement.

Figure 1.- Response of airplane C-A to random gusts for assumed scale length of 335.28 m (1100 ft). Note that units for gust spectrum are different from those for response spectra.

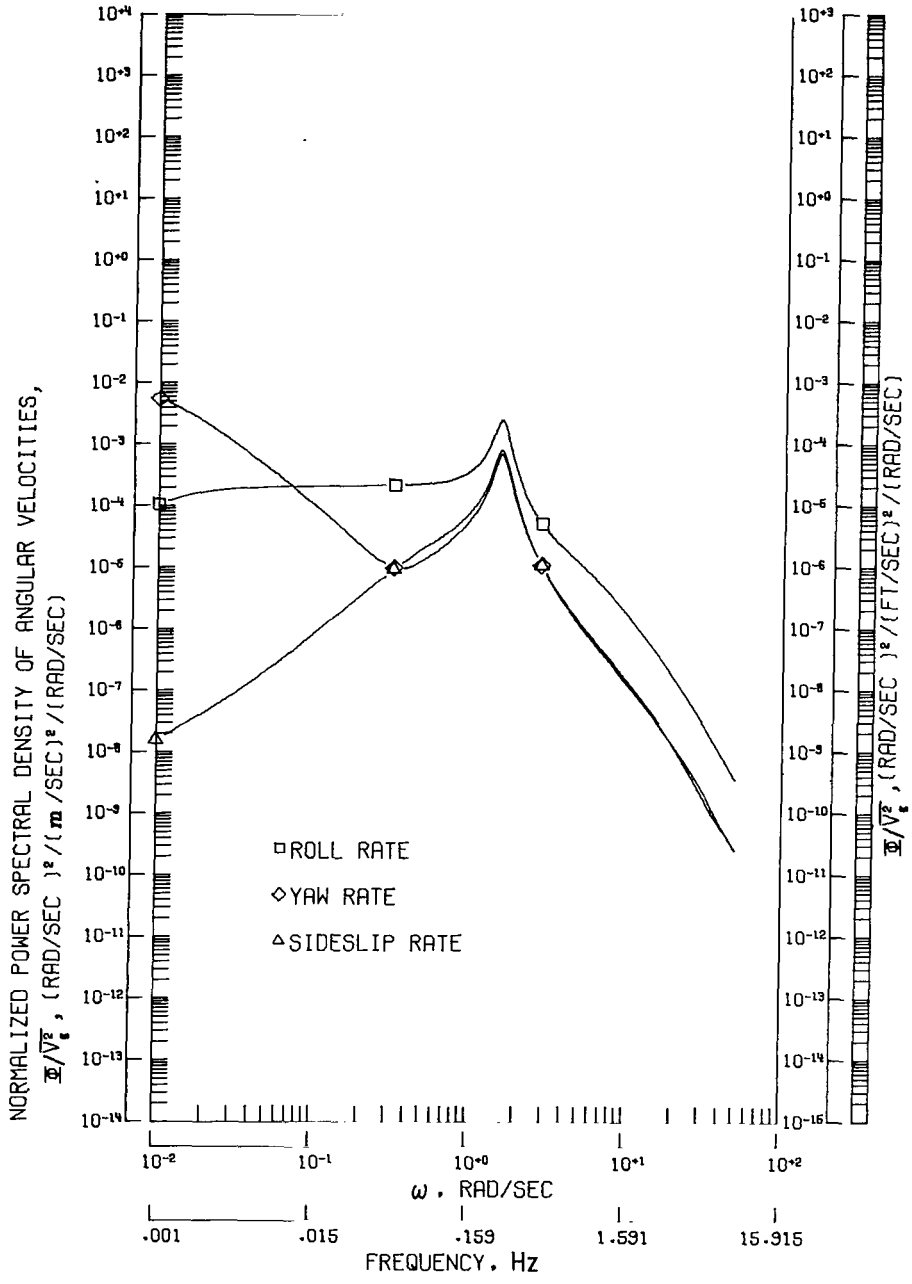


(b) Normalized power spectral density response for each lateral angular rate.

Figure 1.- Continued.

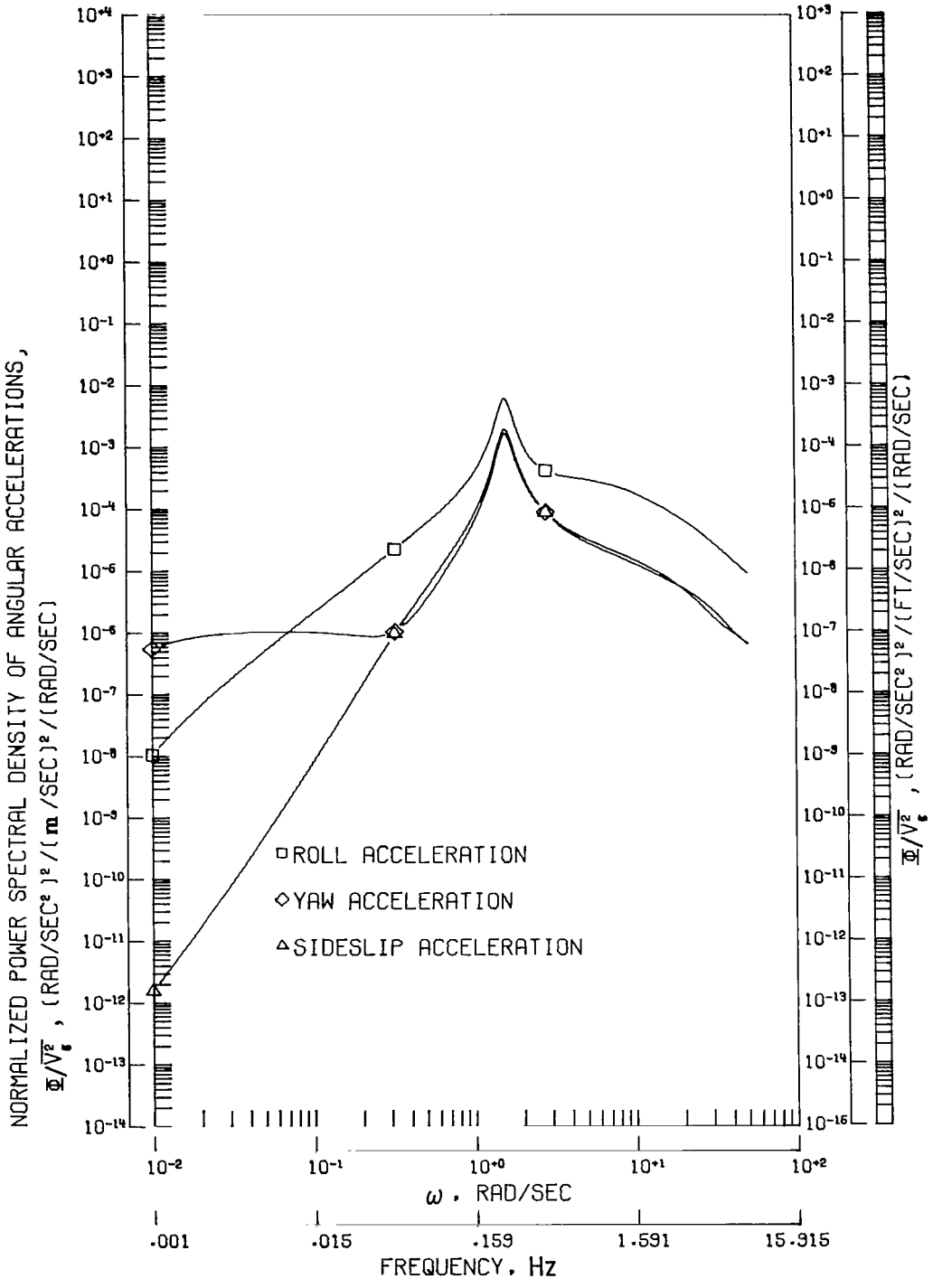


(c) Normalized power spectral density response for each lateral angular acceleration.

Figure 1.- Continued.

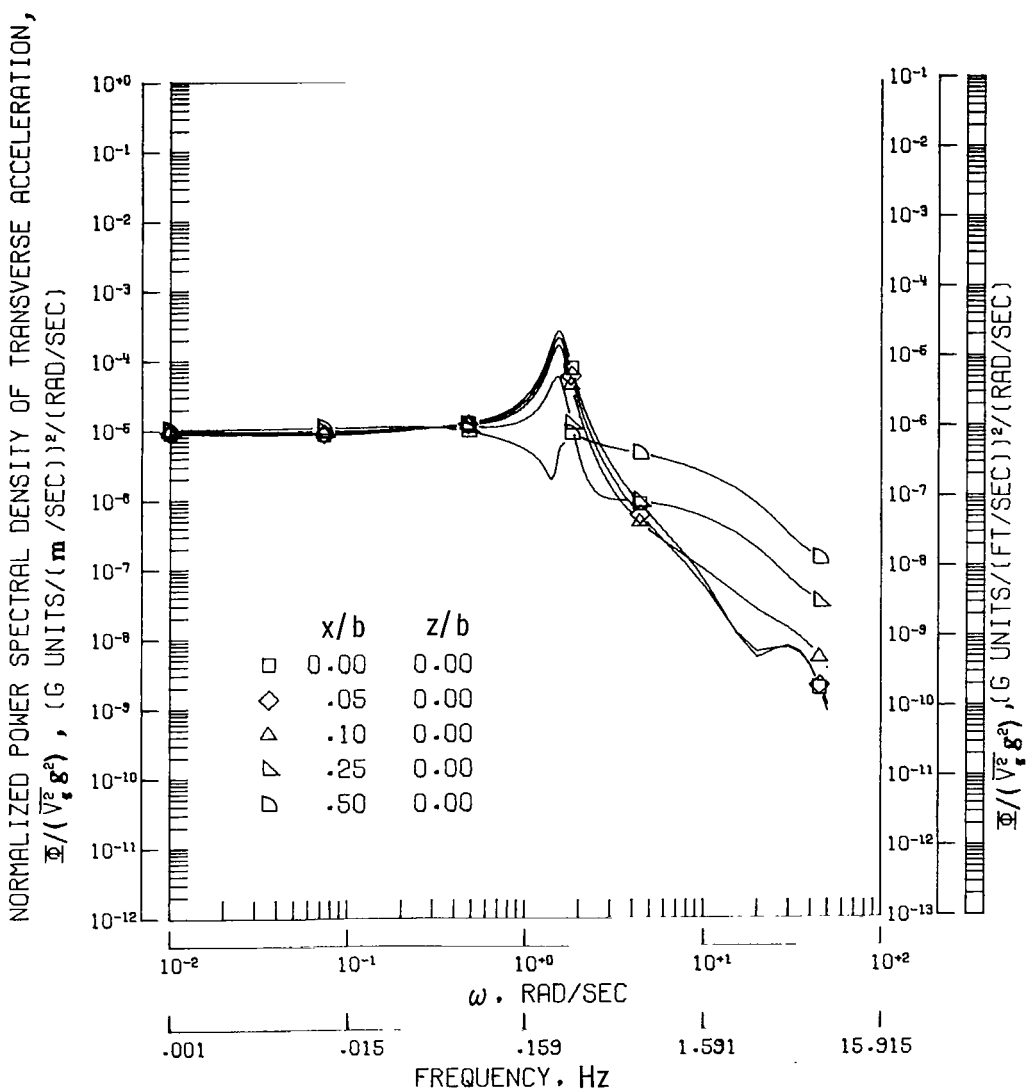


(d) Normalized power spectral density of transverse acceleration for locations forward of center of gravity.

Figure 1.- Continued.

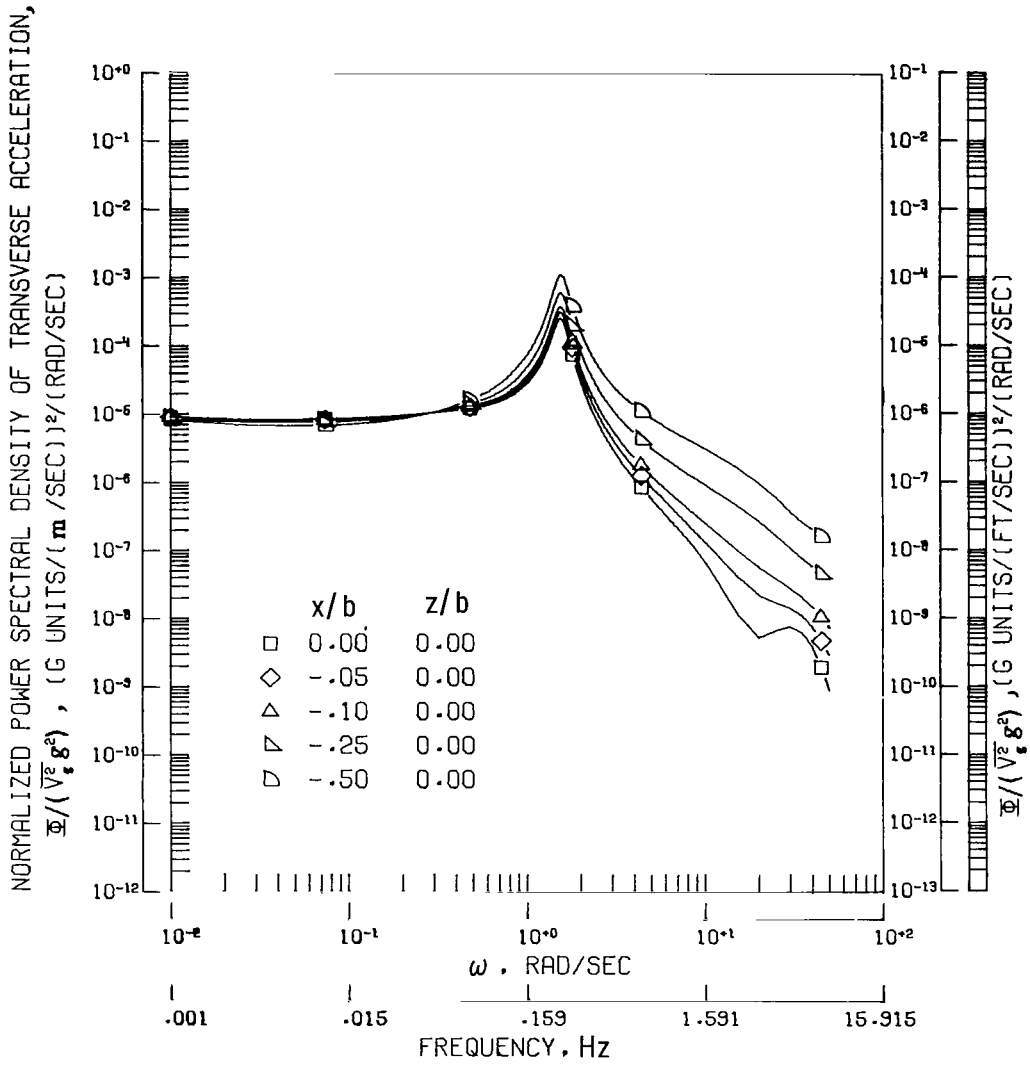


(e) Normalized power spectral density of transverse acceleration for locations rearward of center of gravity.

Figure 1.- Continued.

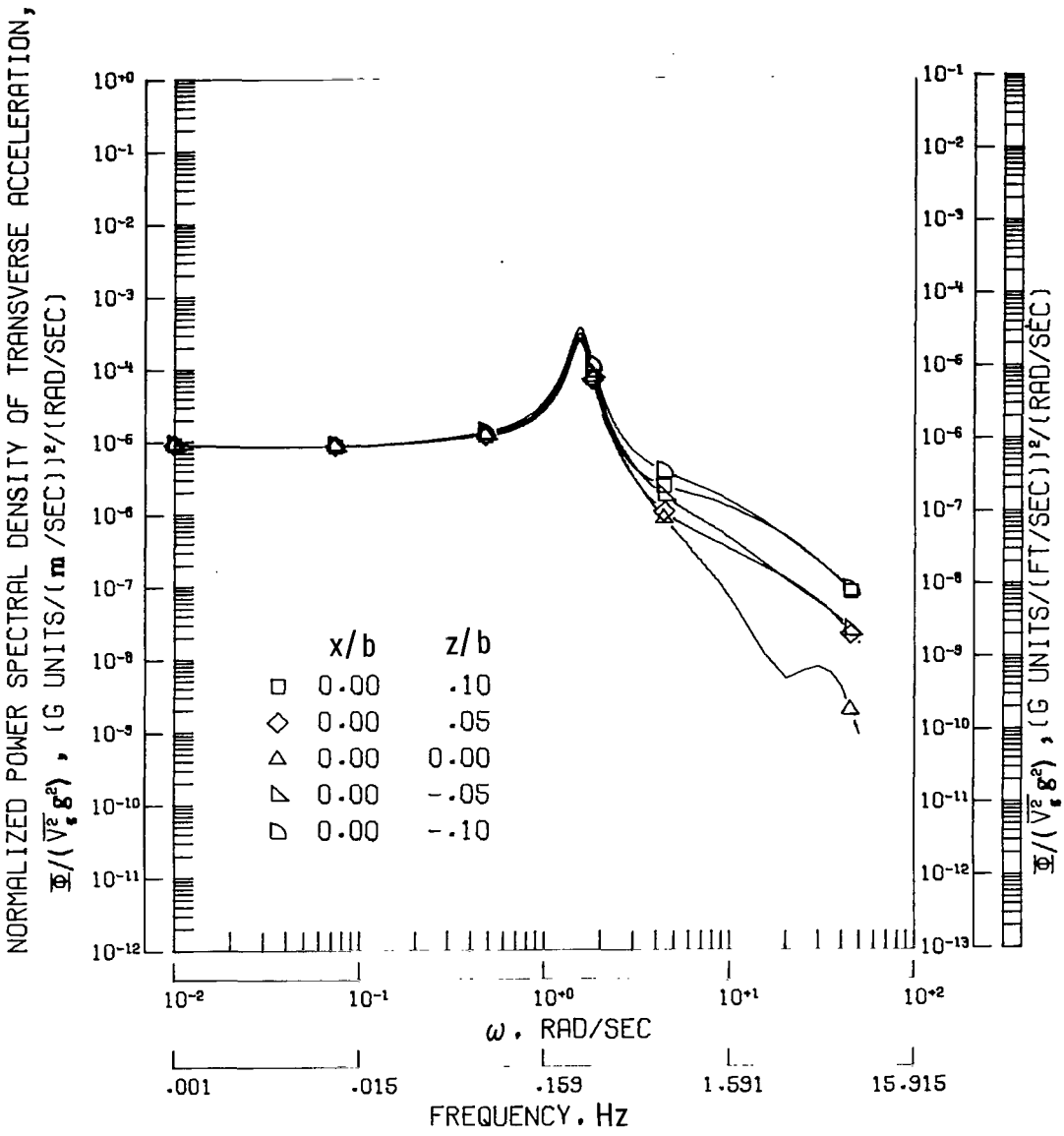


(f) Normalized power spectral density of transverse acceleration for several locations above and below center of gravity.

Figure 1.- Concluded.

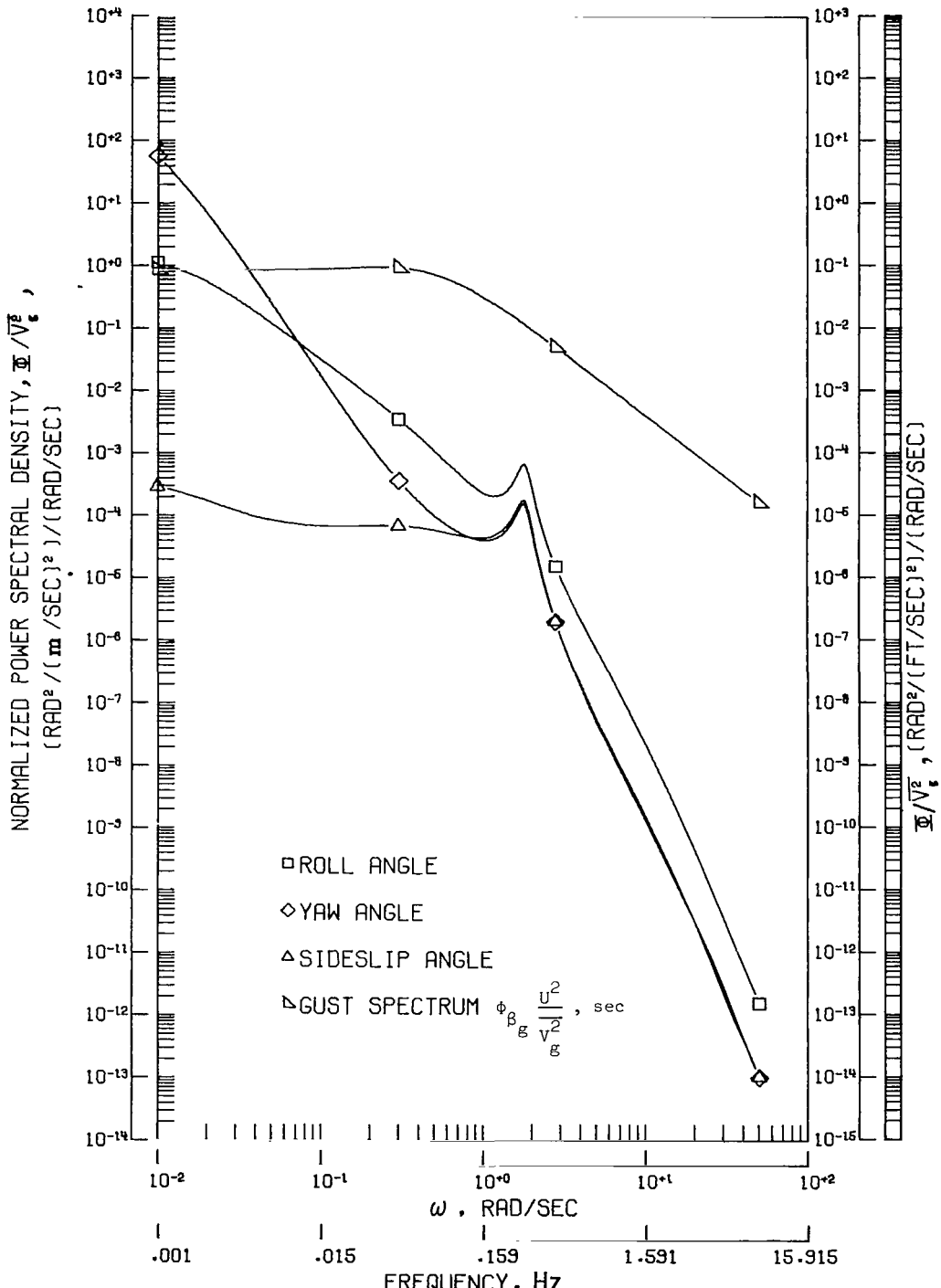


(a) Normalized power spectral density response for each lateral angular displacement.

Figure 2.- Response of airplane C-B to random gusts for assumed scale length of 335.28 m (1100 ft). Note that units for gust spectrum are different from those for response spectra.

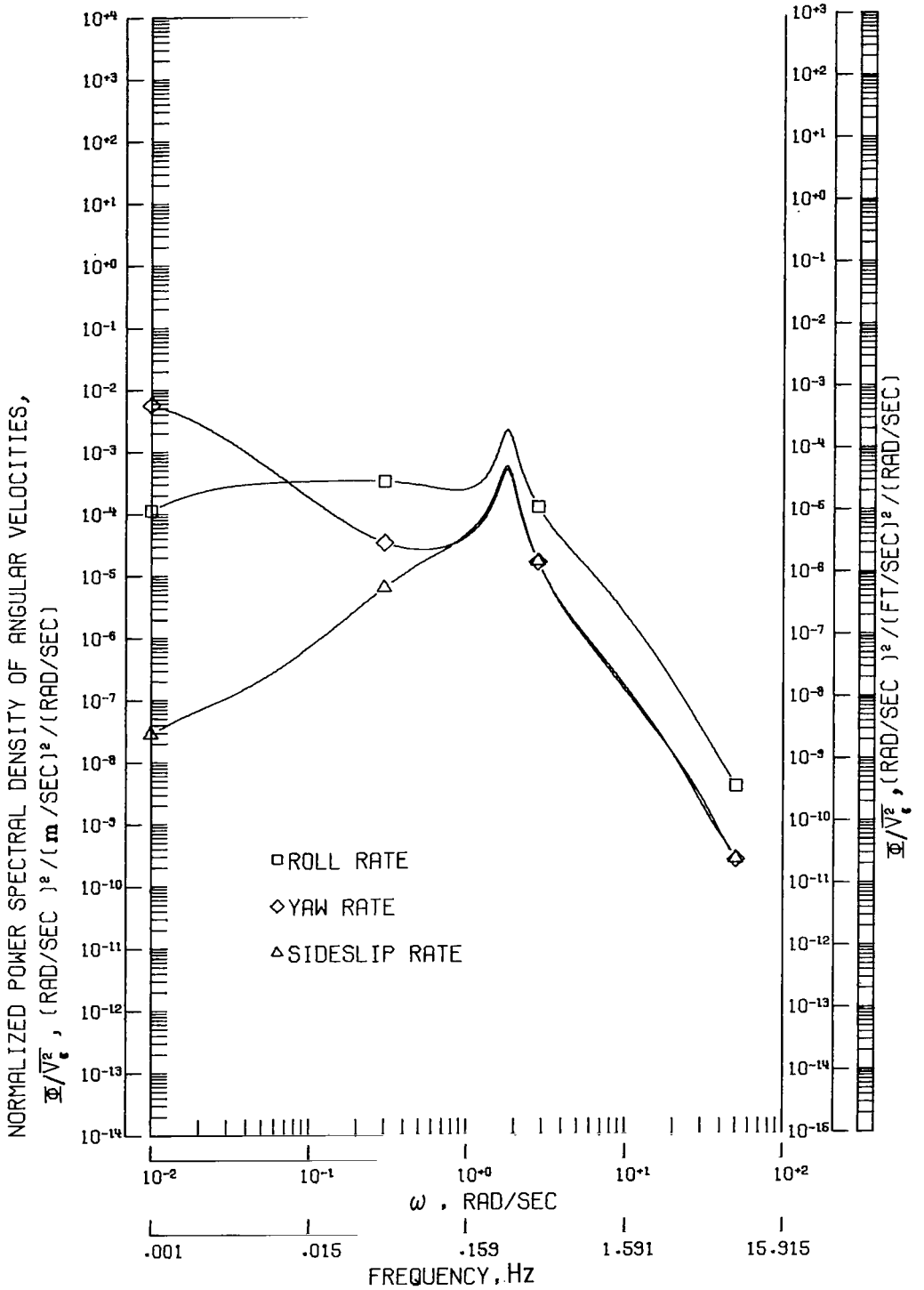


(b) Normalized power spectral density response for each lateral angular rate.

Figure 2.- Continued.

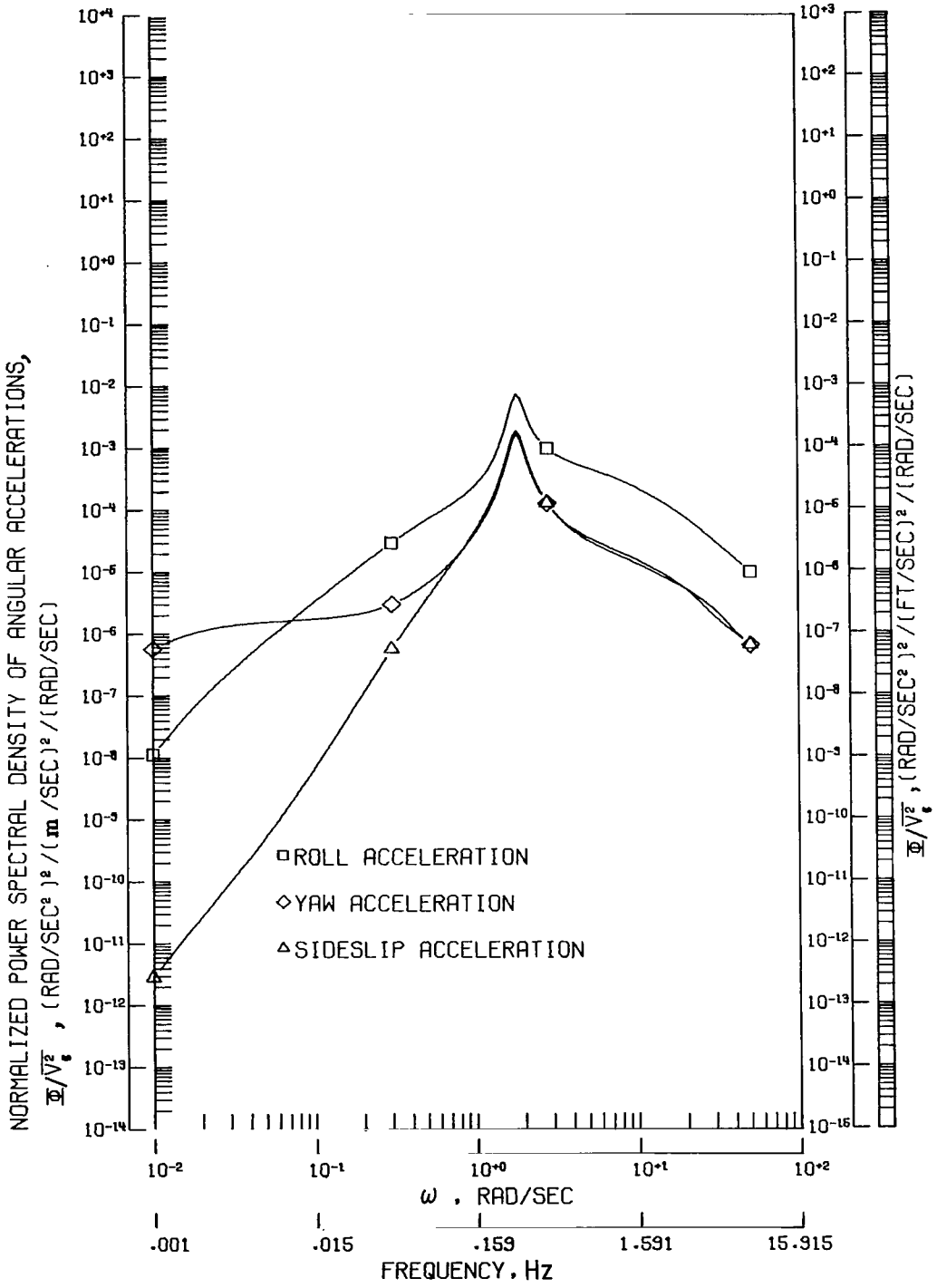


(c) Normalized power spectral density response for each lateral angular acceleration.

Figure 2.- Continued.

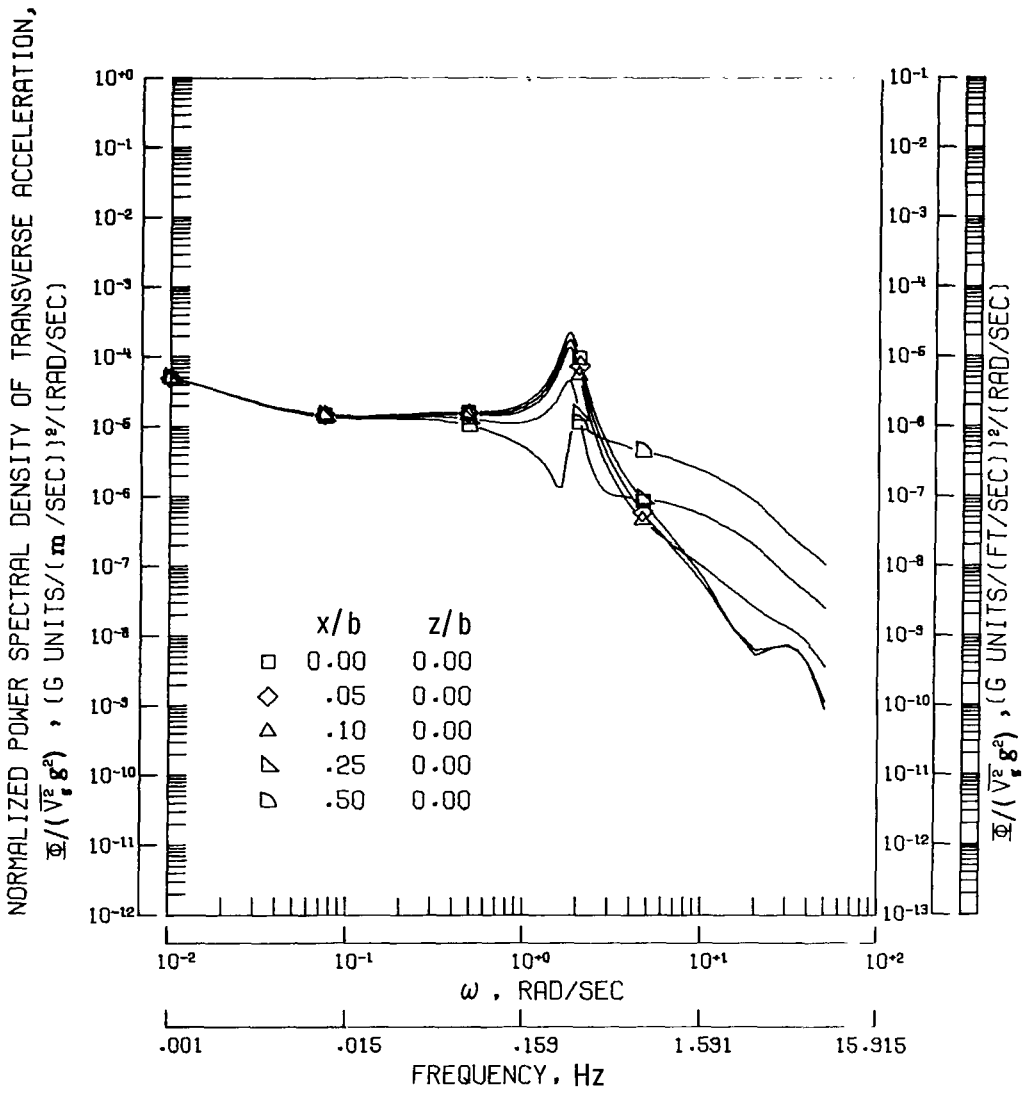


(d) Normalized power spectral density of transverse acceleration for locations forward of center of gravity.

Figure 2.- Continued.

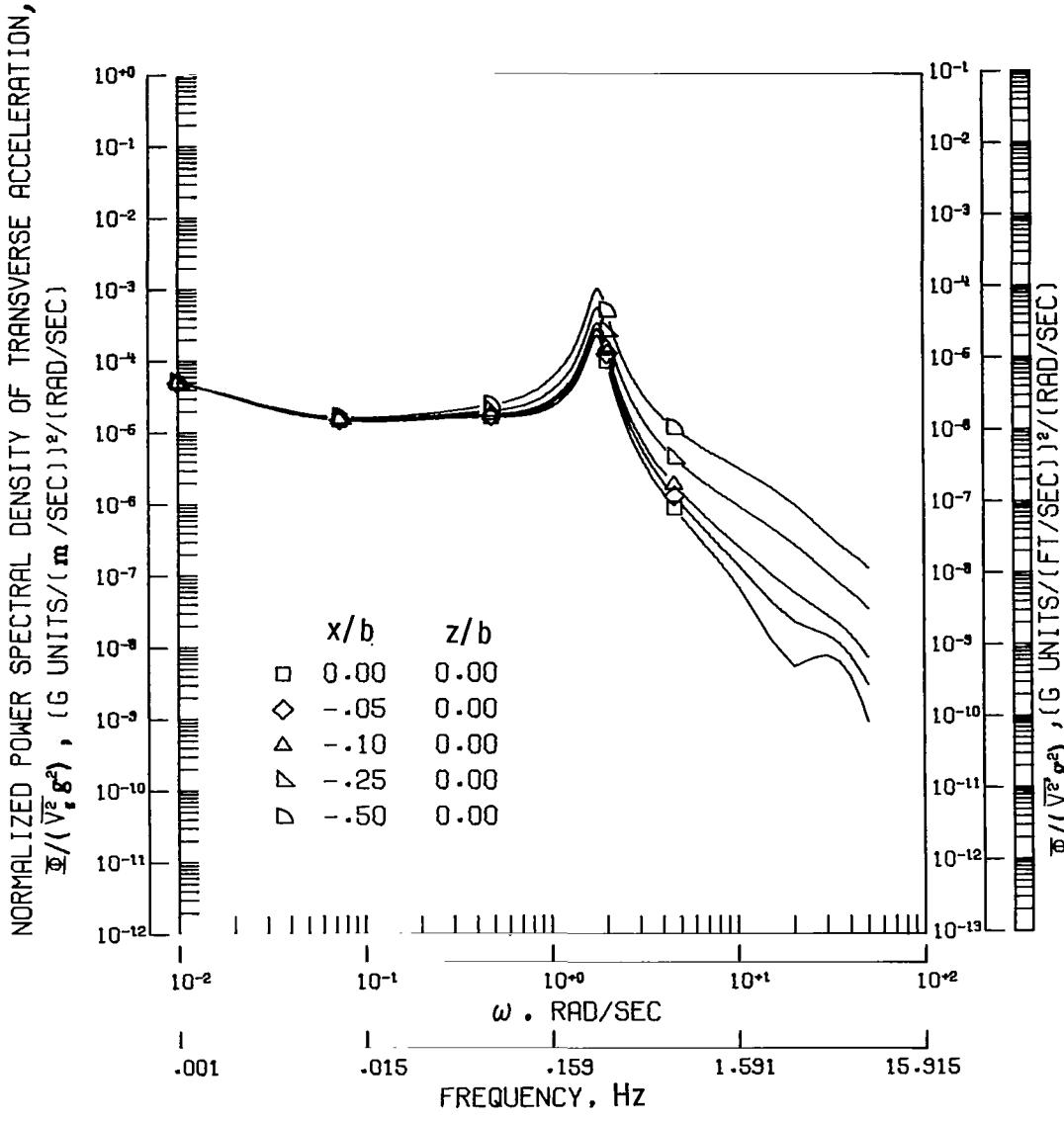


(e) Normalized power spectral density of transverse acceleration for locations rearward of center of gravity.

Figure 2.- Continued.

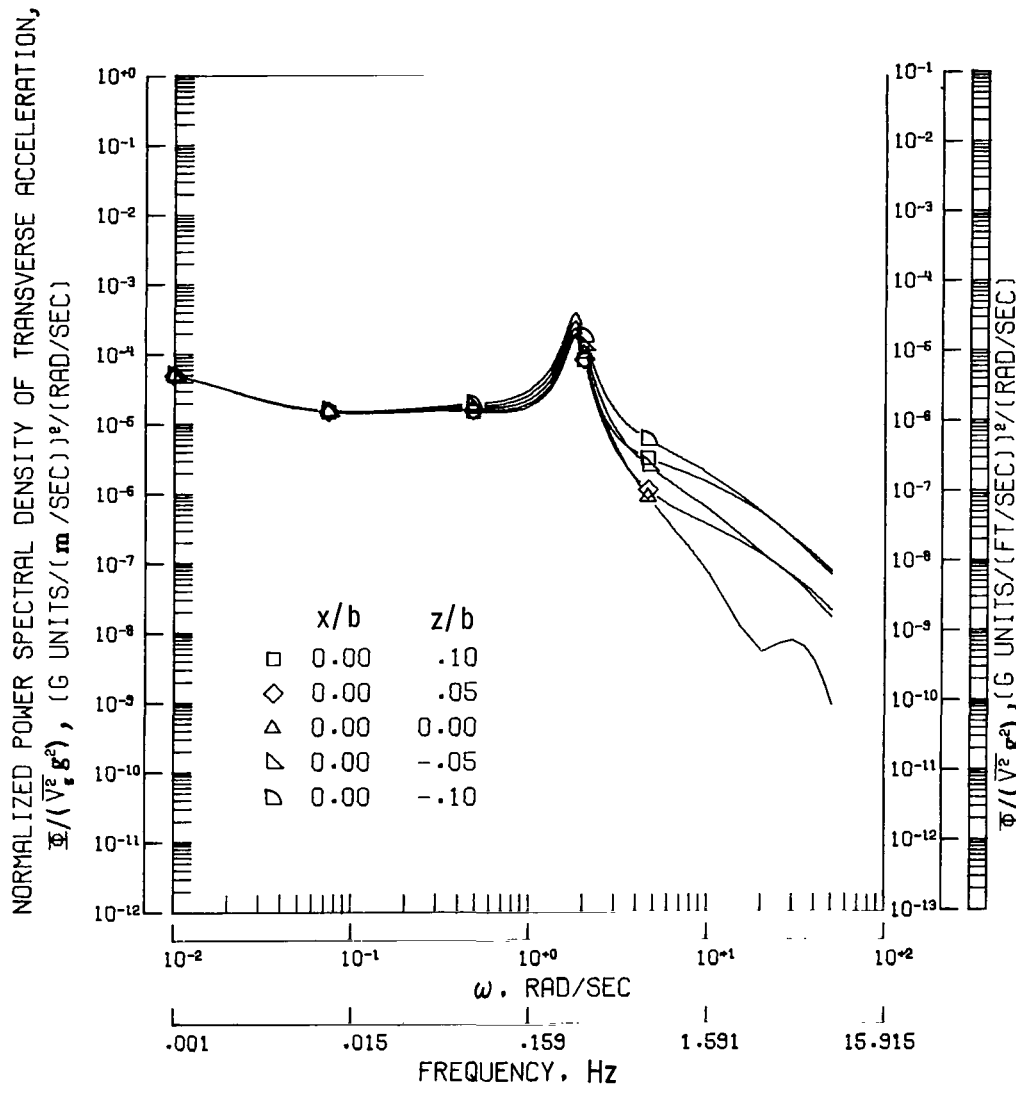


(f) Normalized power spectral density of transverse acceleration for several locations above and below center of gravity.

Figure 2.- Concluded.

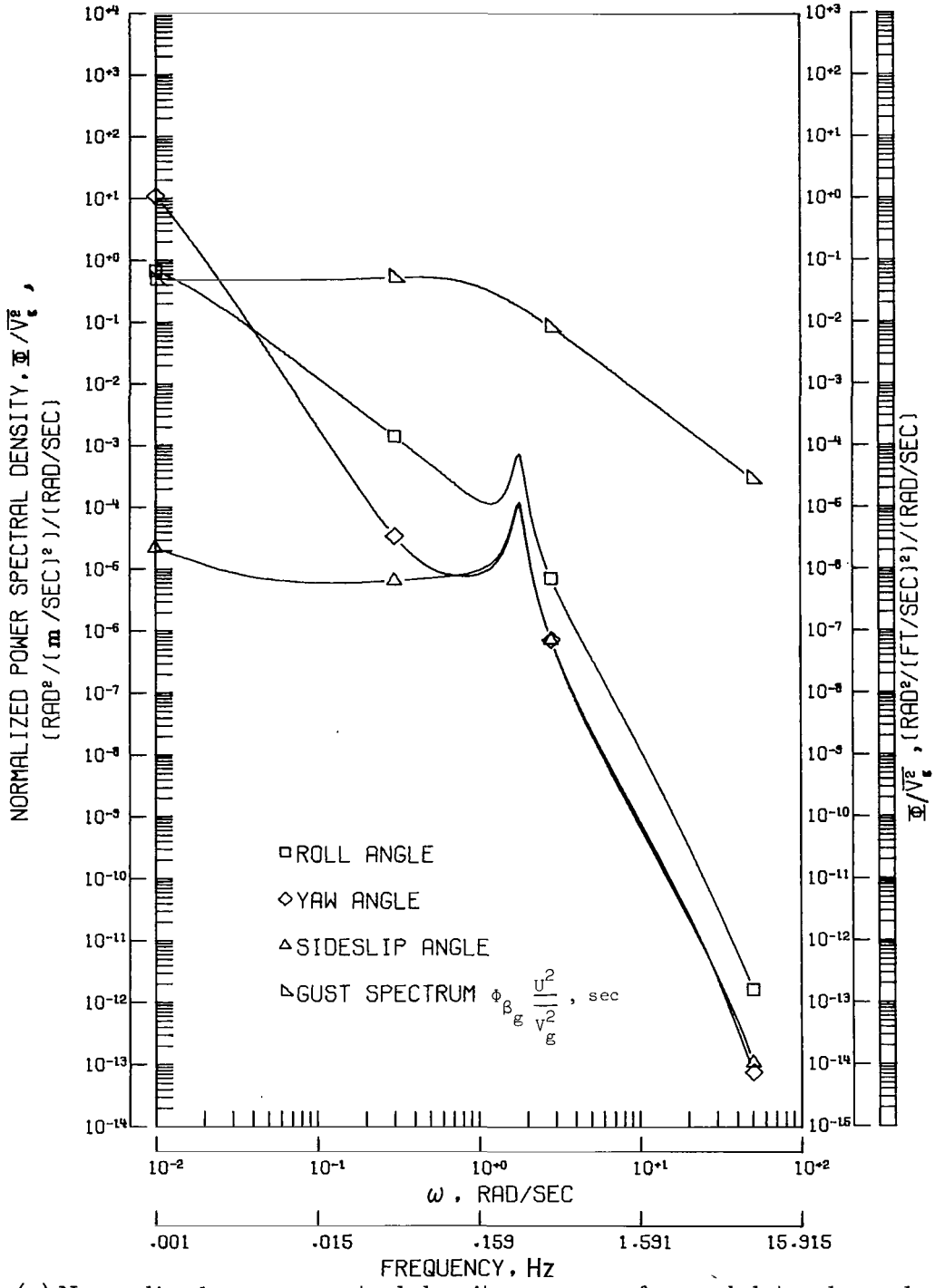


(a) Normalized power spectral density response for each lateral angular displacement.

Figure 3.- Response of airplane C-C to random gusts for assumed scale length of 335.28 m (1100 ft). Note that units for gust spectrum are different from those for response spectra.

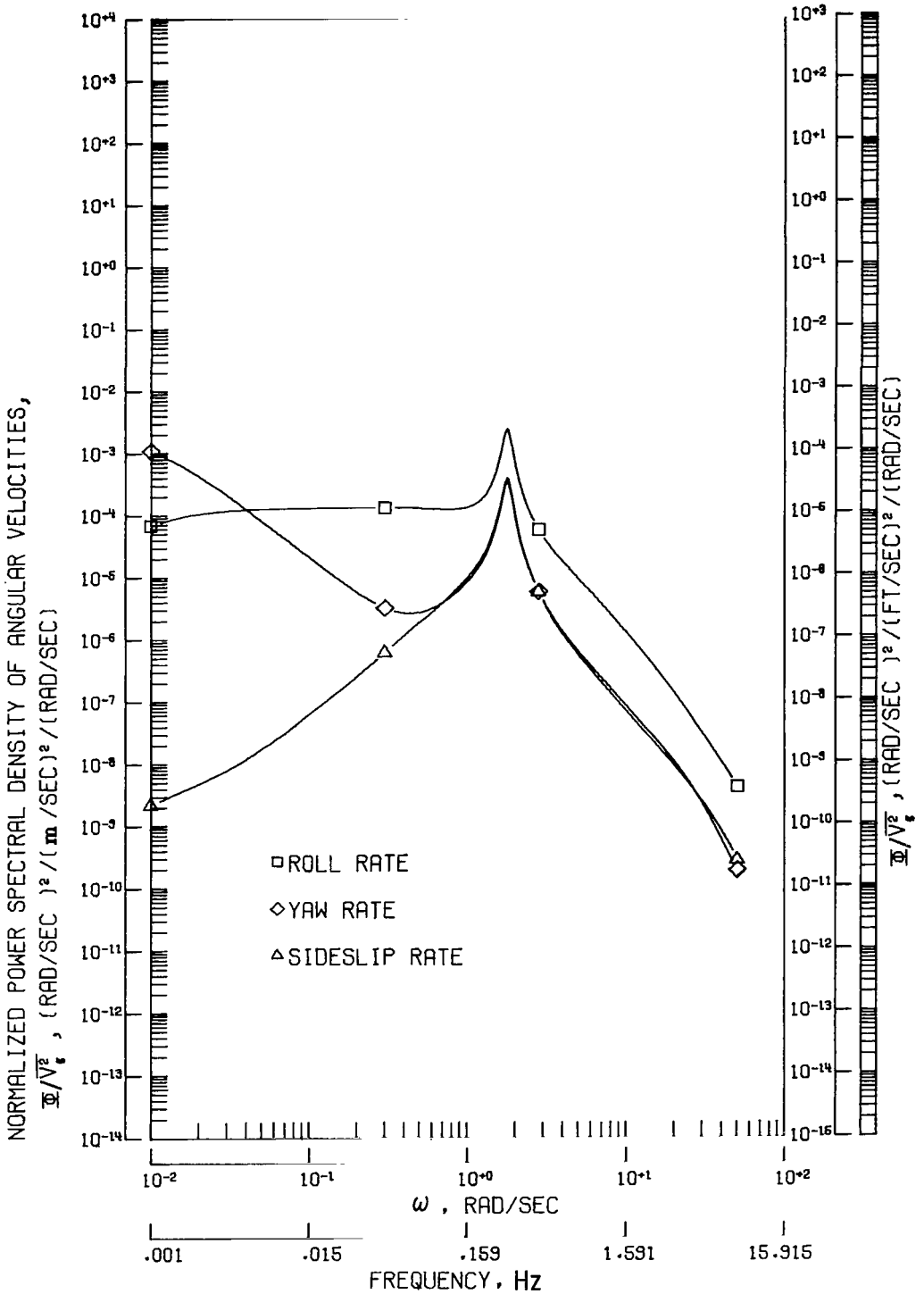


(b) Normalized power spectral density response for each lateral angular rate.

Figure 3.- Continued.

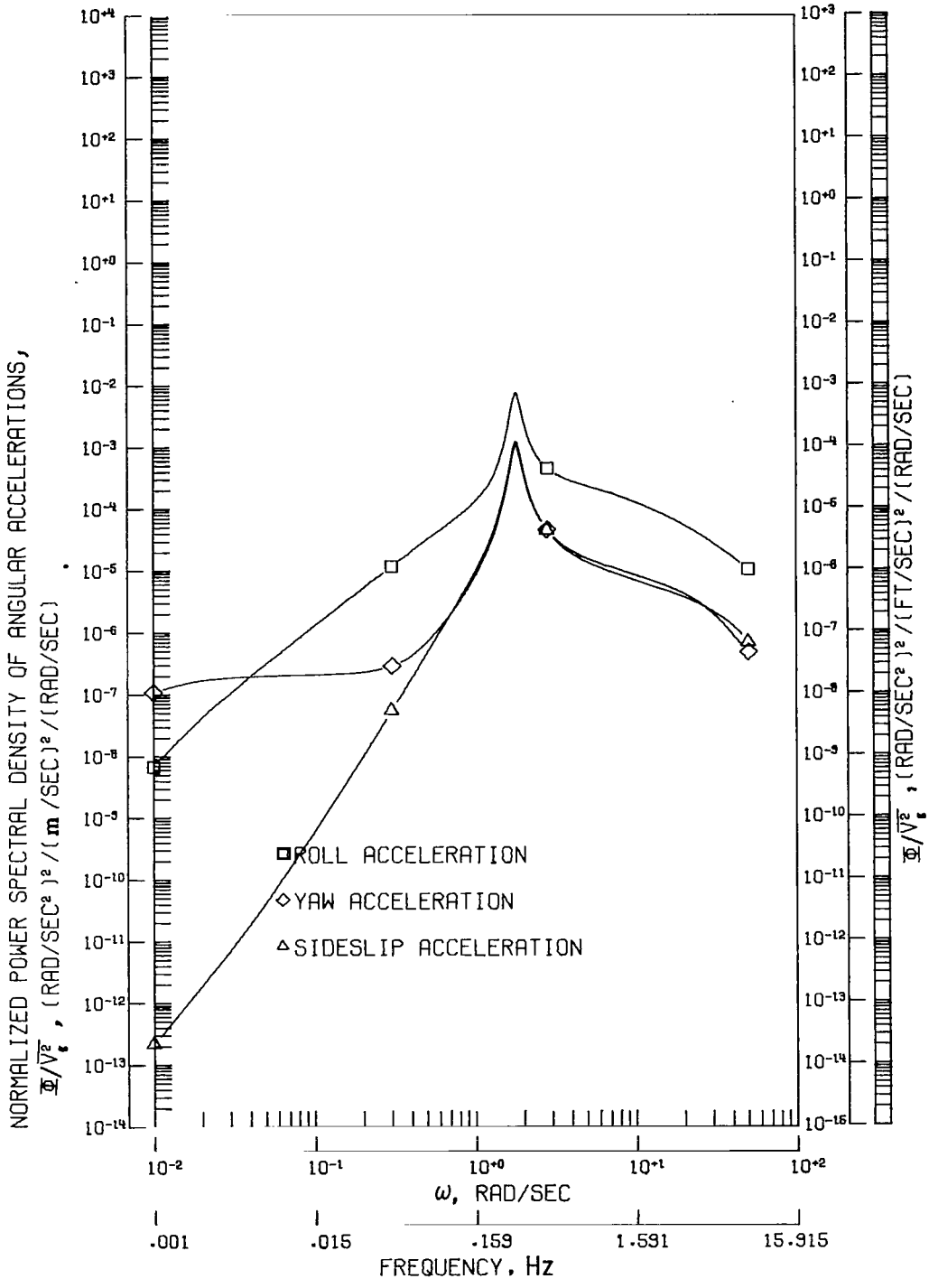


(c) Normalized power spectral density response for each lateral angular acceleration.

Figure 3.- Continued.

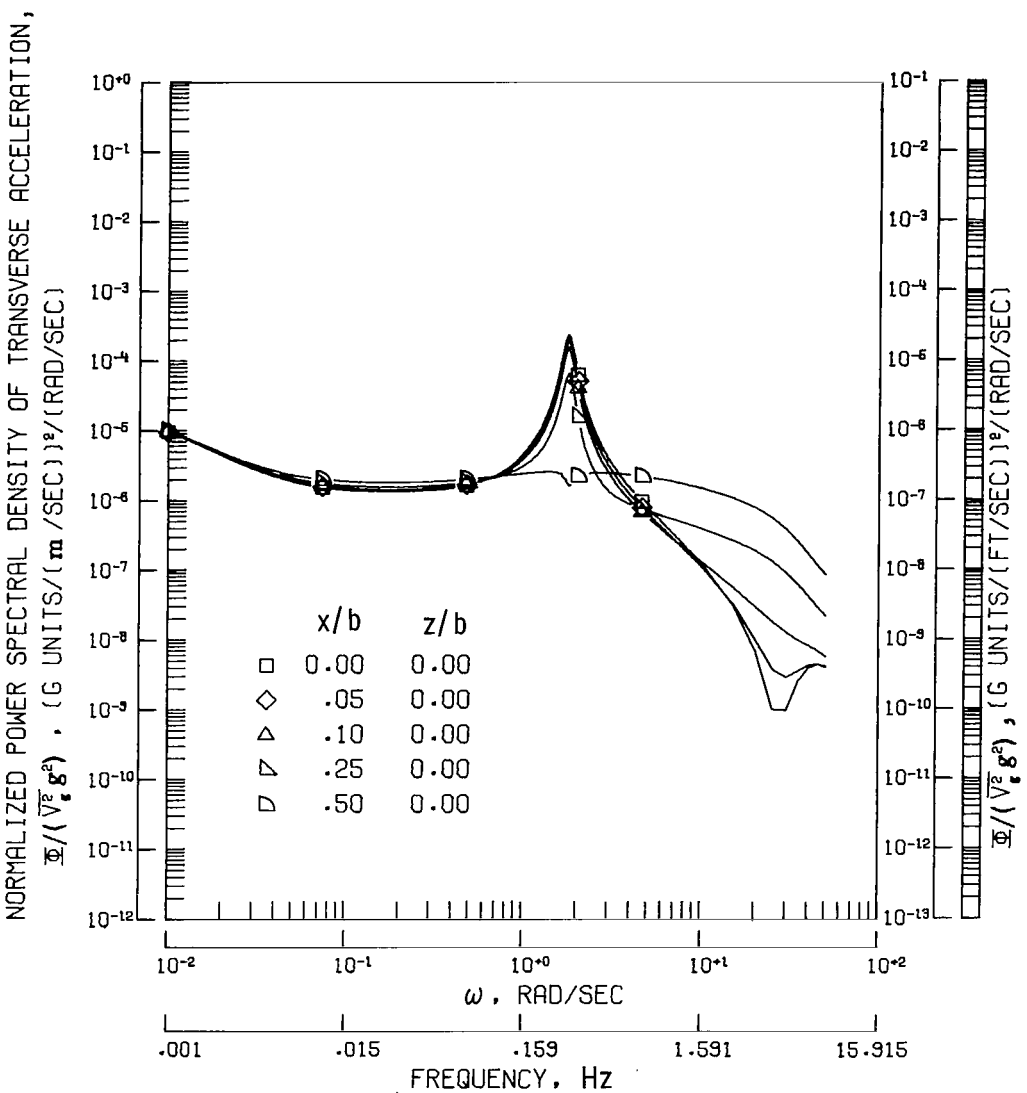


(d) Normalized power spectral density of transverse acceleration for locations forward of center of gravity.

Figure 3.- Continued.

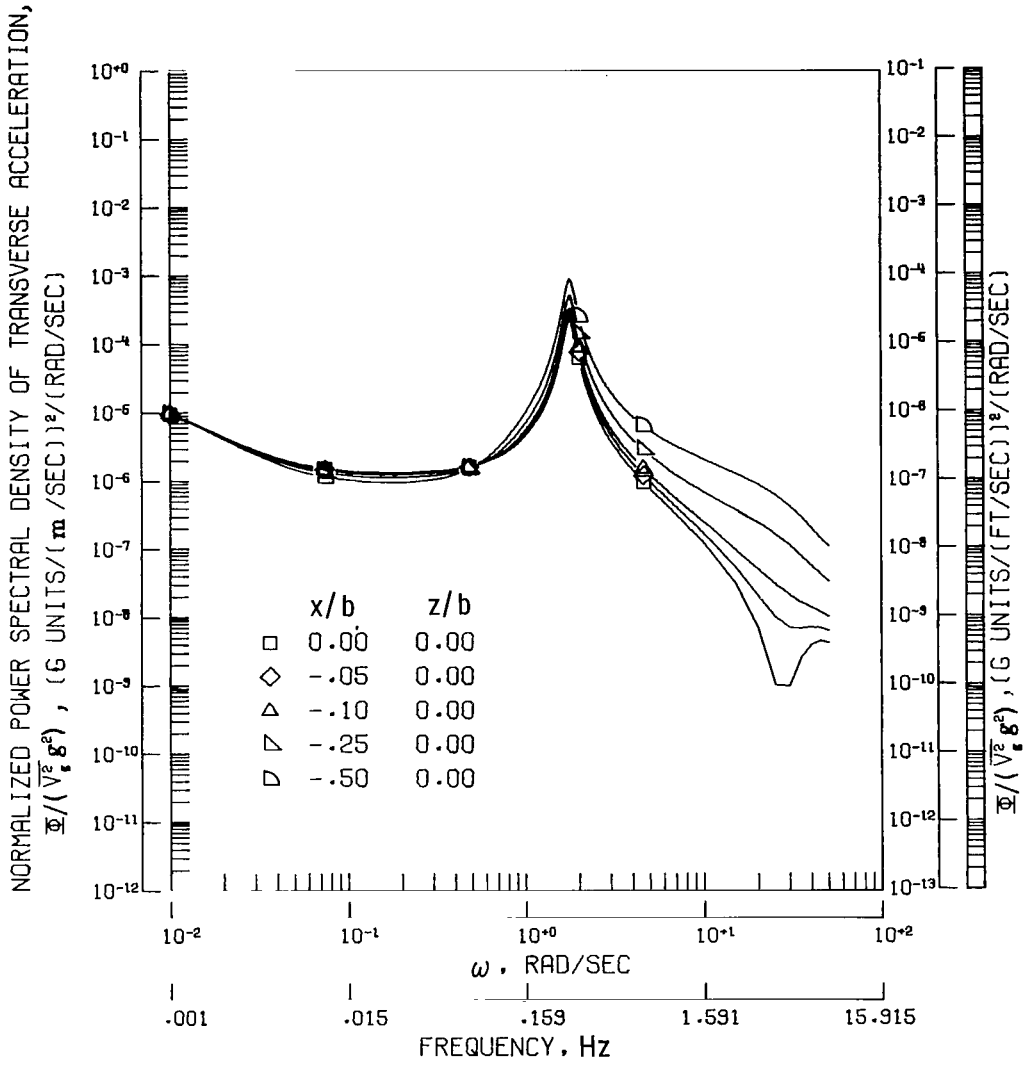


(e) Normalized power spectral density of transverse acceleration for locations rearward of center of gravity.

Figure 3.- Continued.

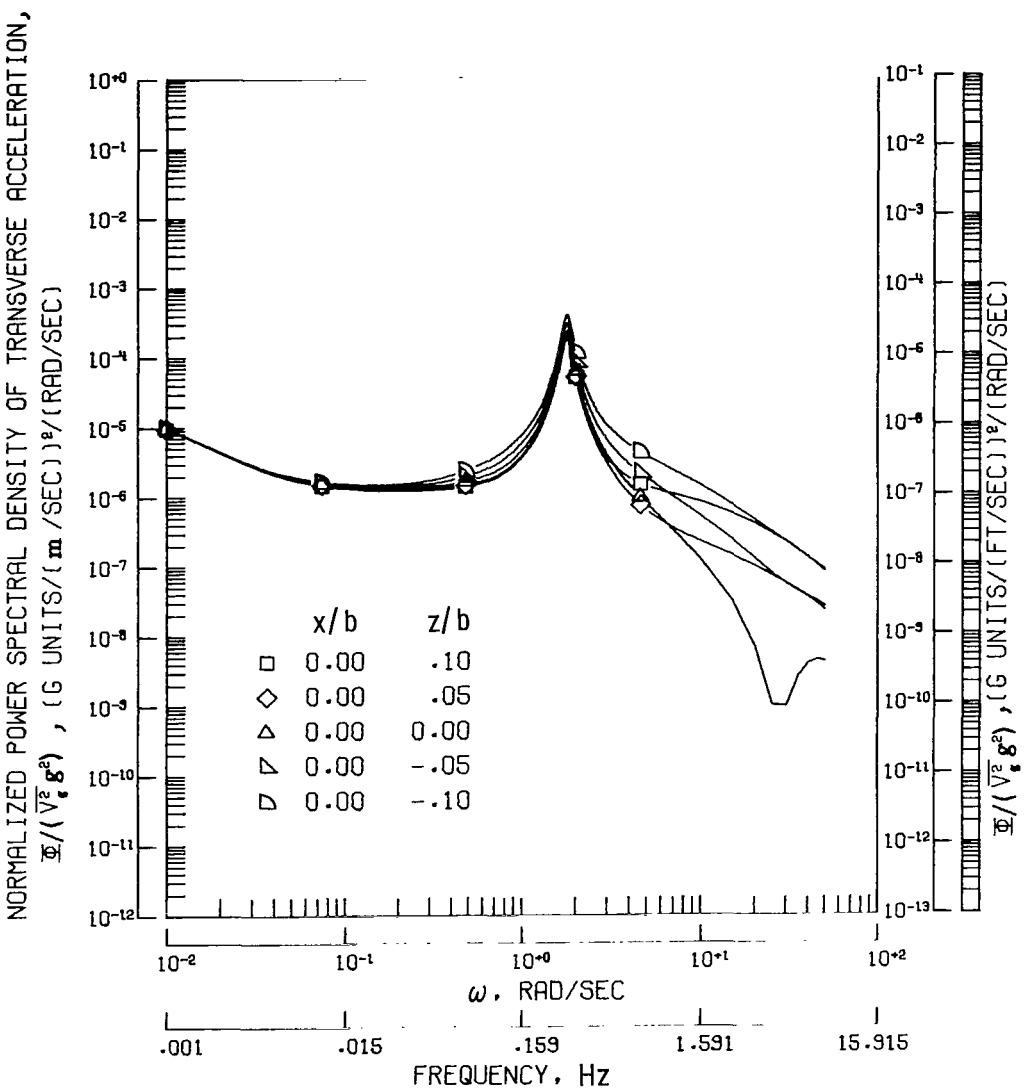


(f) Normalized power spectral density of transverse acceleration for several locations above and below center of gravity.

Figure 3.- Concluded.

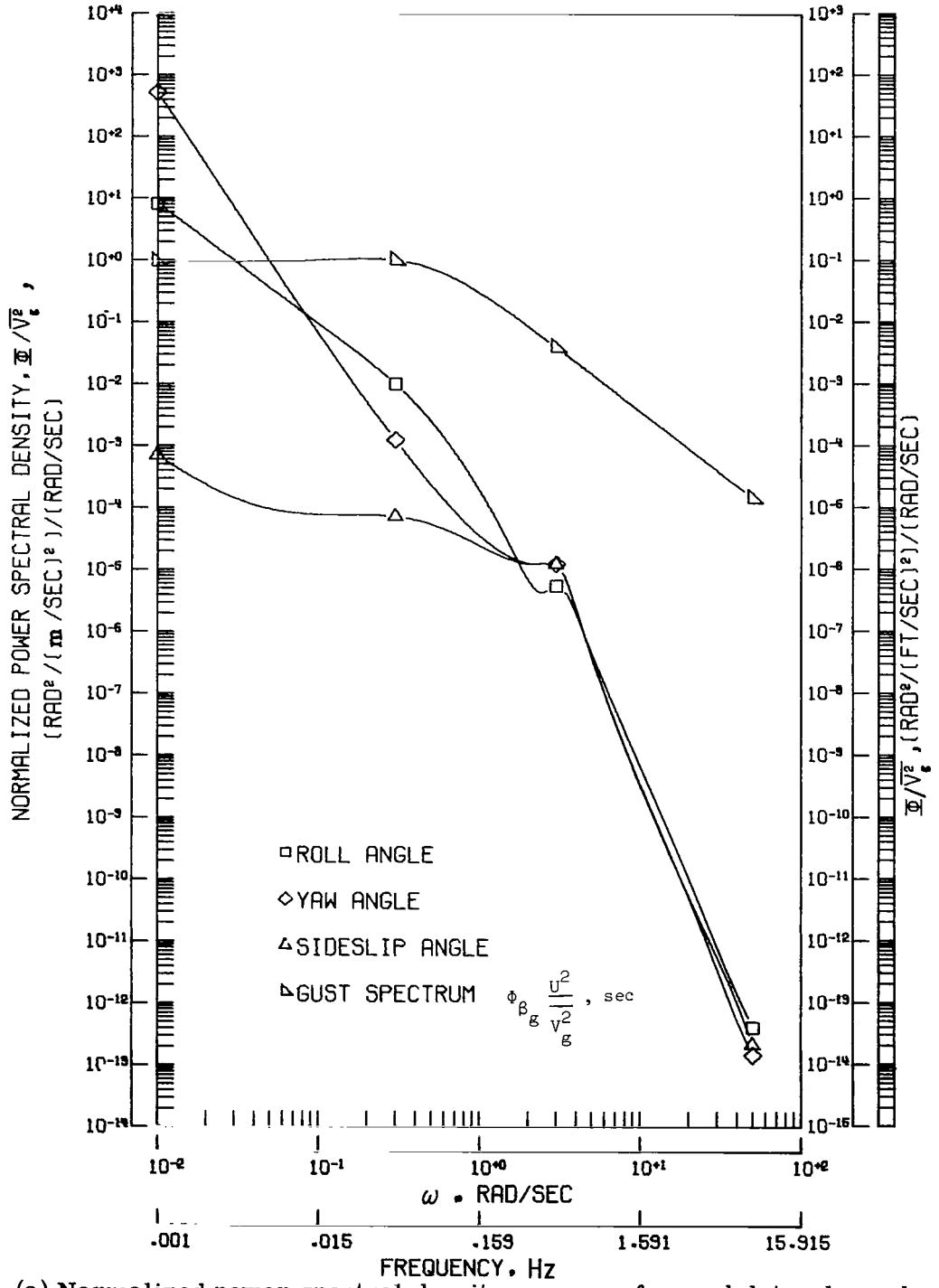


(a) Normalized power spectral density response for each lateral angular displacement.

Figure 4.- Response of airplane LS-A to random gusts for assumed scale length of 335.28 m (1100 ft). Note that units for gust spectrum are different from those for response spectra.

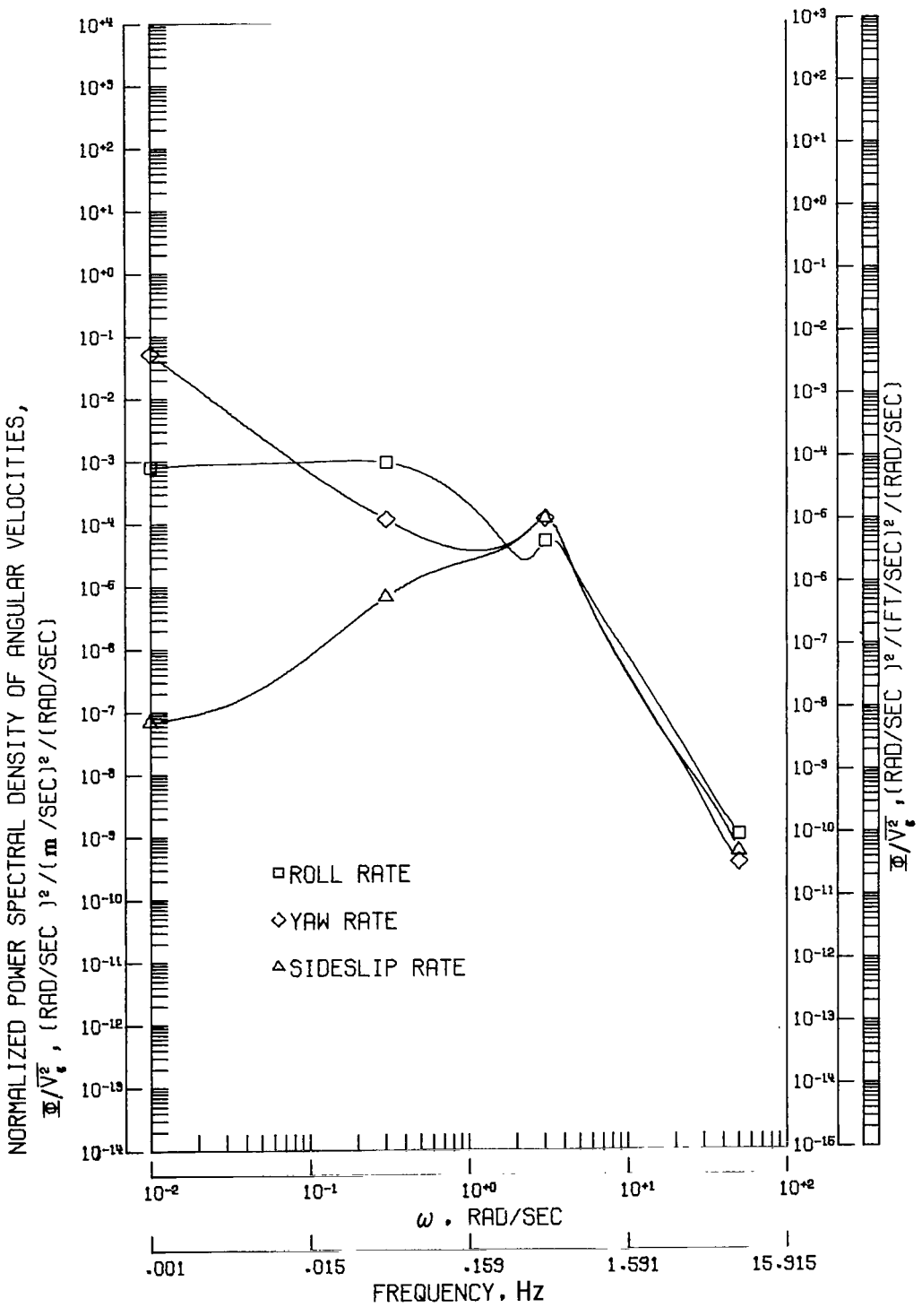


(b) Normalized power spectral density response for each lateral angular rate.

Figure 4.- Continued.

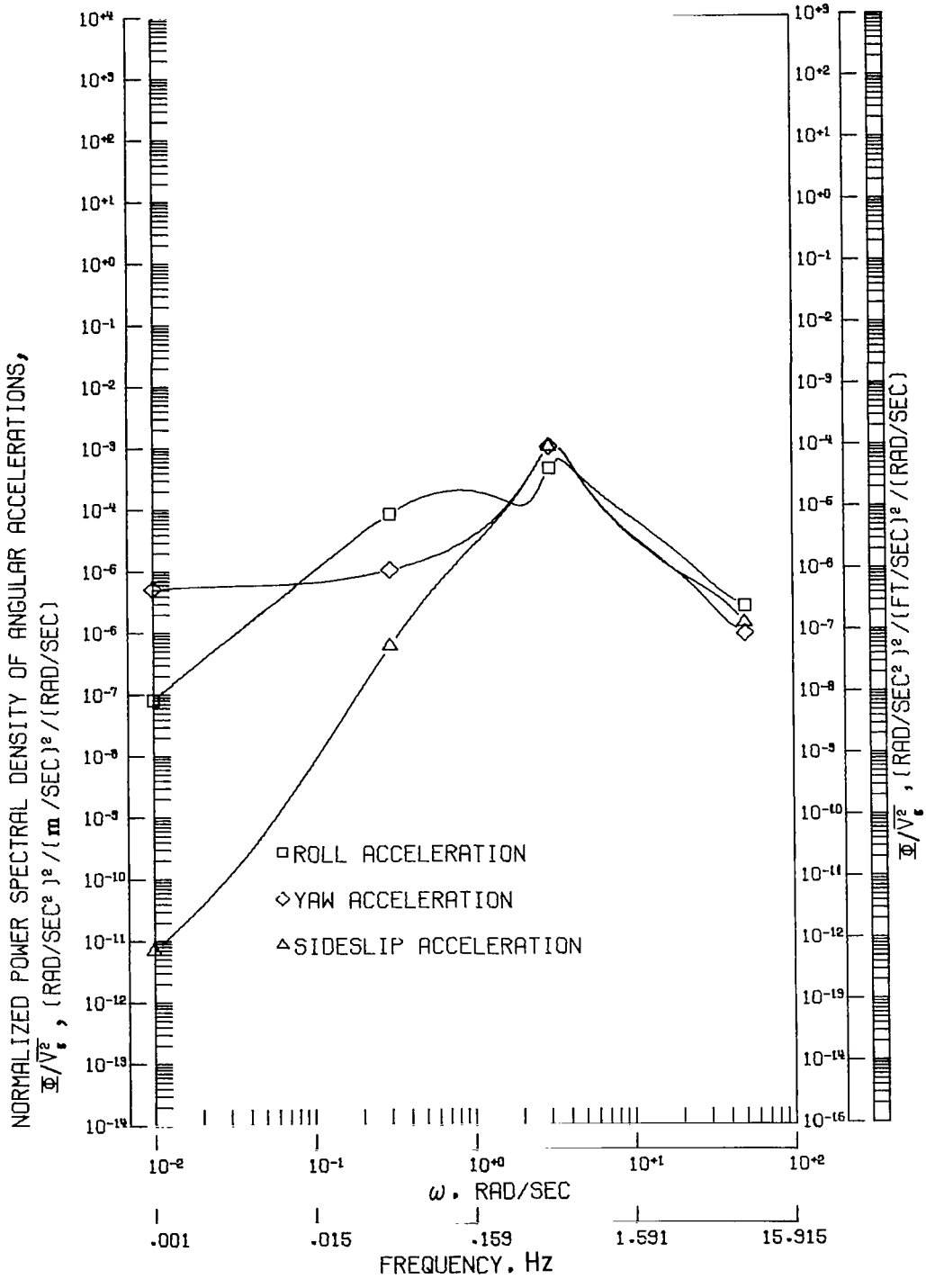


(c) Normalized power spectral density response for each lateral angular acceleration.

Figure 4.- Continued.

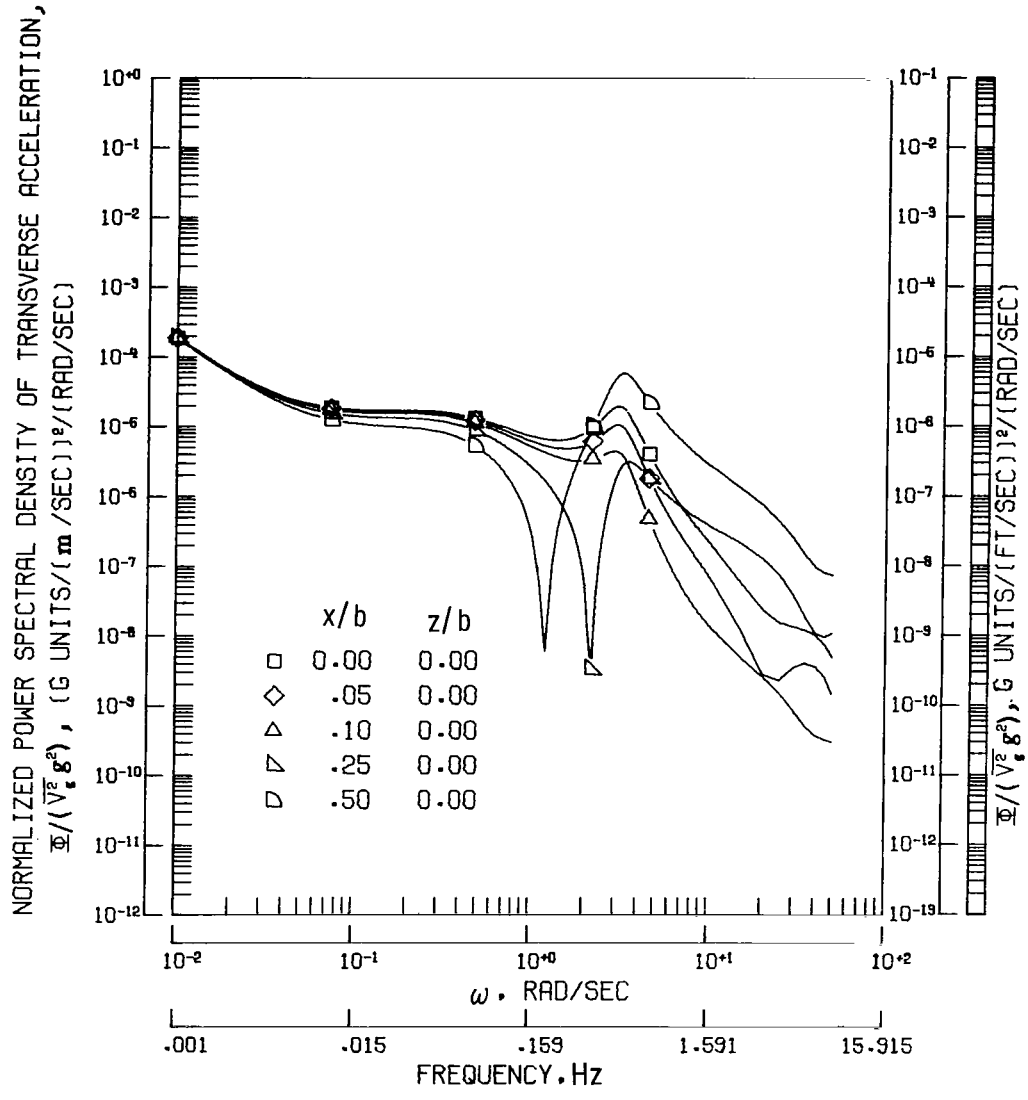


(d) Normalized power spectral density of transverse acceleration for locations forward of center of gravity.

Figure 4.- Continued.

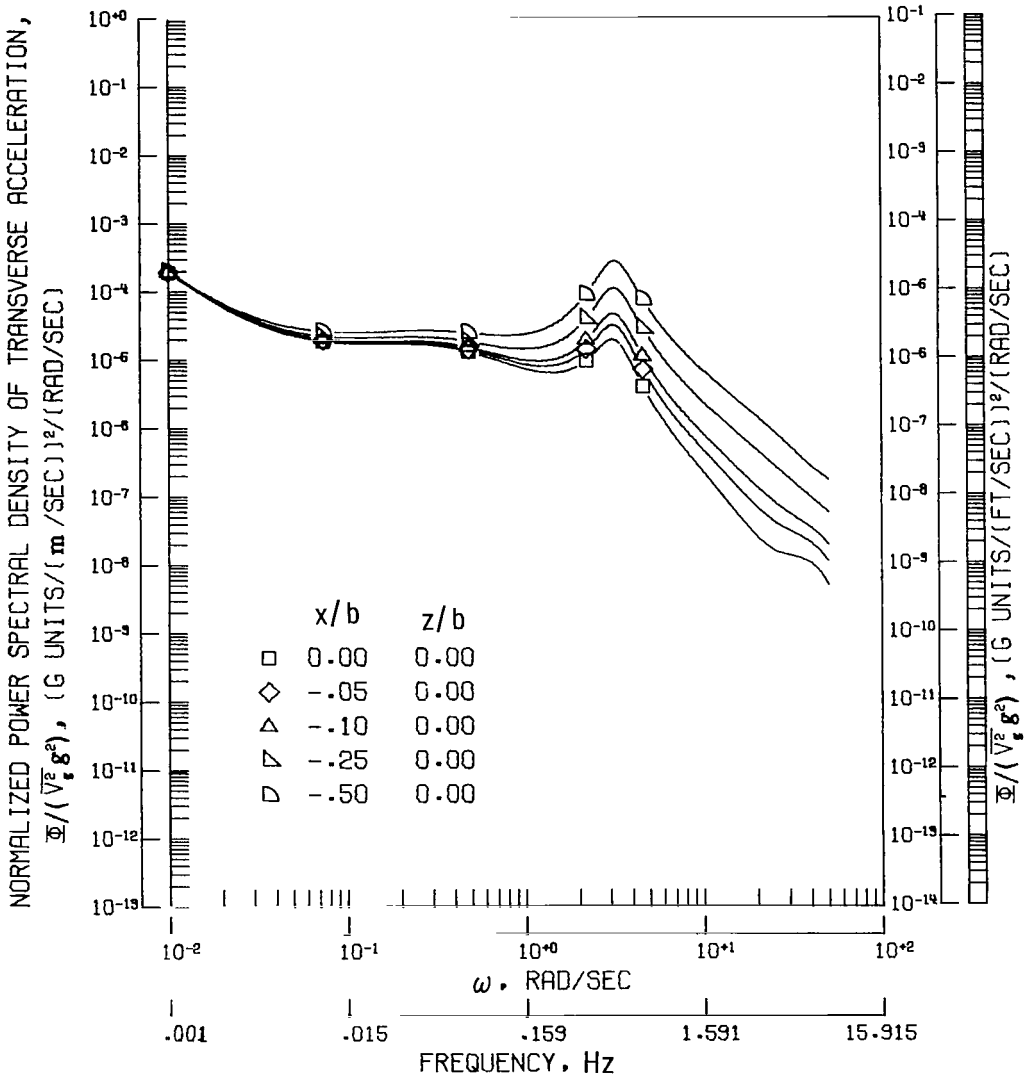


(e) Normalized power spectral density of transverse acceleration for locations rearward of center of gravity.

Figure 4.- Continued.

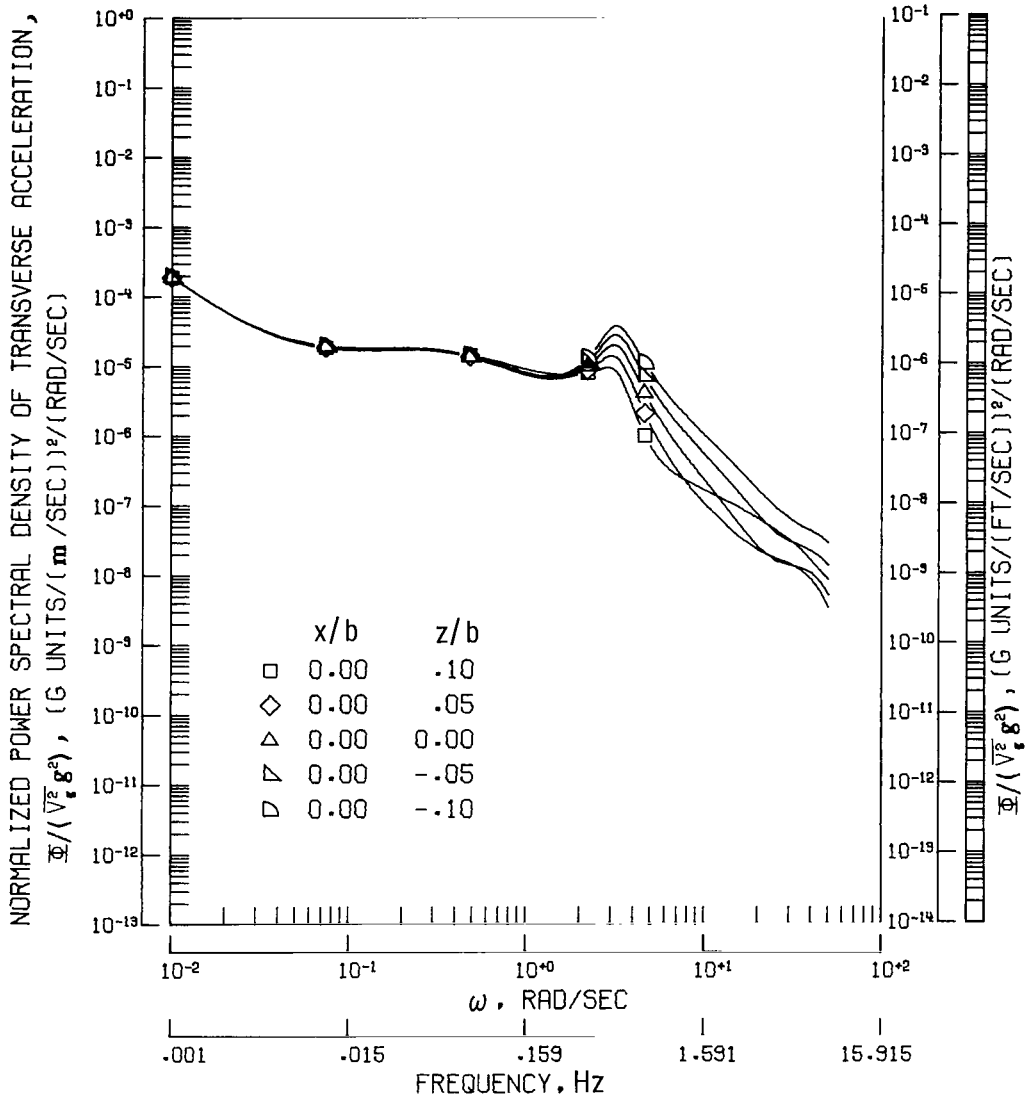


(f) Normalized power spectral density of transverse acceleration for several locations above and below center of gravity.

Figure 4.- Concluded.

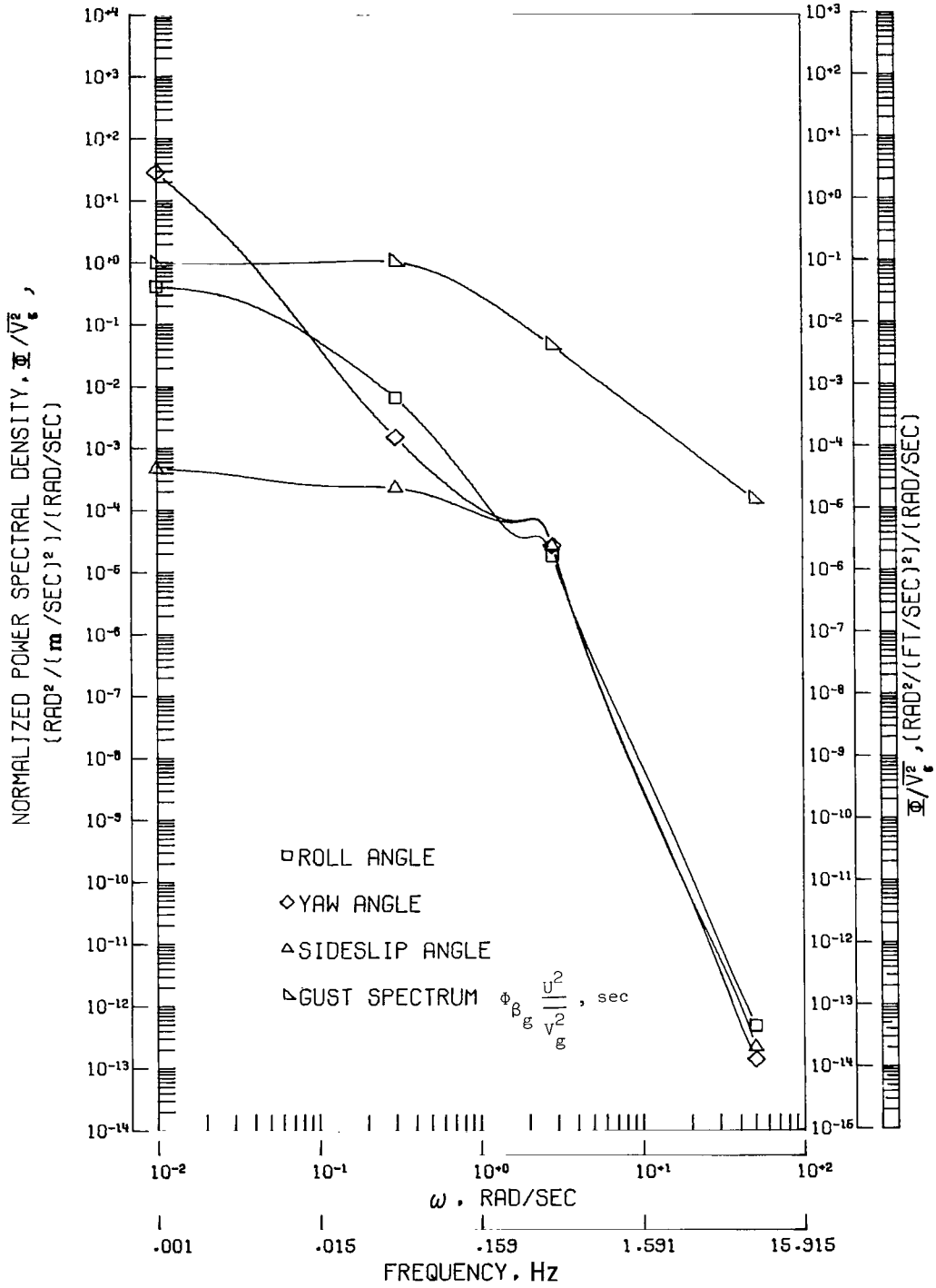


(a) Normalized power spectral density response for each lateral angular displacement.

Figure 5.- Response of airplane LS-B to random gusts for assumed scale length of 335.28 m (1100 ft). Note that units for gust spectrum are different from those for response spectra.

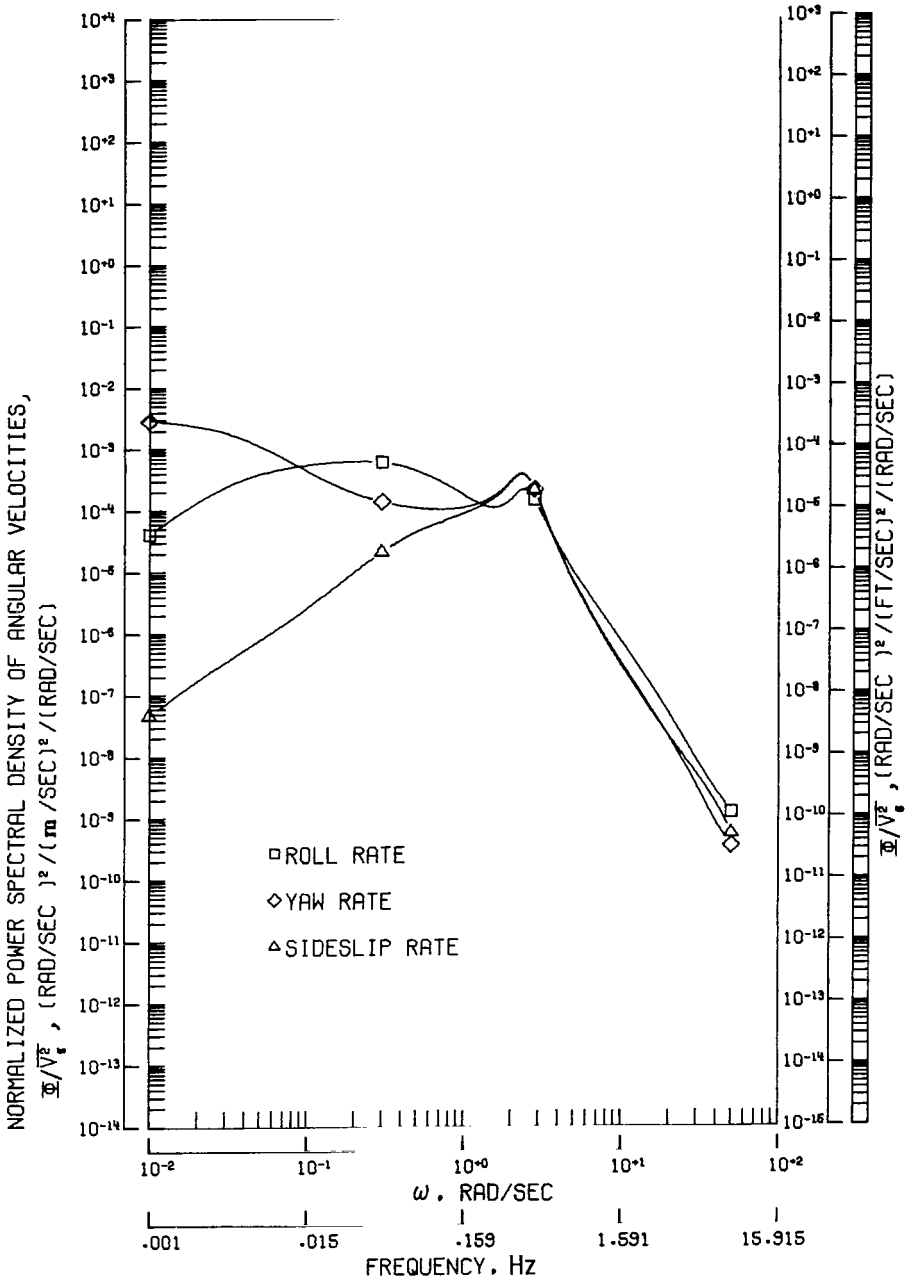


(b) Normalized power spectral density response for each lateral angular rate.

Figure 5.- Continued.

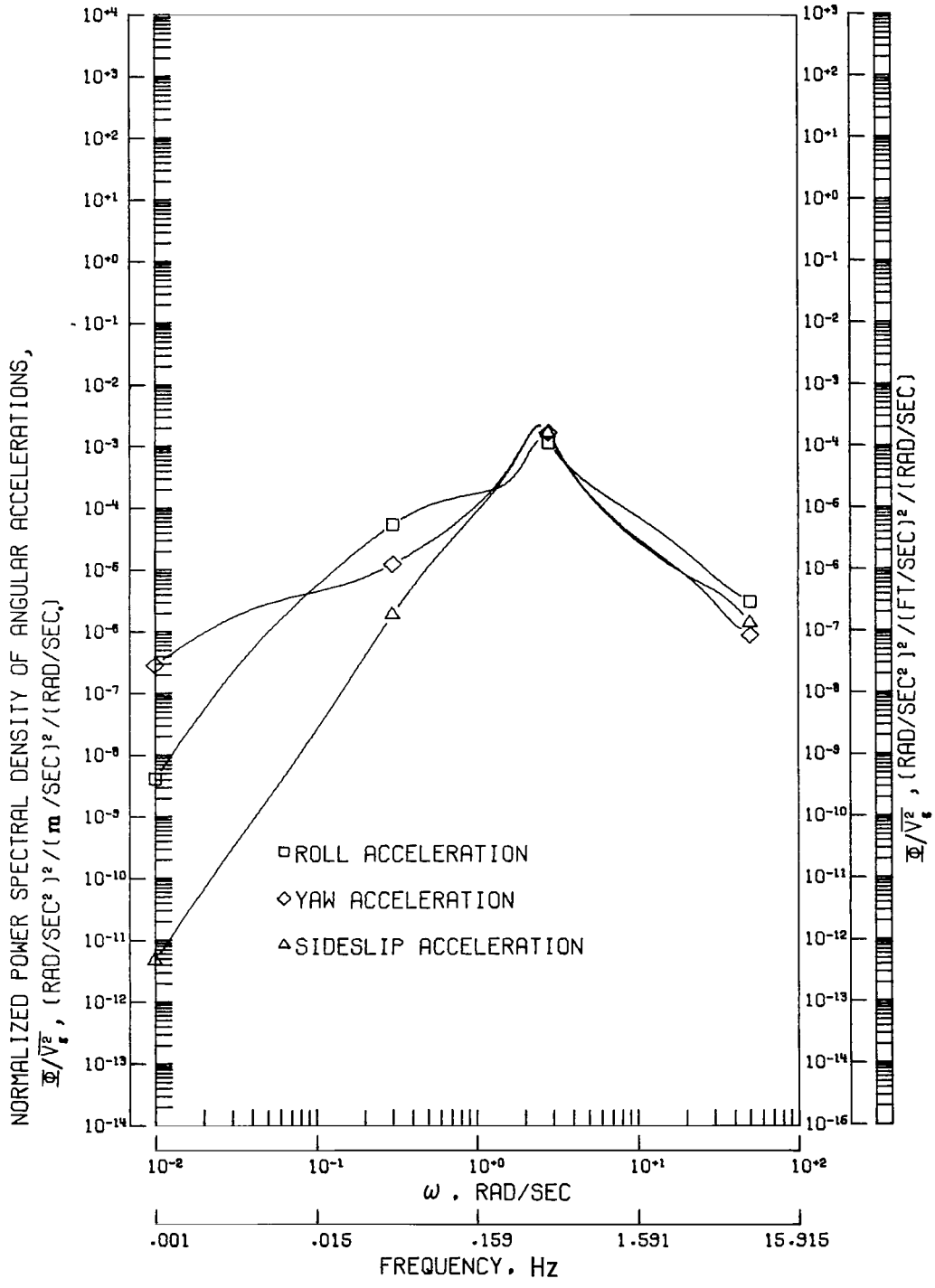


(c) Normalized power spectral density response for each lateral angular acceleration.

Figure 5.- Continued.

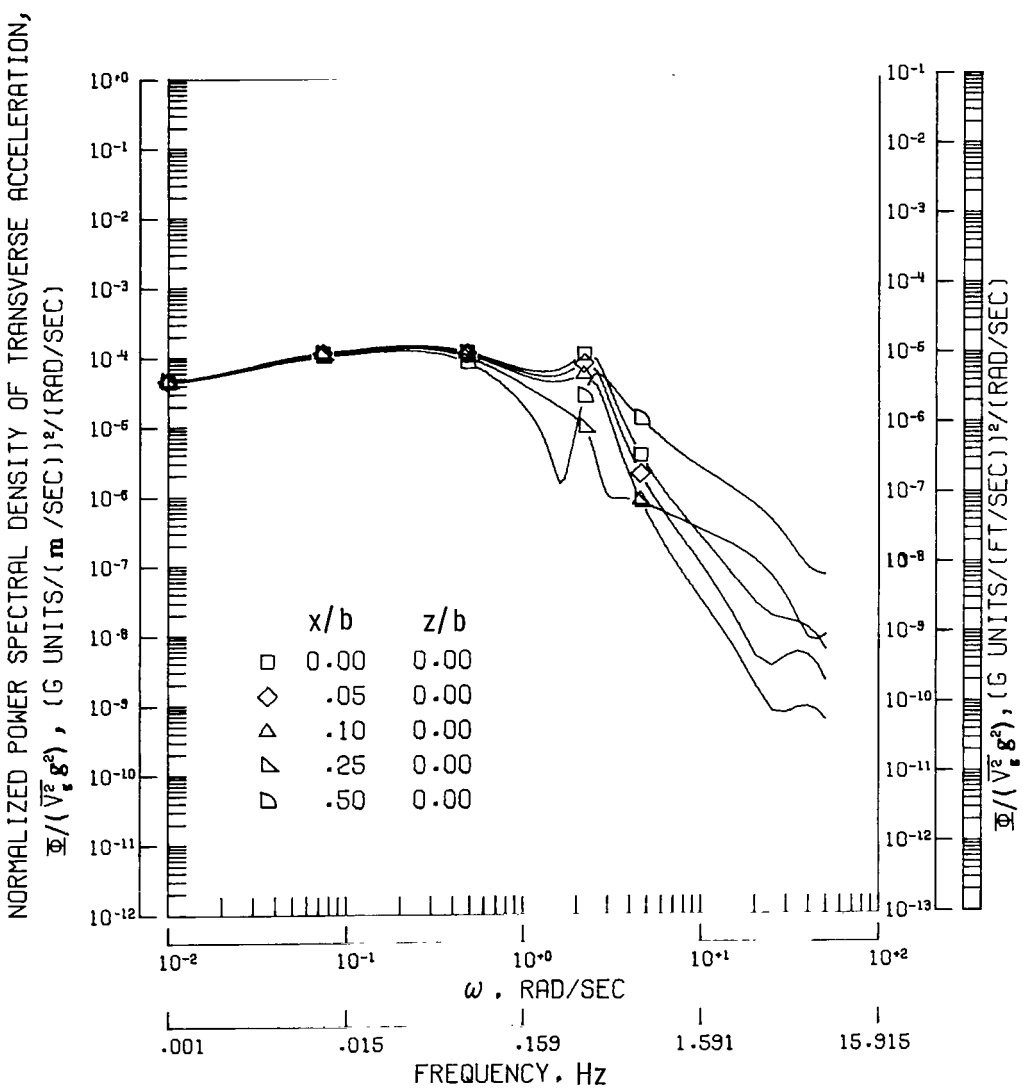


(d) Normalized power spectral density of transverse acceleration for locations forward of center of gravity.

Figure 5.- Continued.

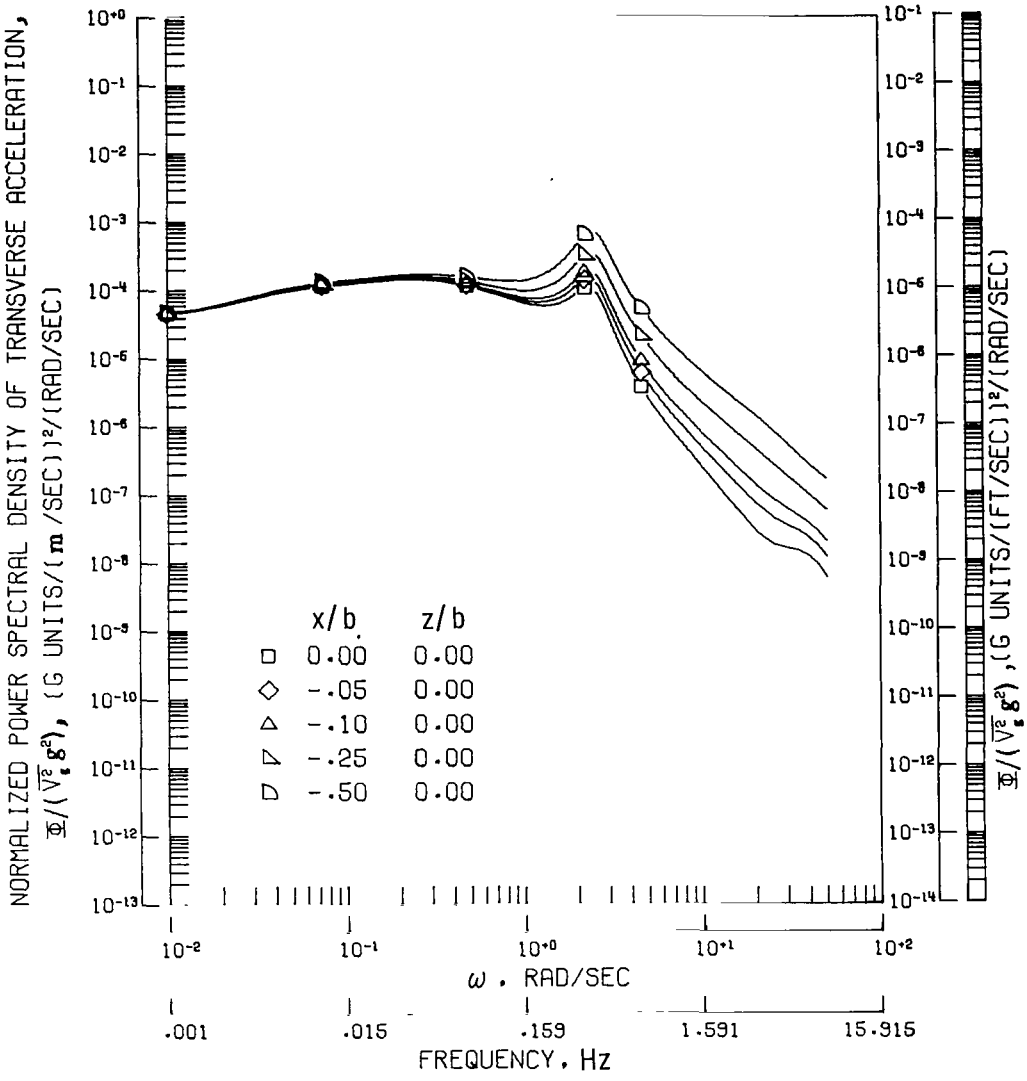


(e) Normalized power spectral density of transverse acceleration for locations rearward of center of gravity.

Figure 5.- Continued.

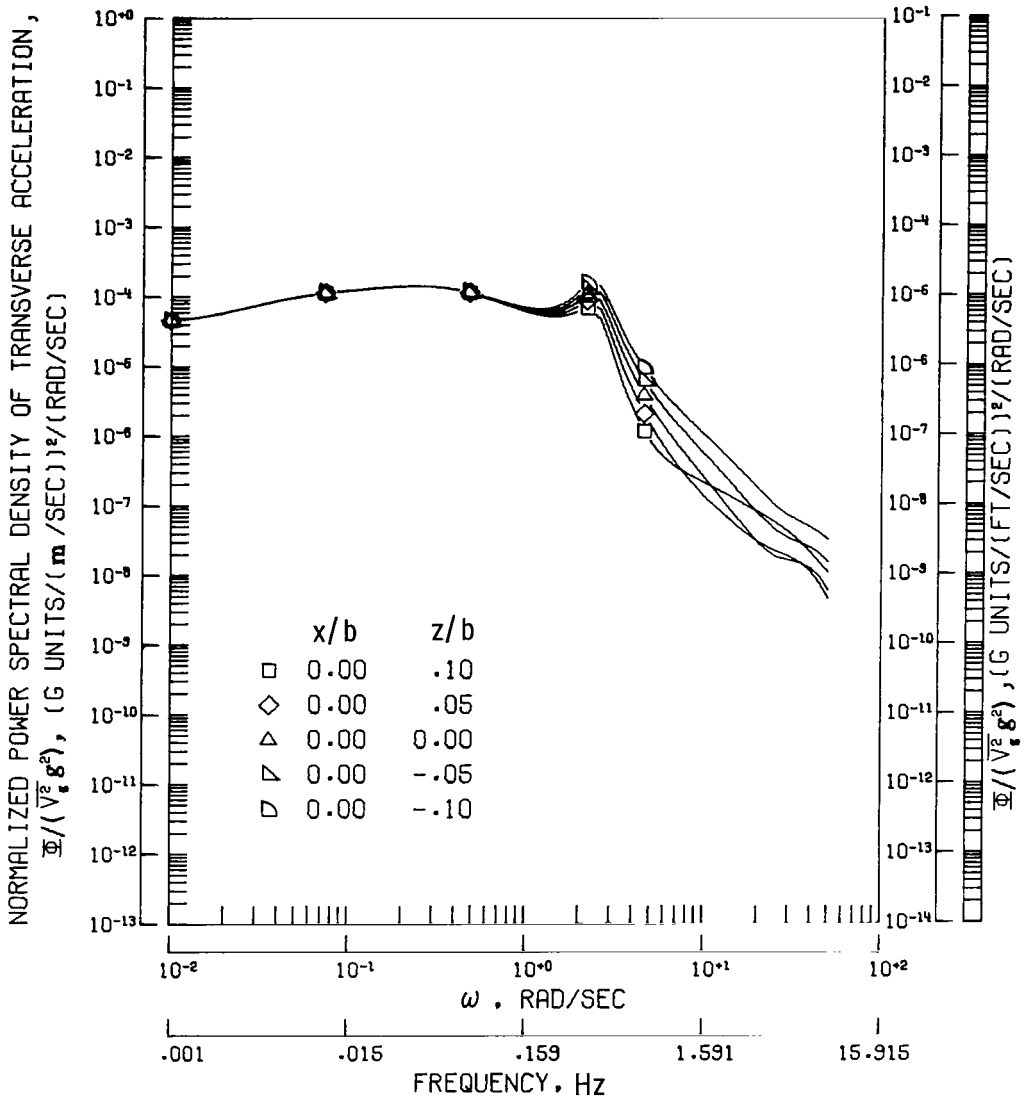


(f) Normalized power spectral density of transverse acceleration for several locations above and below center of gravity.

Figure 5.- Concluded.

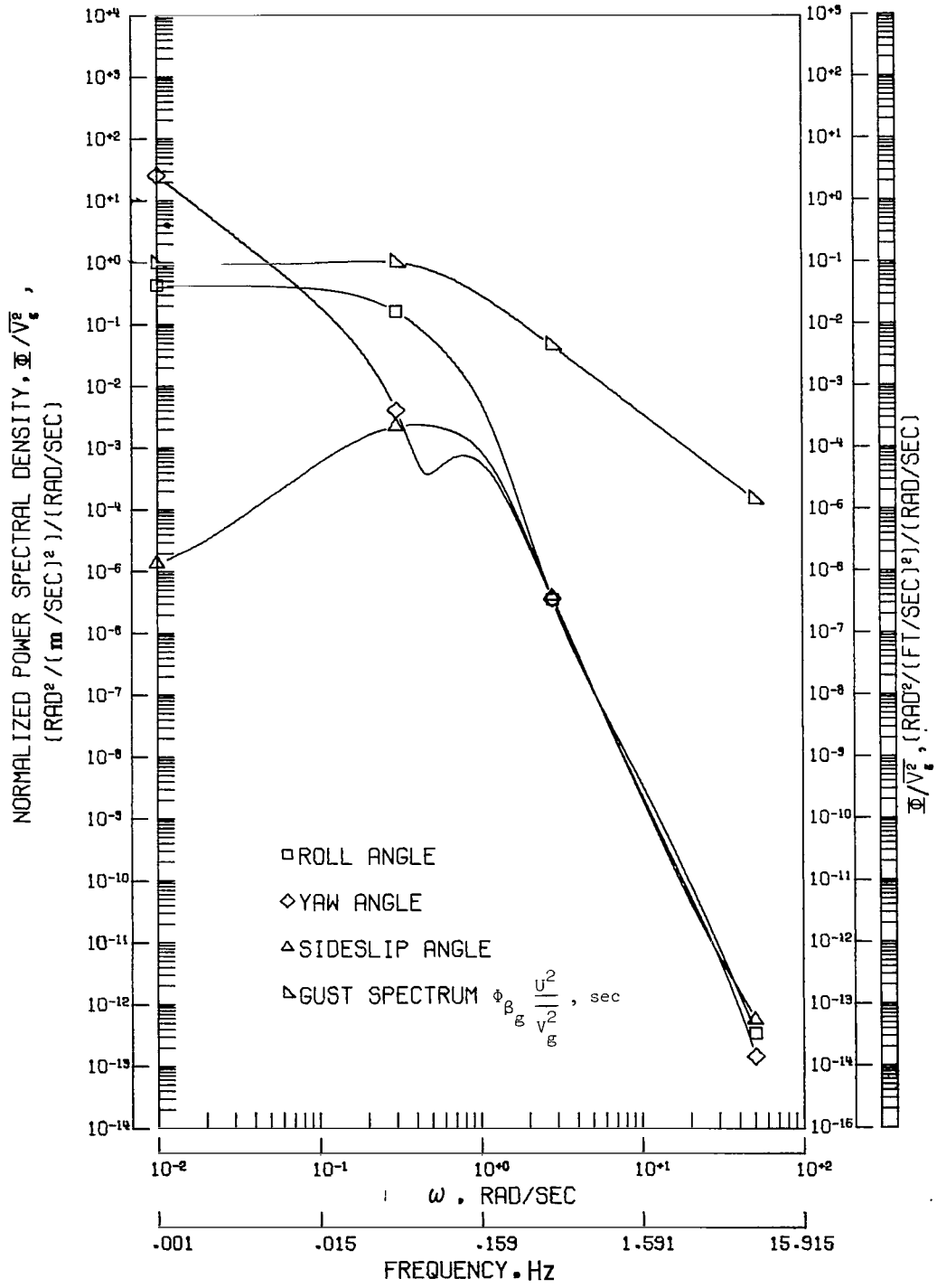


(a) Normalized power spectral density response for each lateral angular displacement.

Figure 6.- Response of airplane LS-C to random gusts for assumed scale length of 335.28 m (1100 ft). Note that units for gust spectrum are different from those for response spectra.

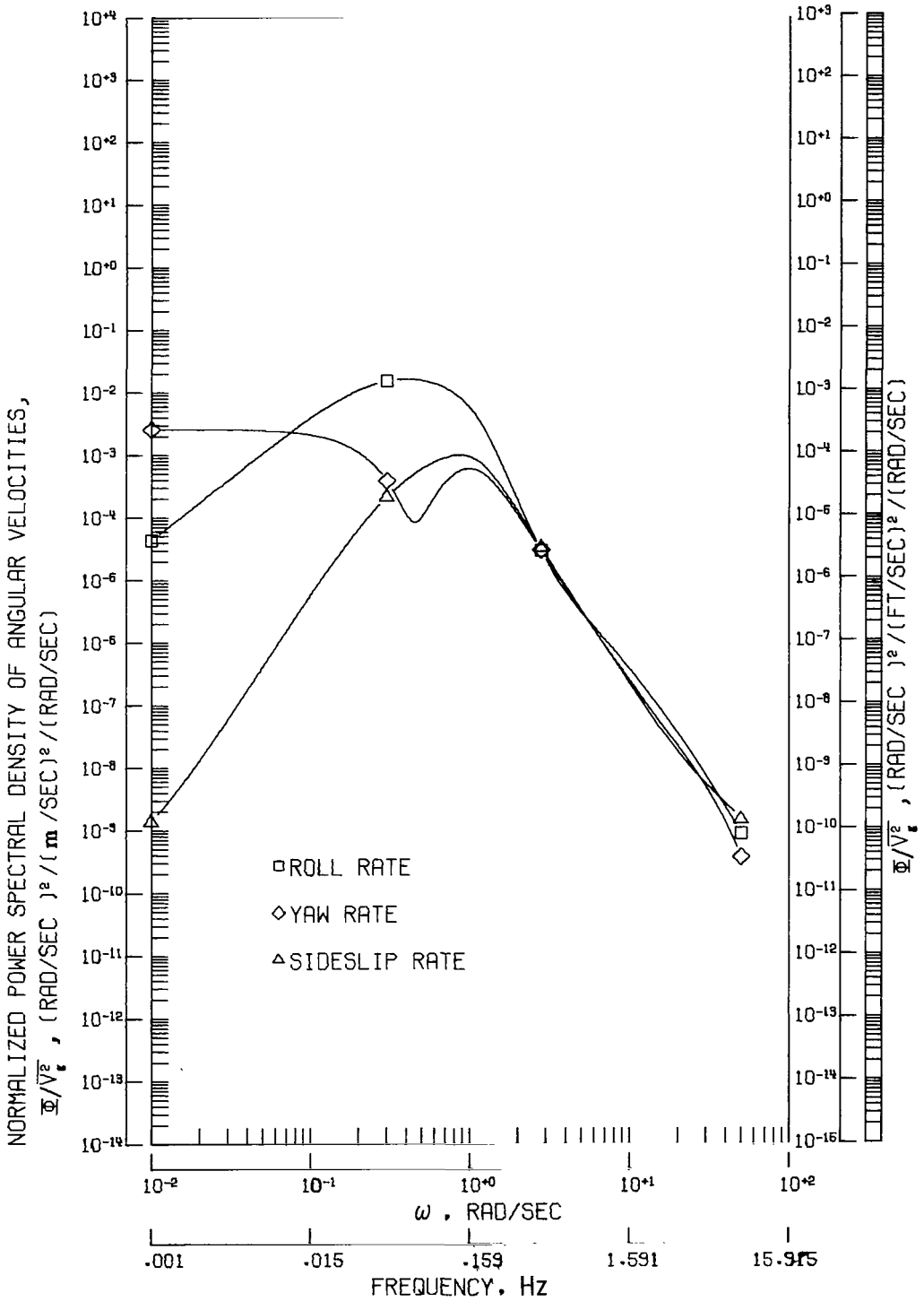


(b) Normalized power spectral density response for each lateral angular rate.

Figure 6.- Continued.

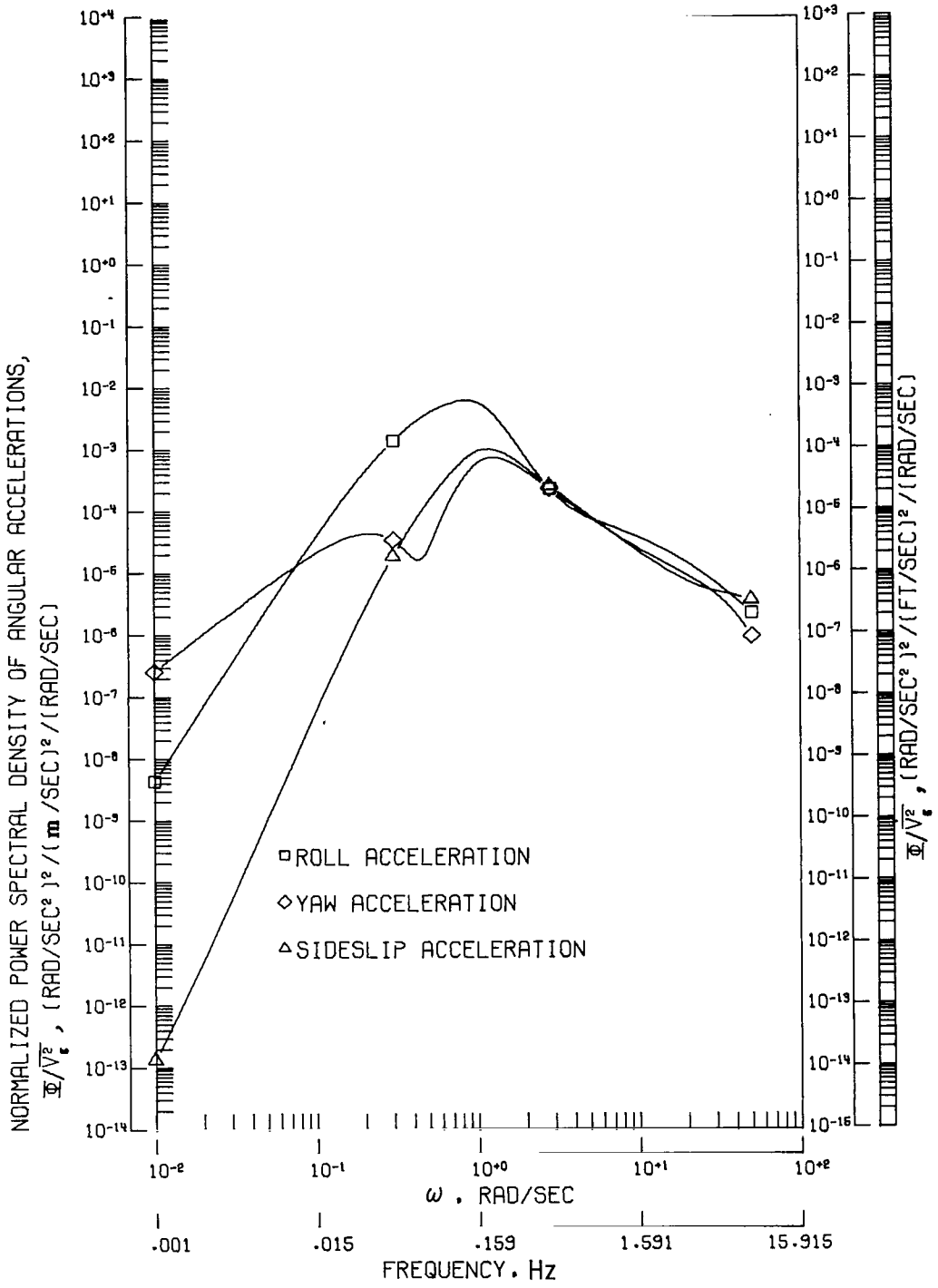


(c) Normalized power spectral density response for each lateral angular acceleration.

Figure 6.- Continued.

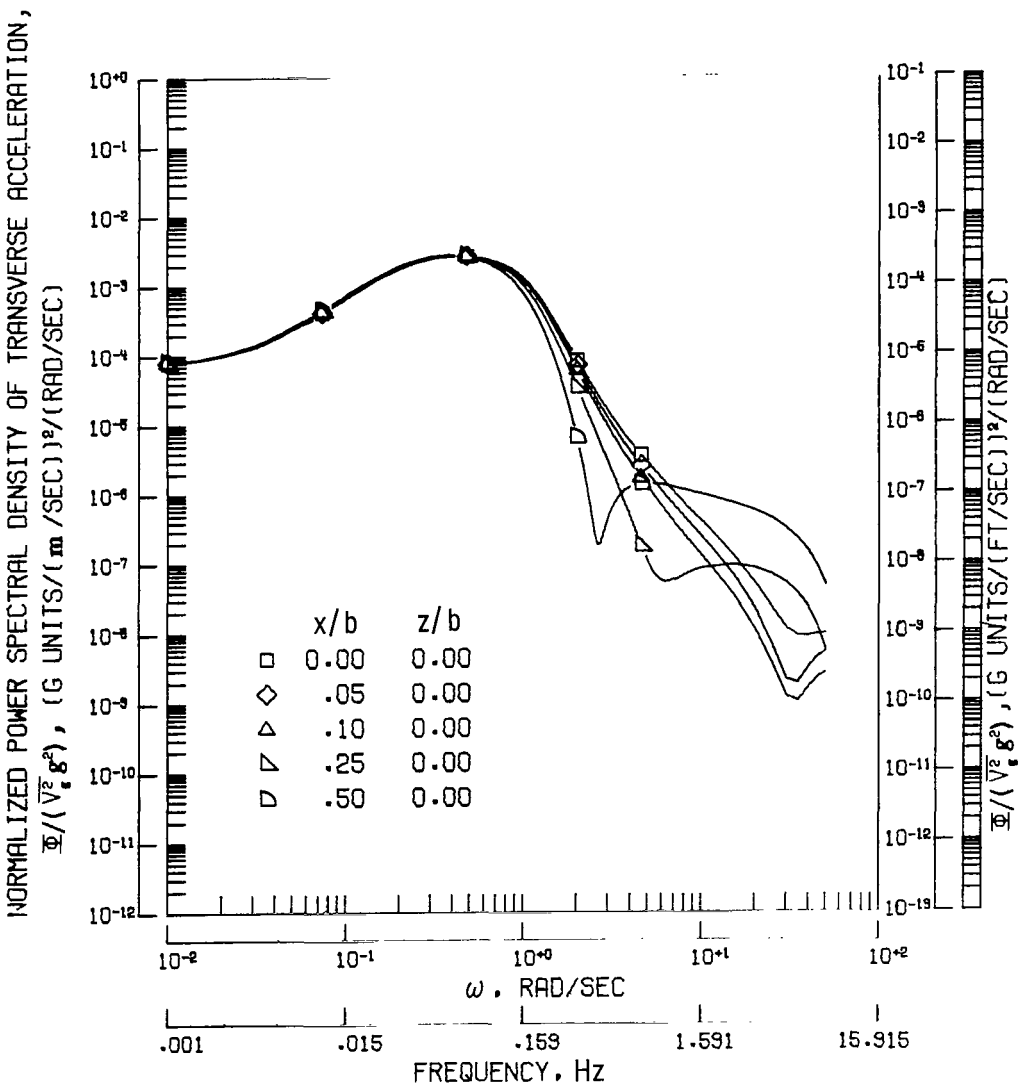


(d) Normalized power spectral density of transverse acceleration for locations forward of center of gravity.

Figure 6.- Continued.

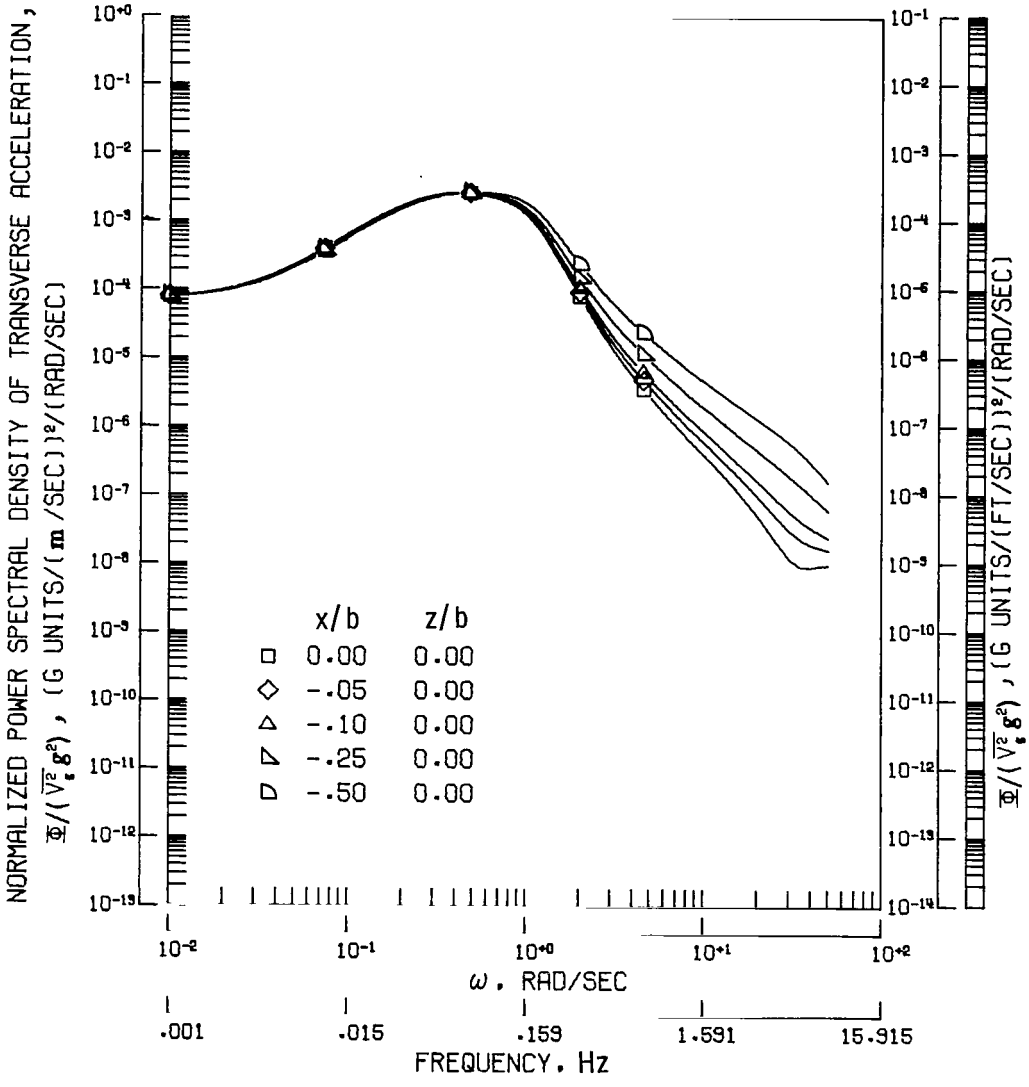


(e) Normalized power spectral density of transverse acceleration for locations rearward of center of gravity.

Figure 6.- Continued.

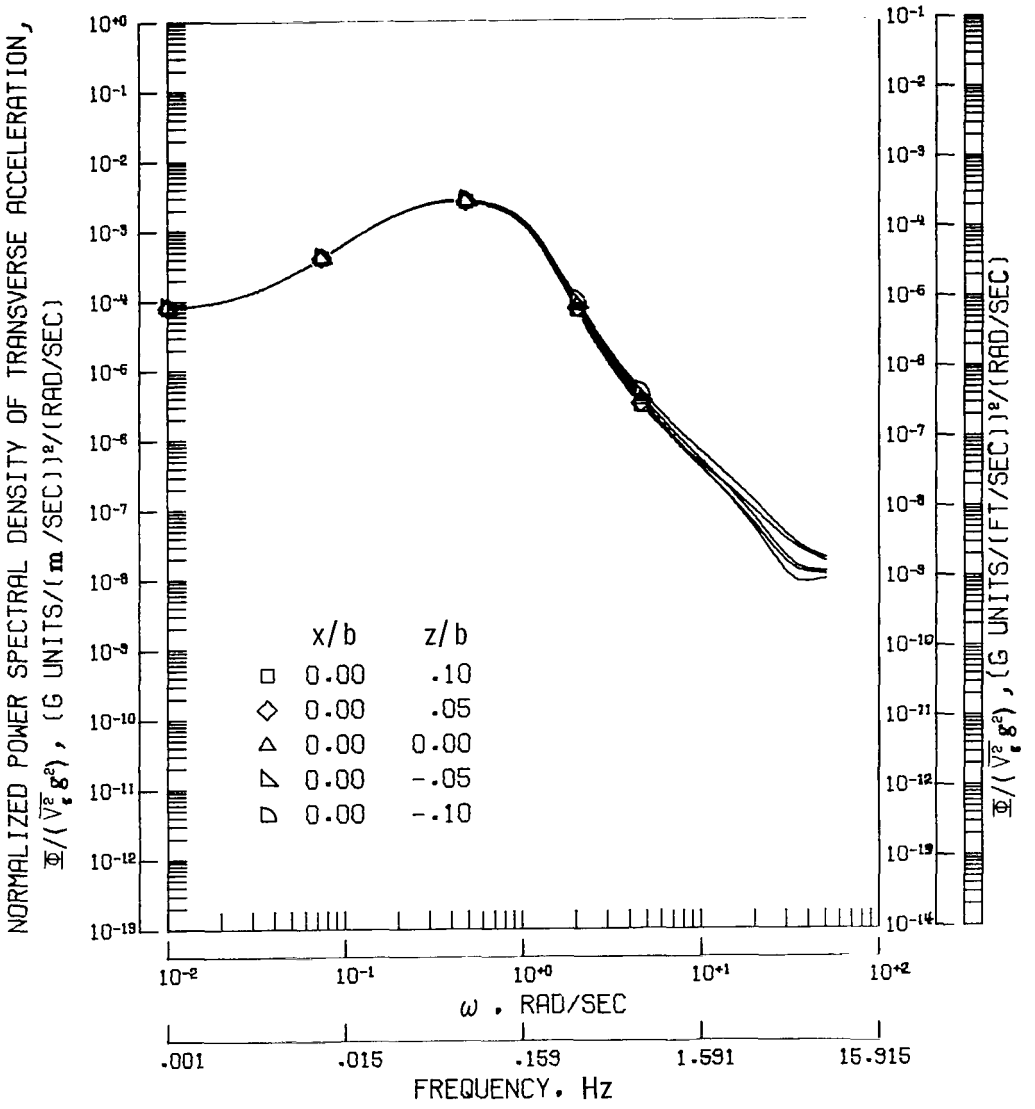


(f) Normalized power spectral density of transverse acceleration for several locations above and below center of gravity.

Figure 6.- Concluded.

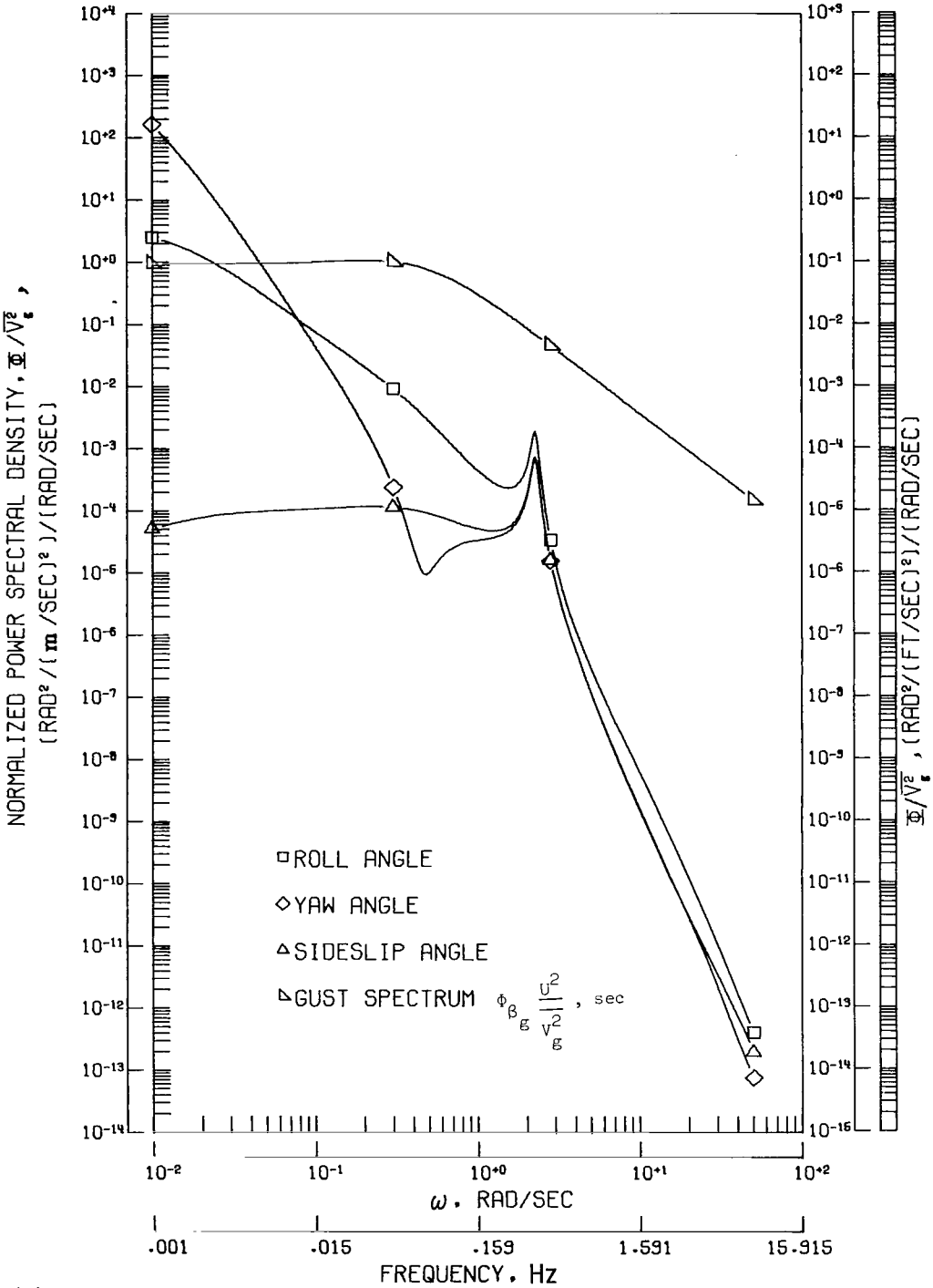


(a) Normalized power spectral density response for each lateral angular displacement.

Figure 7.- Response of airplane LS-D to random gusts for assumed scale length of 335.28 m (1100 ft). Note that units for gust spectrum are different from those for response spectra.

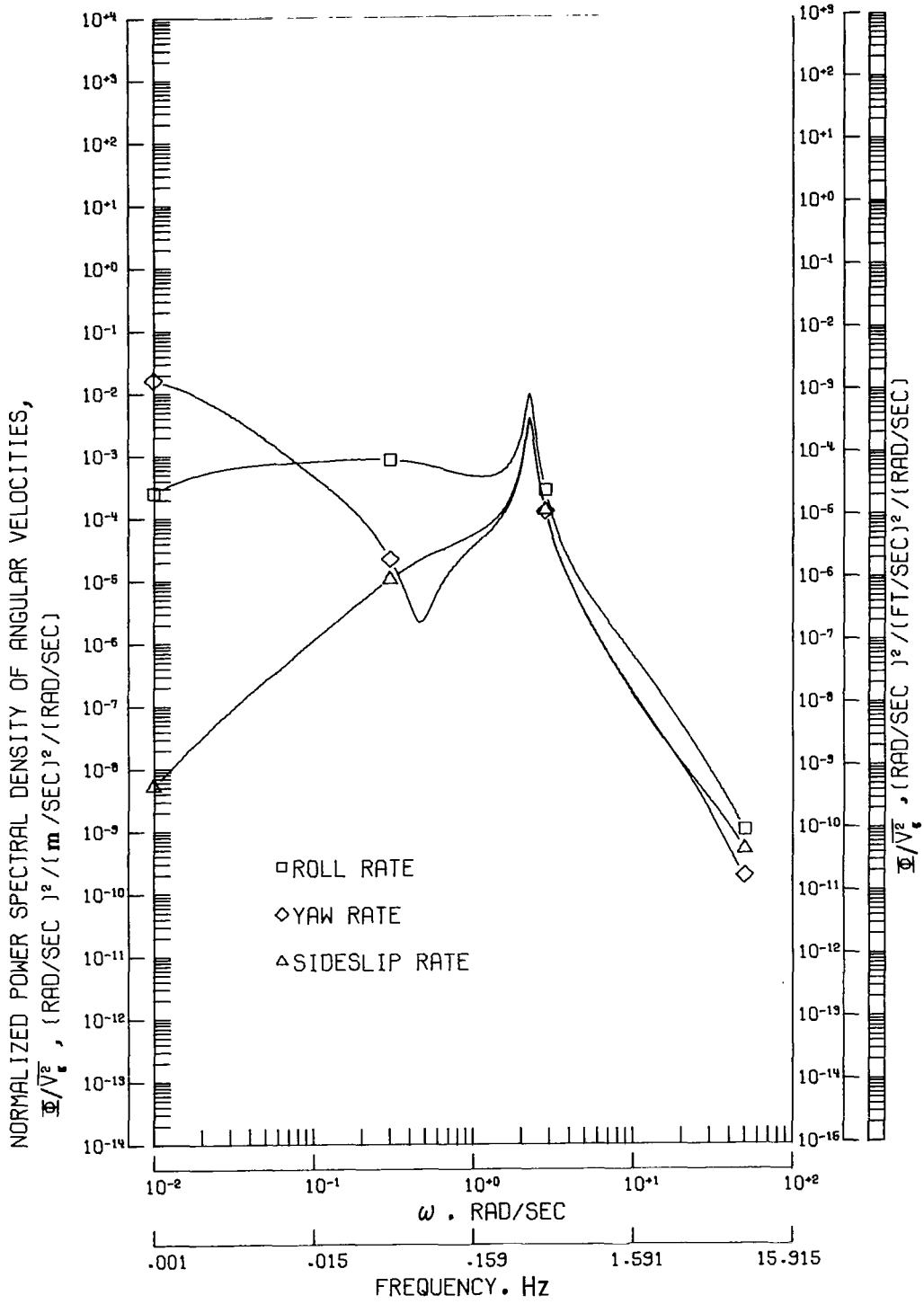


(b) Normalized power spectral density response for each lateral angular rate.

Figure 7.- Continued.

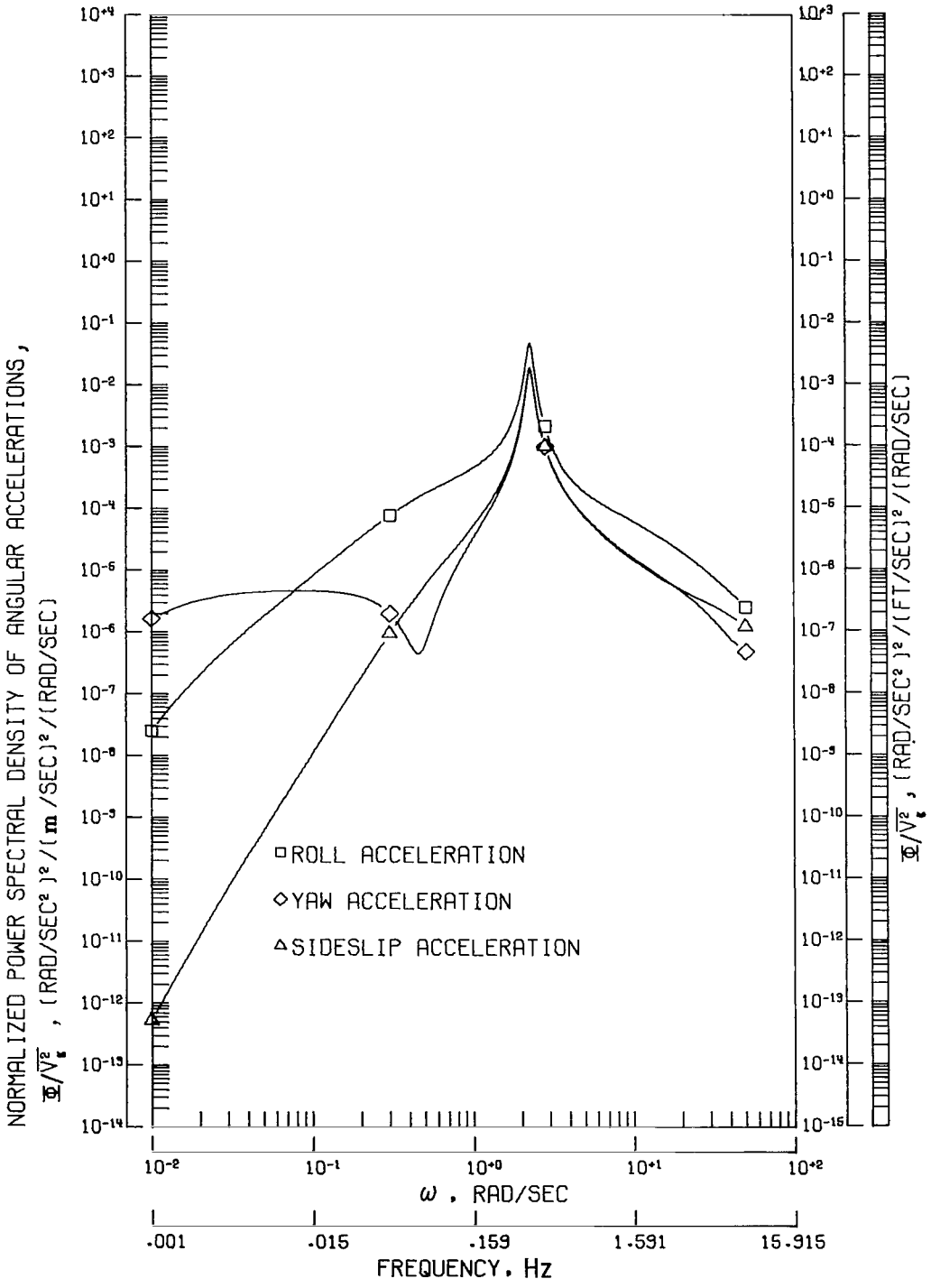


(c) Normalized power spectral density response for each lateral angular acceleration.

Figure 7.- Continued.

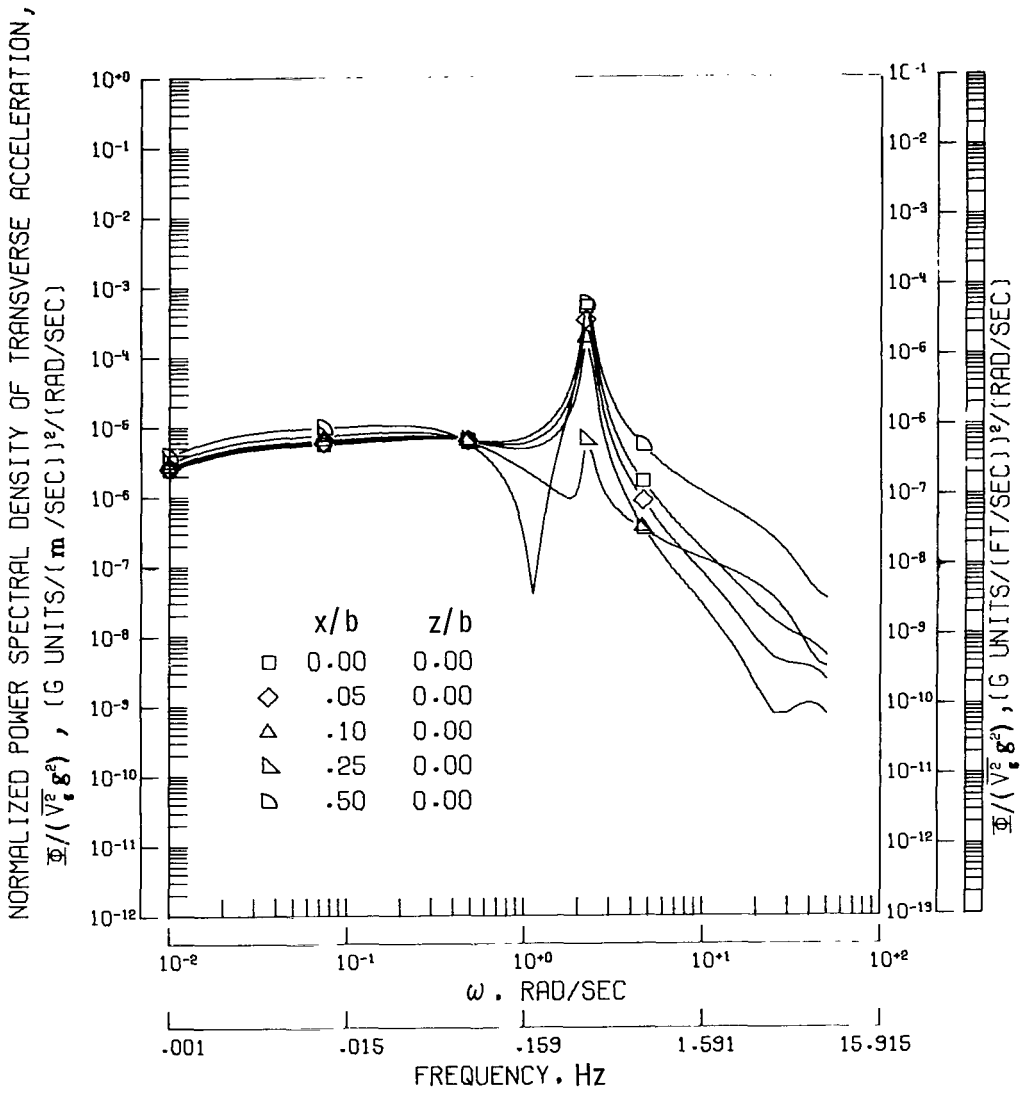


(d) Normalized power spectral density of transverse acceleration for locations forward of center of gravity.

Figure 7.- Continued.

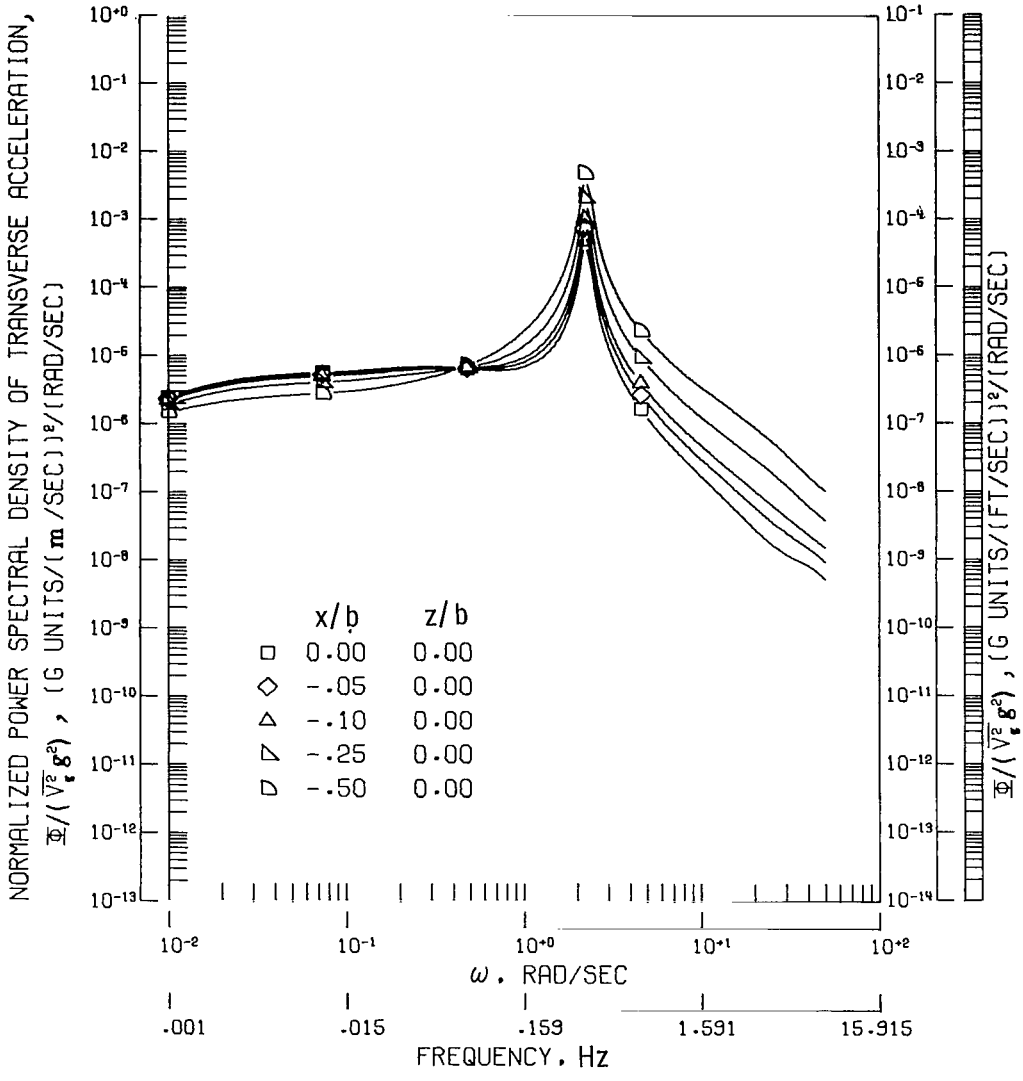


(e) Normalized power spectral density of transverse acceleration for locations rearward of center of gravity.

Figure 7.- Continued.

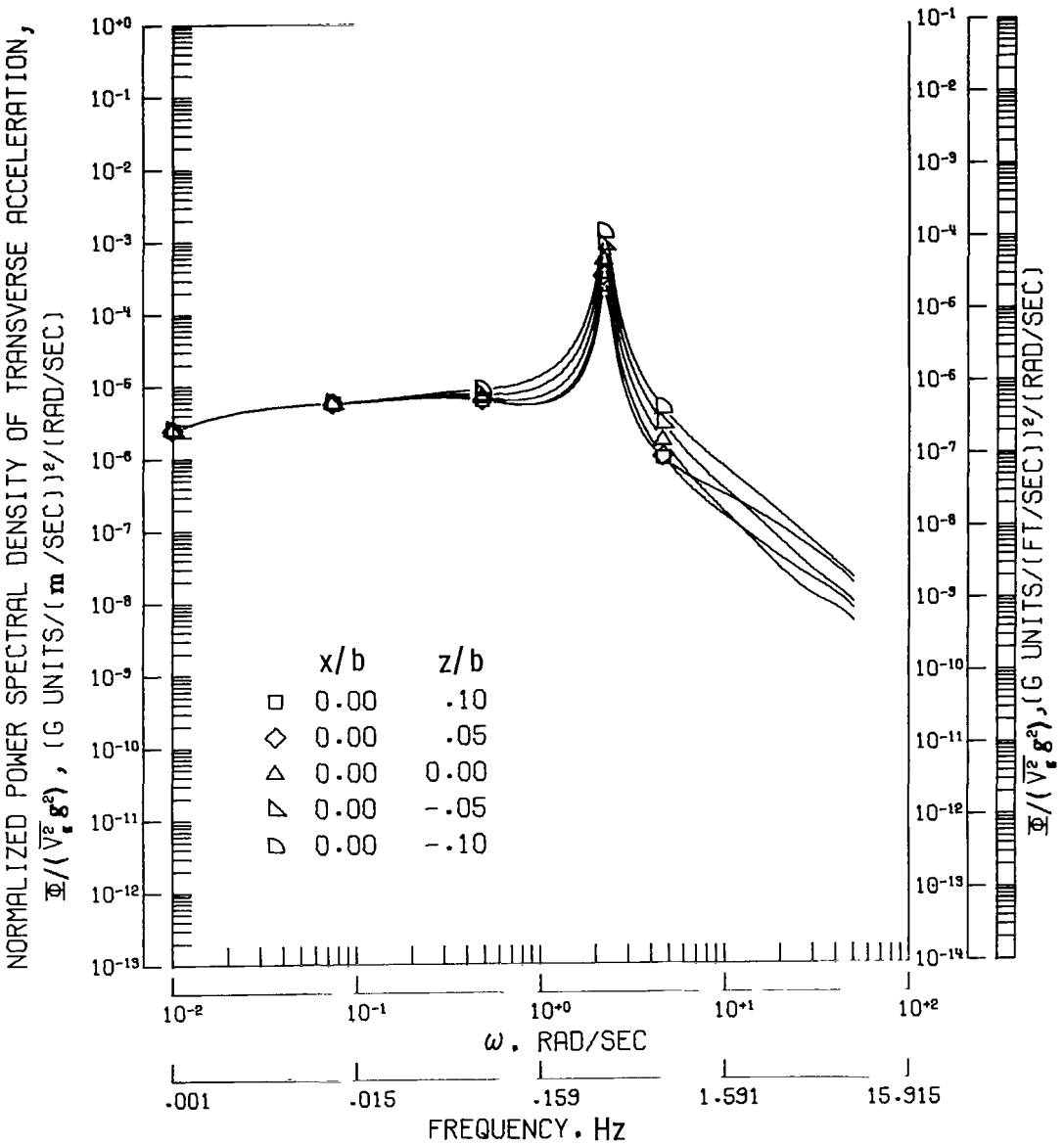


(f) Normalized power spectral density of transverse acceleration for several locations above and below center of gravity.

Figure 7.- Concluded.

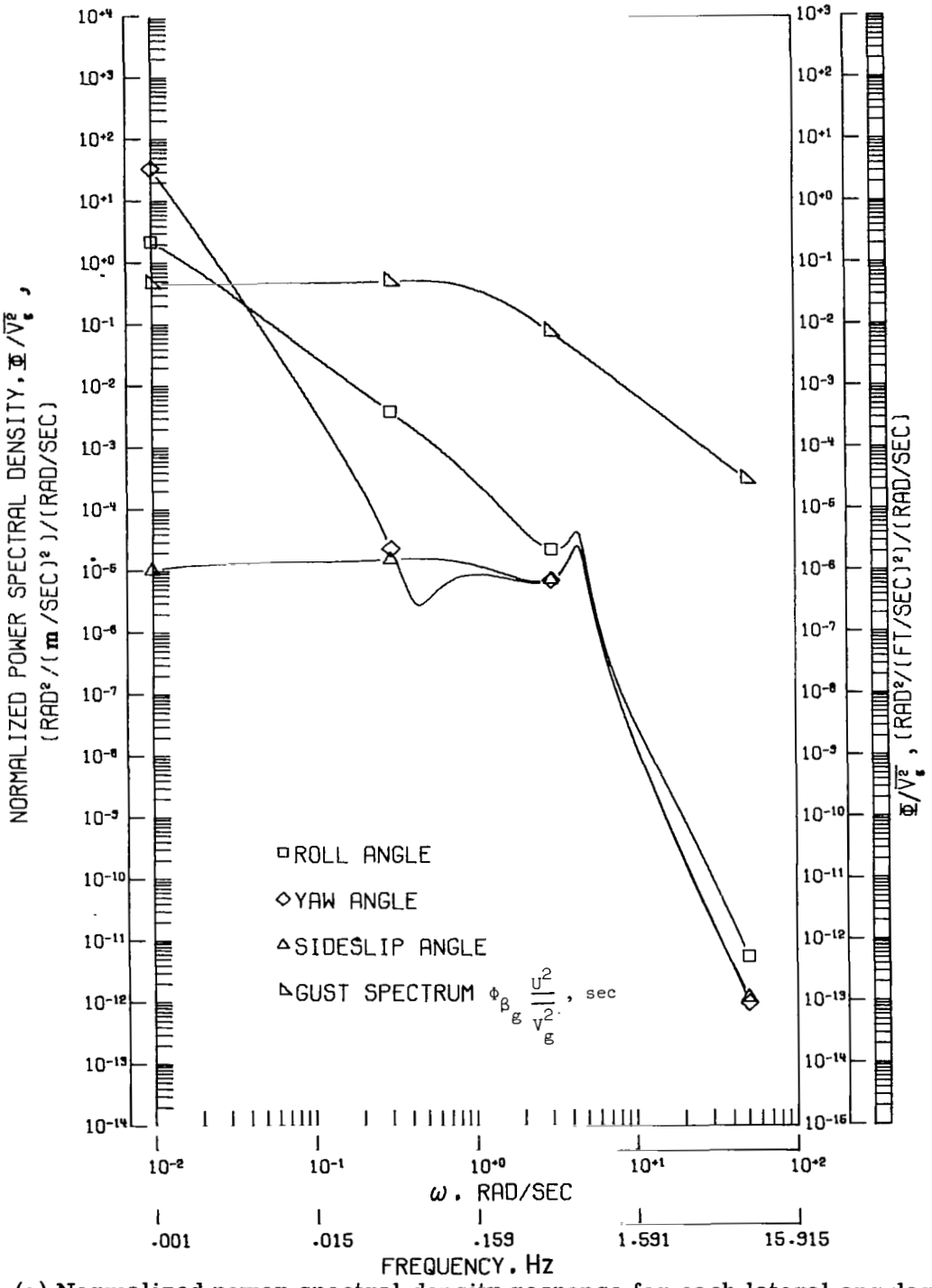


(a) Normalized power spectral density response for each lateral angular displacement.

Figure 8.- Response of airplane LS-E to random gusts for assumed scale length of 335.28 m (1100 ft). Note that units for gust spectrum are different from those for response spectra.

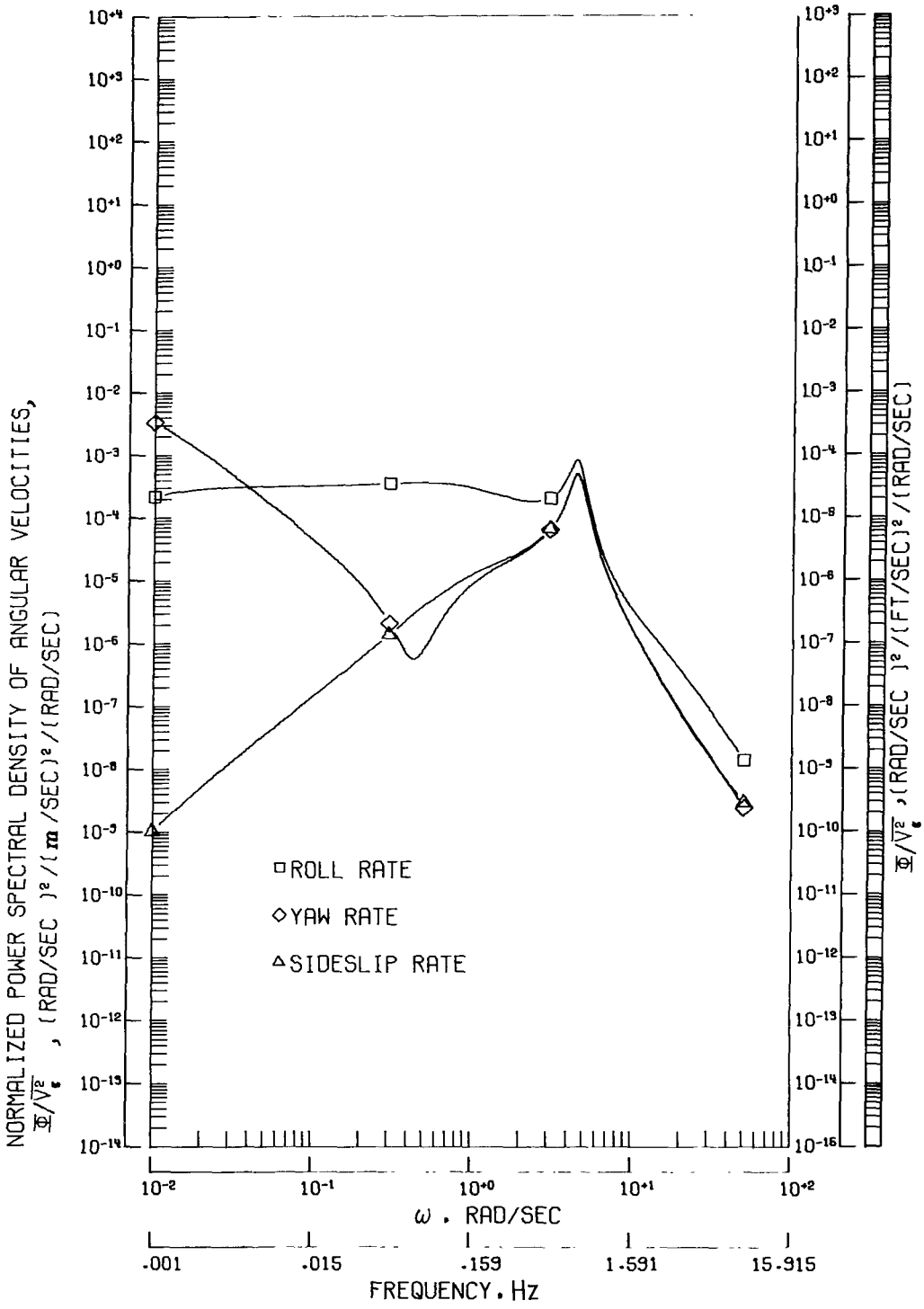


(b) Normalized power spectral density response for each lateral angular rate.

Figure 8.- Continued.

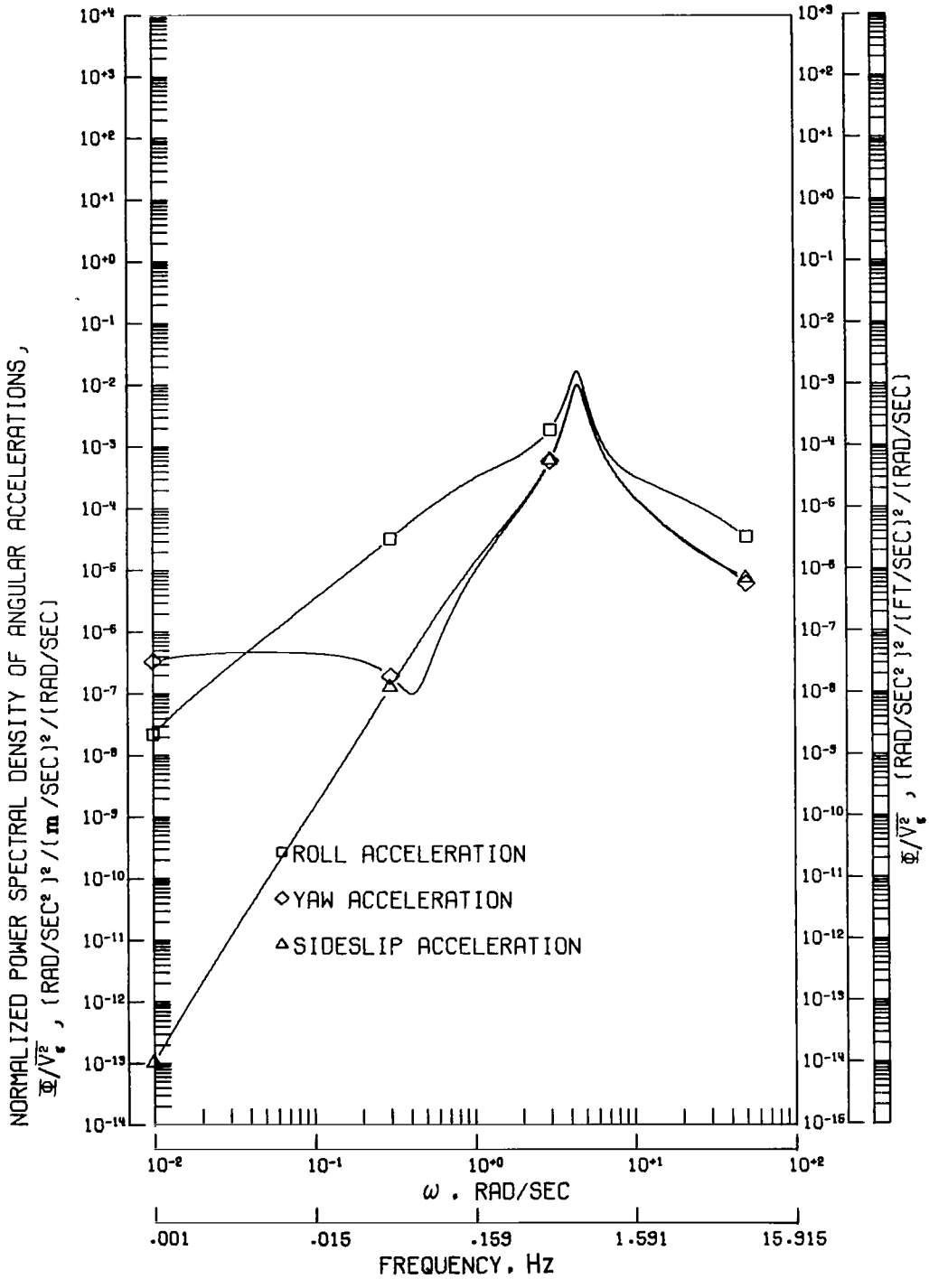


(c) Normalized power spectral density response for each lateral angular acceleration.

Figure 8.- Continued.

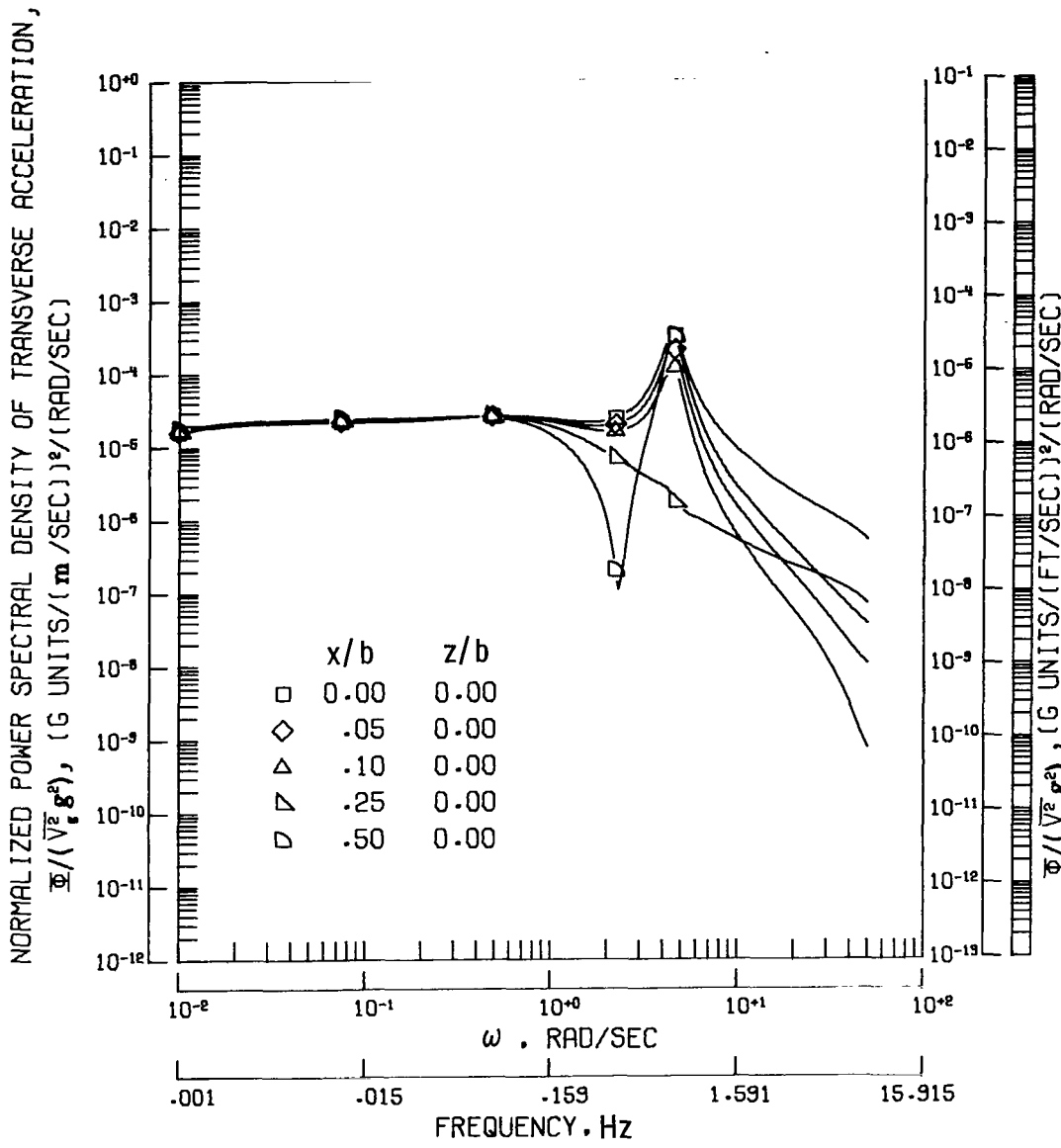


(d) Normalized power spectral density of transverse acceleration for locations forward of center of gravity.

Figure 8.- Continued.

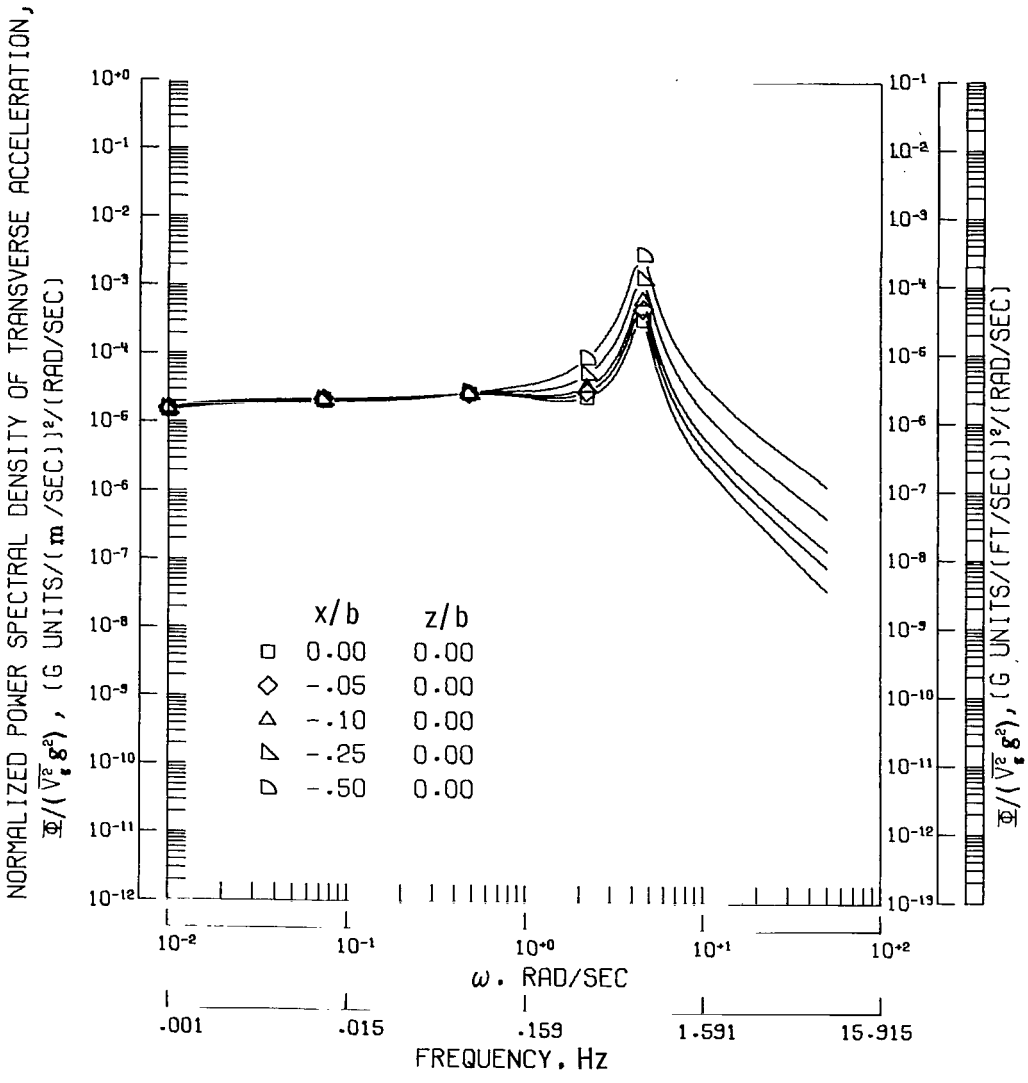


(e) Normalized power spectral density of transverse acceleration for locations rearward of center of gravity.

Figure 8.- Continued.

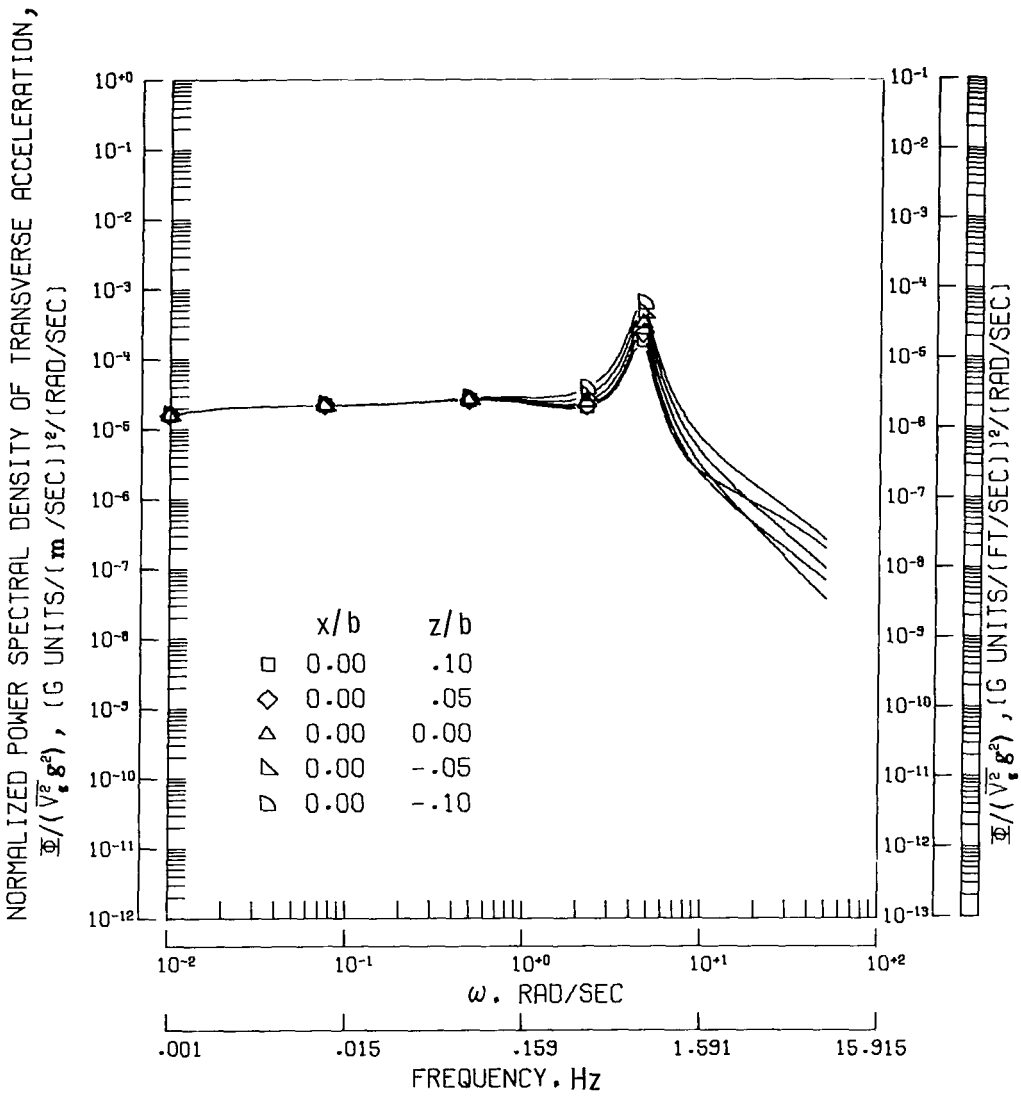


(f) Normalized power spectral density of transverse acceleration for several locations above and below center of gravity.

Figure 8.- Concluded.

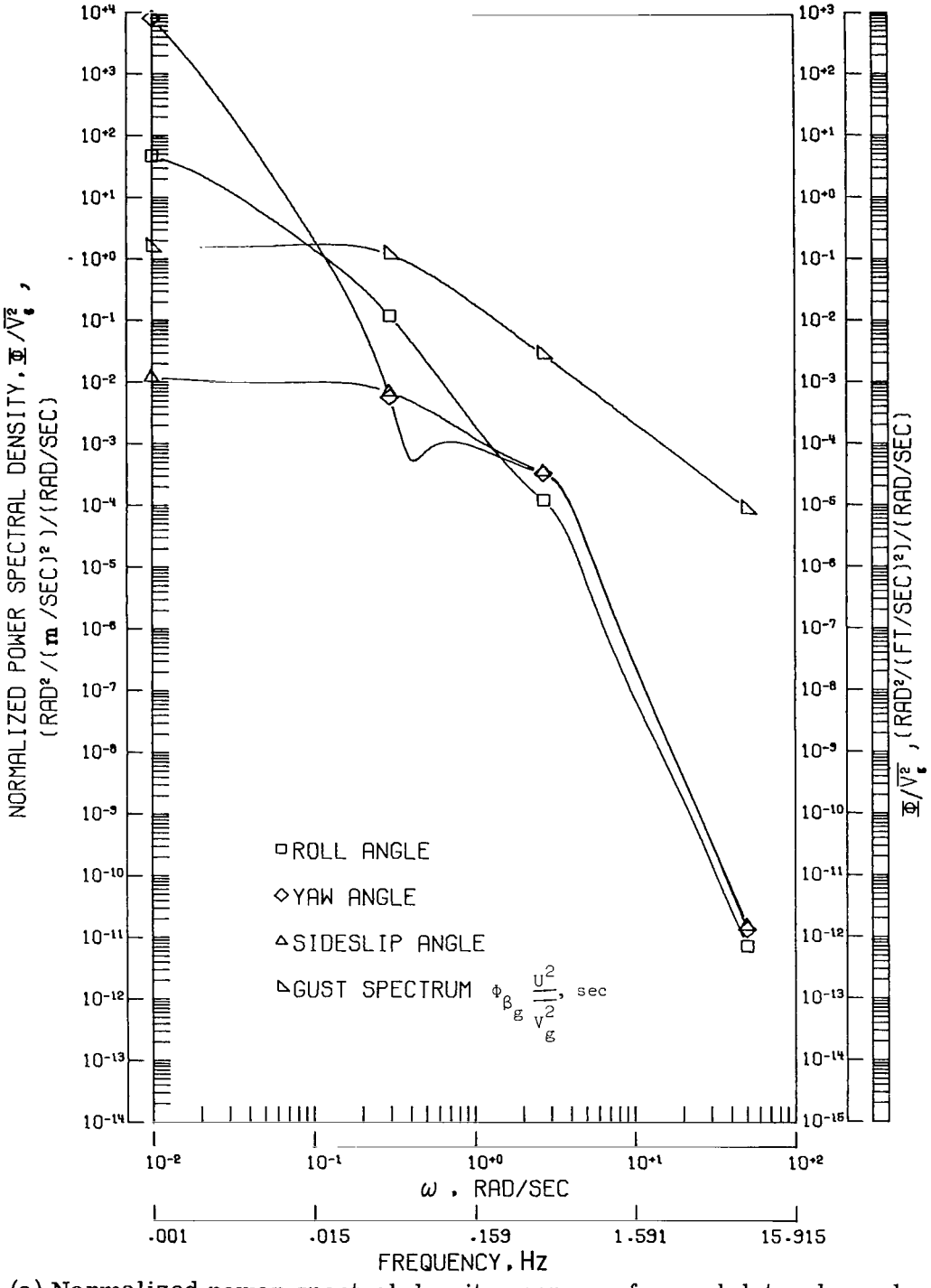


(a) Normalized power spectral density response for each lateral angular displacement.

Figure 9.- Response of airplane SS-A to random gusts for assumed scale length of 335.28 m (1100 ft). Note that units for gust spectrum are different from those for response spectra.

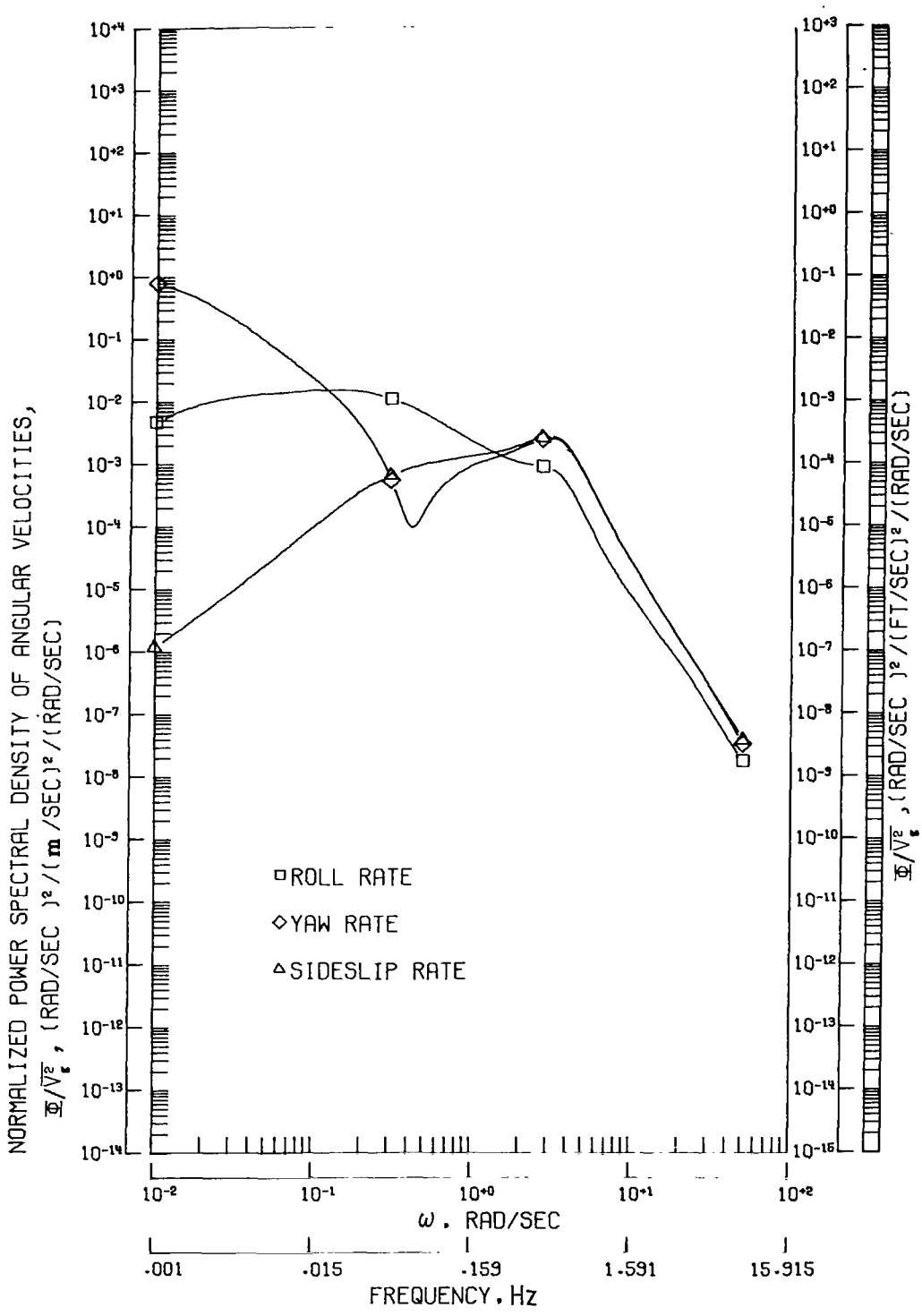


(b) Normalized power spectral density response for each lateral angular rate.

Figure 9.- Continued.

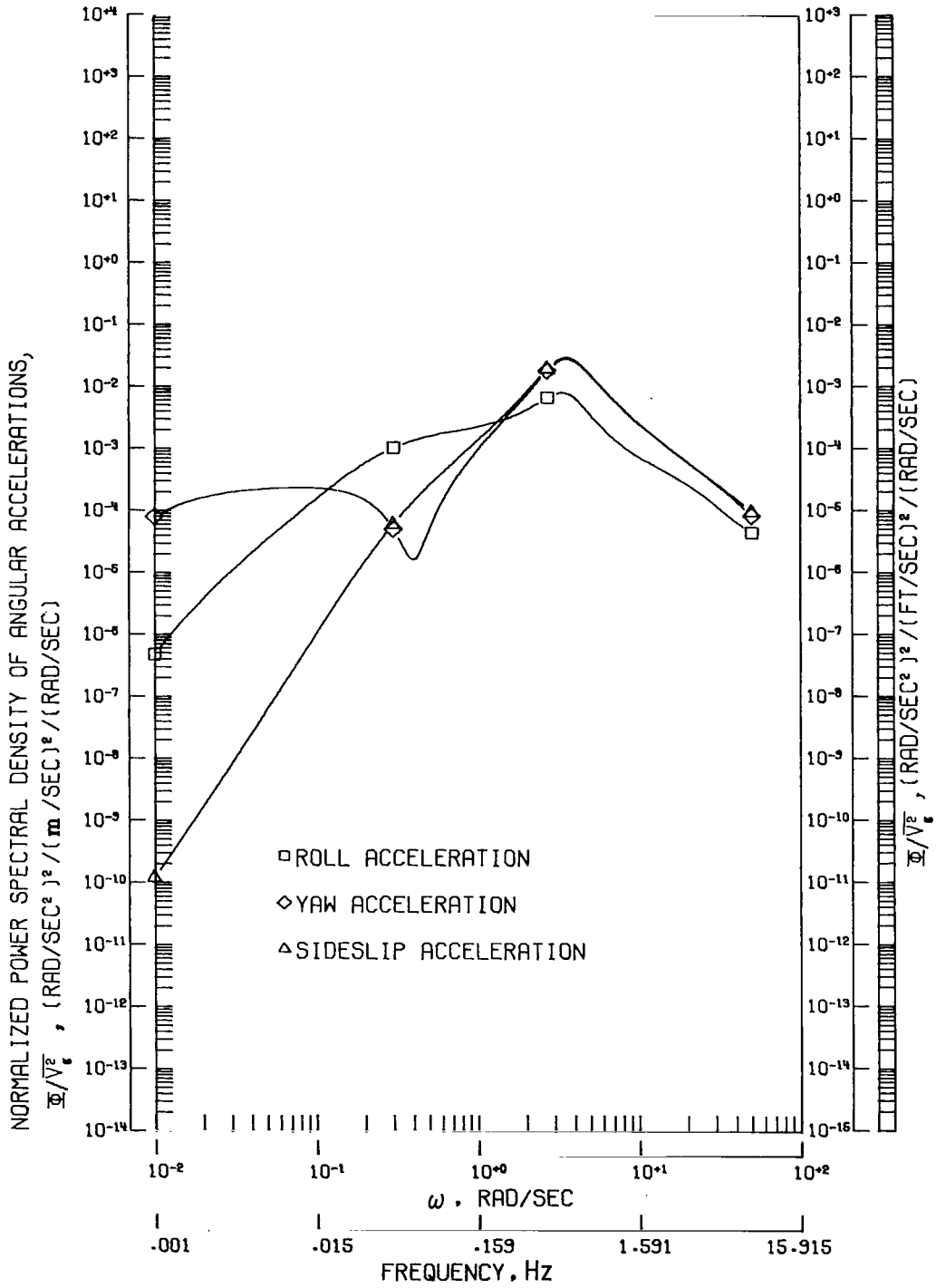


(c) Normalized power spectral density response for each lateral angular acceleration.

Figure 9.- Continued.

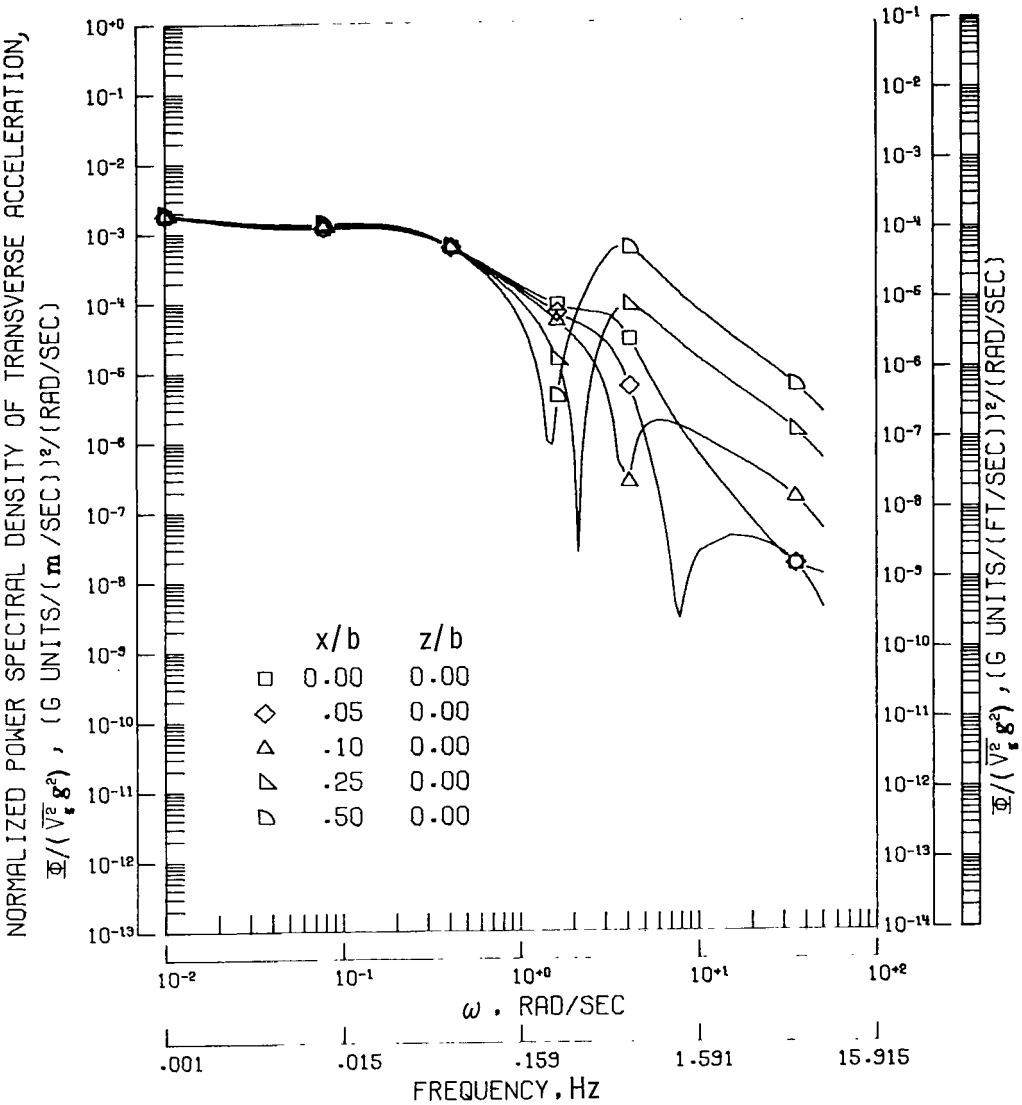


(d) Normalized power spectral density of transverse acceleration for locations forward of center of gravity.

Figure 9.- Continued.

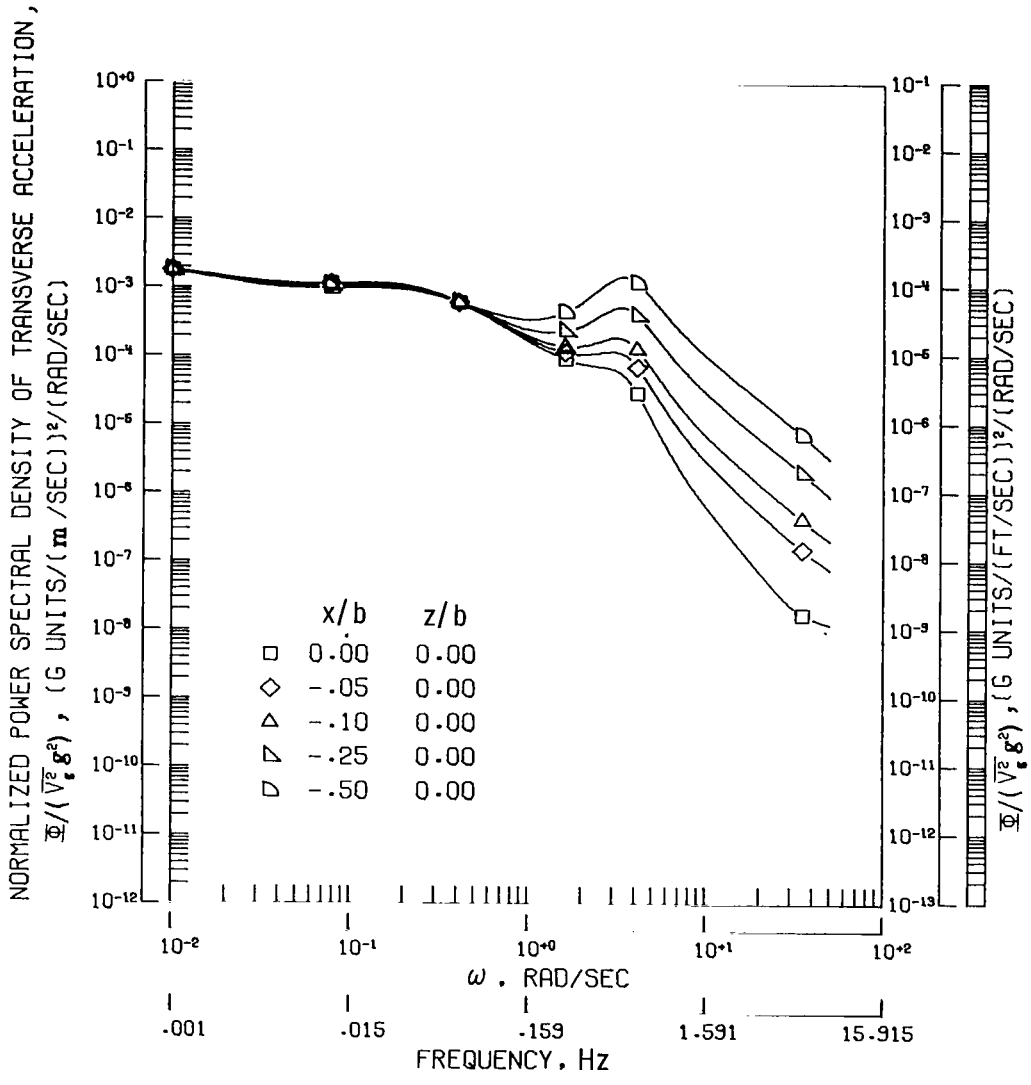


(e) Normalized power spectral density of transverse acceleration for locations rearward of center of gravity.

Figure 9.- Continued.

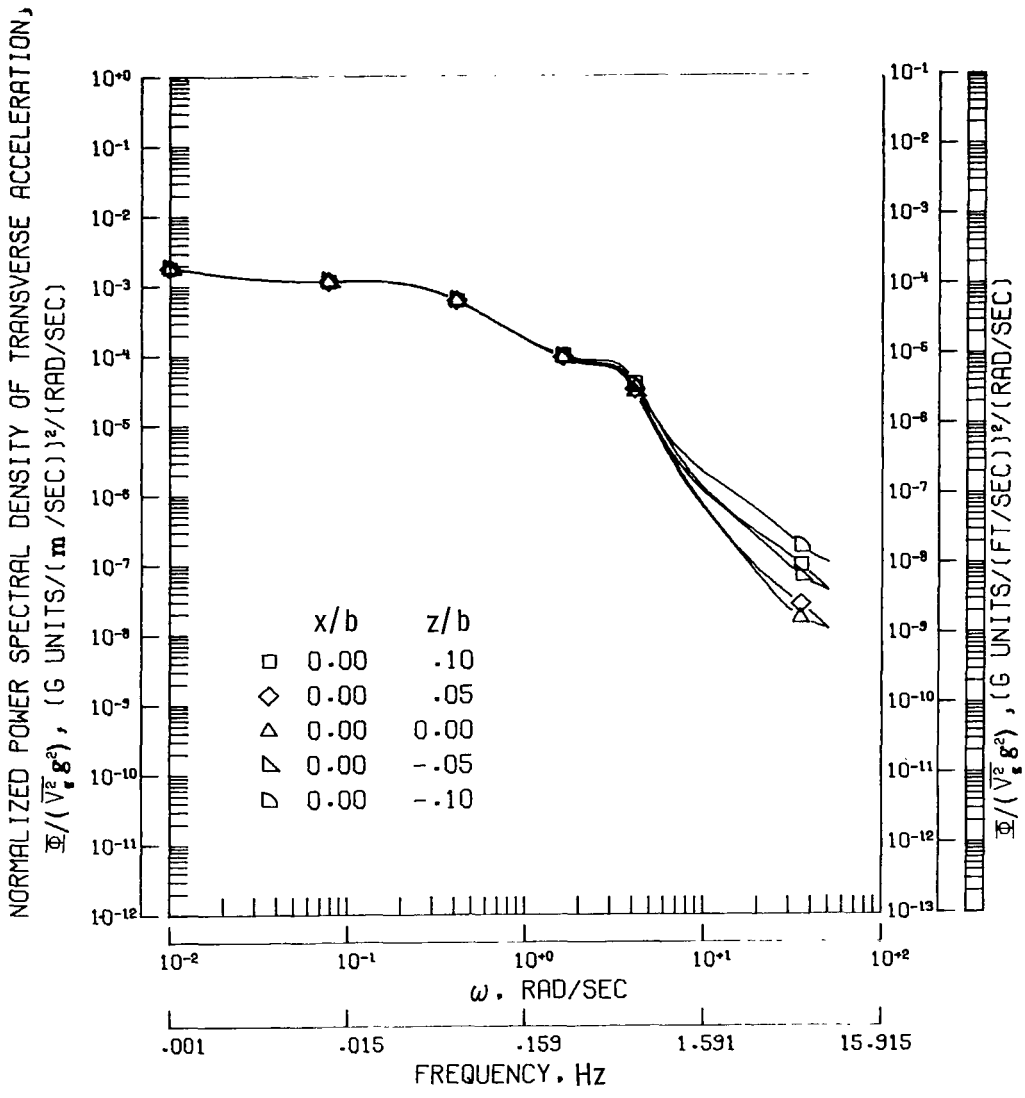


(f) Normalized power spectral density of transverse acceleration for several locations above and below center of gravity.

Figure 9.- Concluded.

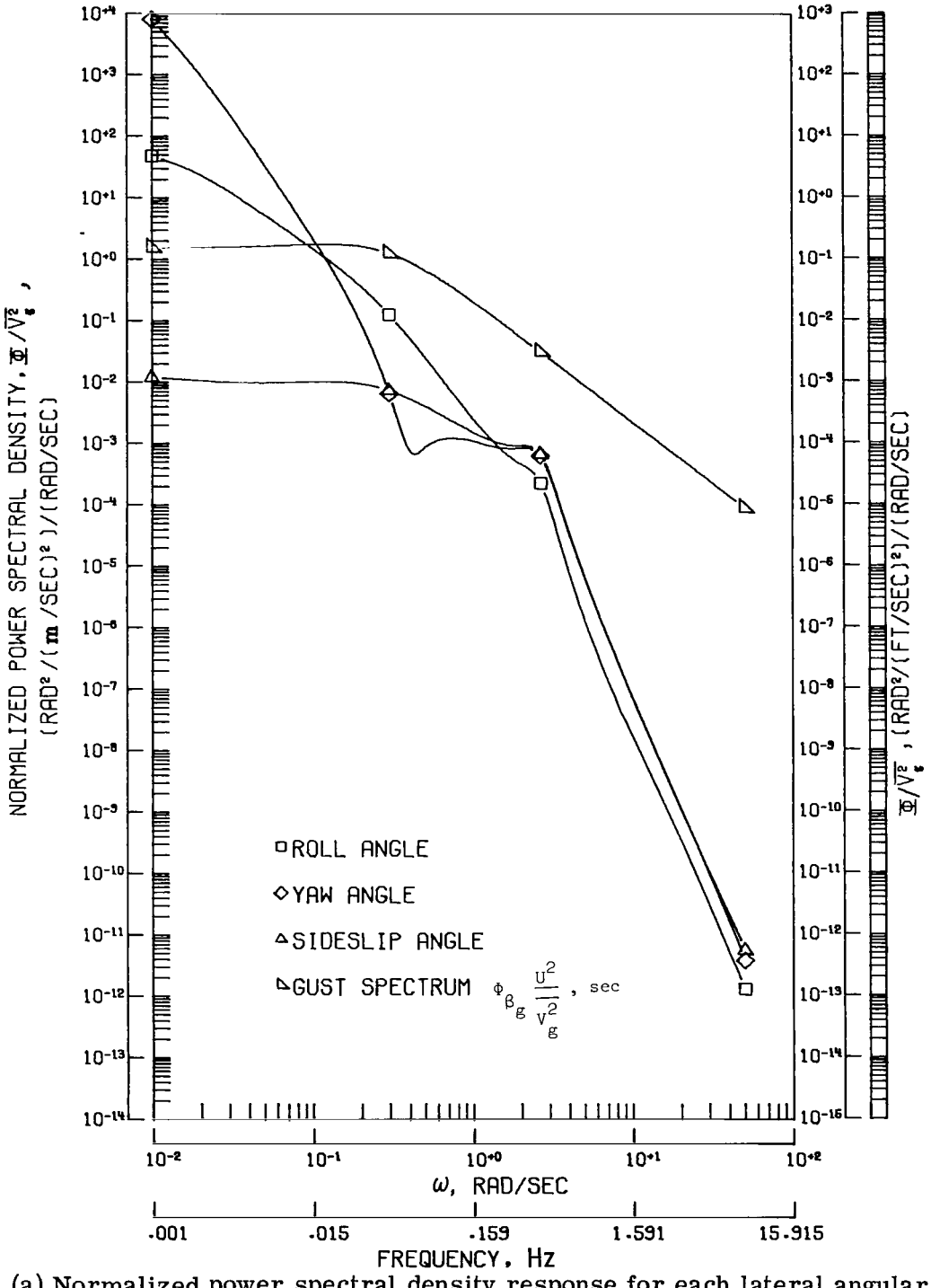


(a) Normalized power spectral density response for each lateral angular displacement.

Figure 10.- Response of airplane SS-B to random gusts for assumed scale length of 335.28 m (1100 ft). Note that units for gust spectrum are different from those for response spectra.

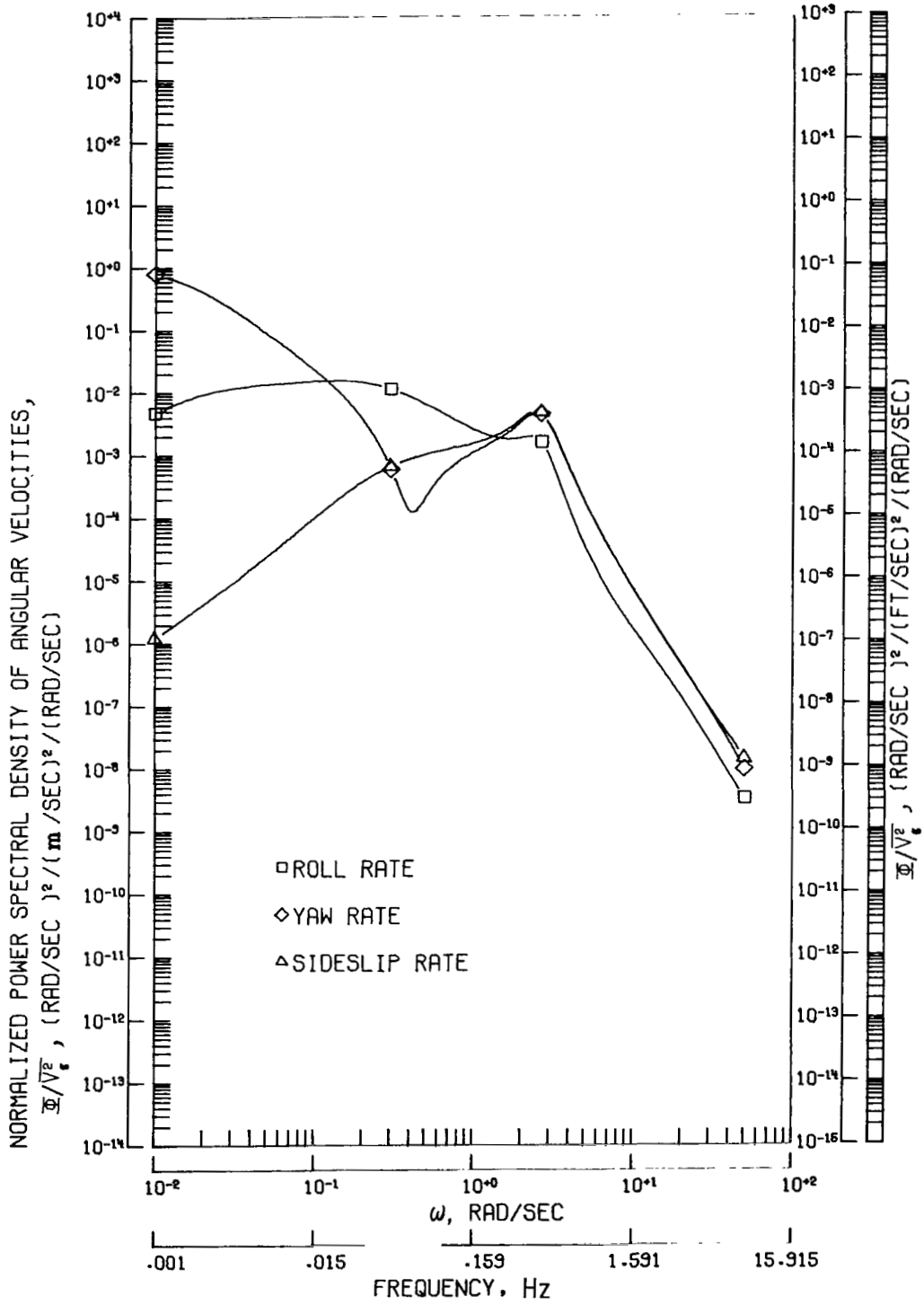


(b) Normalized power spectral density response for each lateral angular rate.

Figure 10.- Continued.

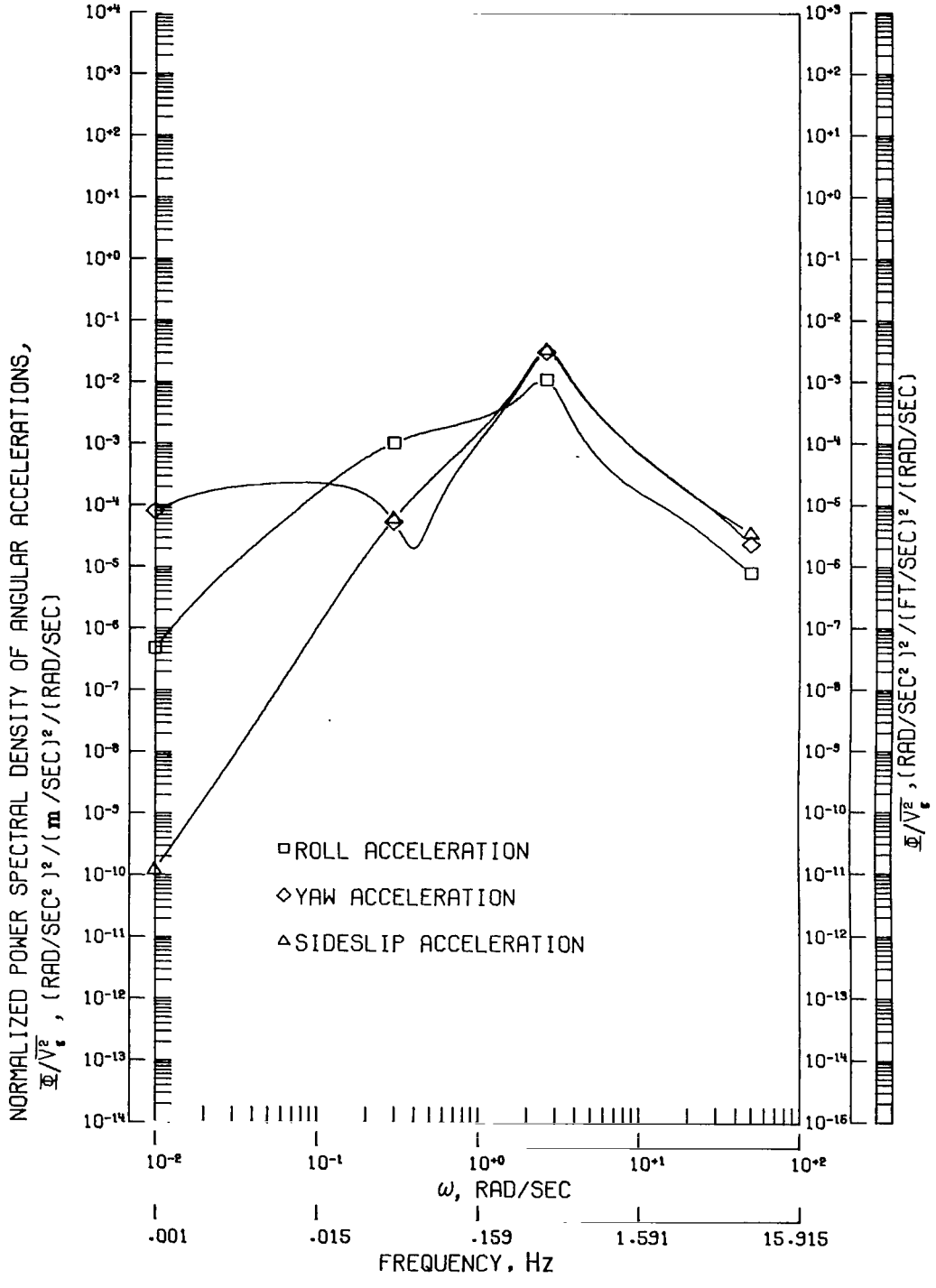


(c) Normalized power spectral density response for each lateral angular acceleration.

Figure 10.- Continued.

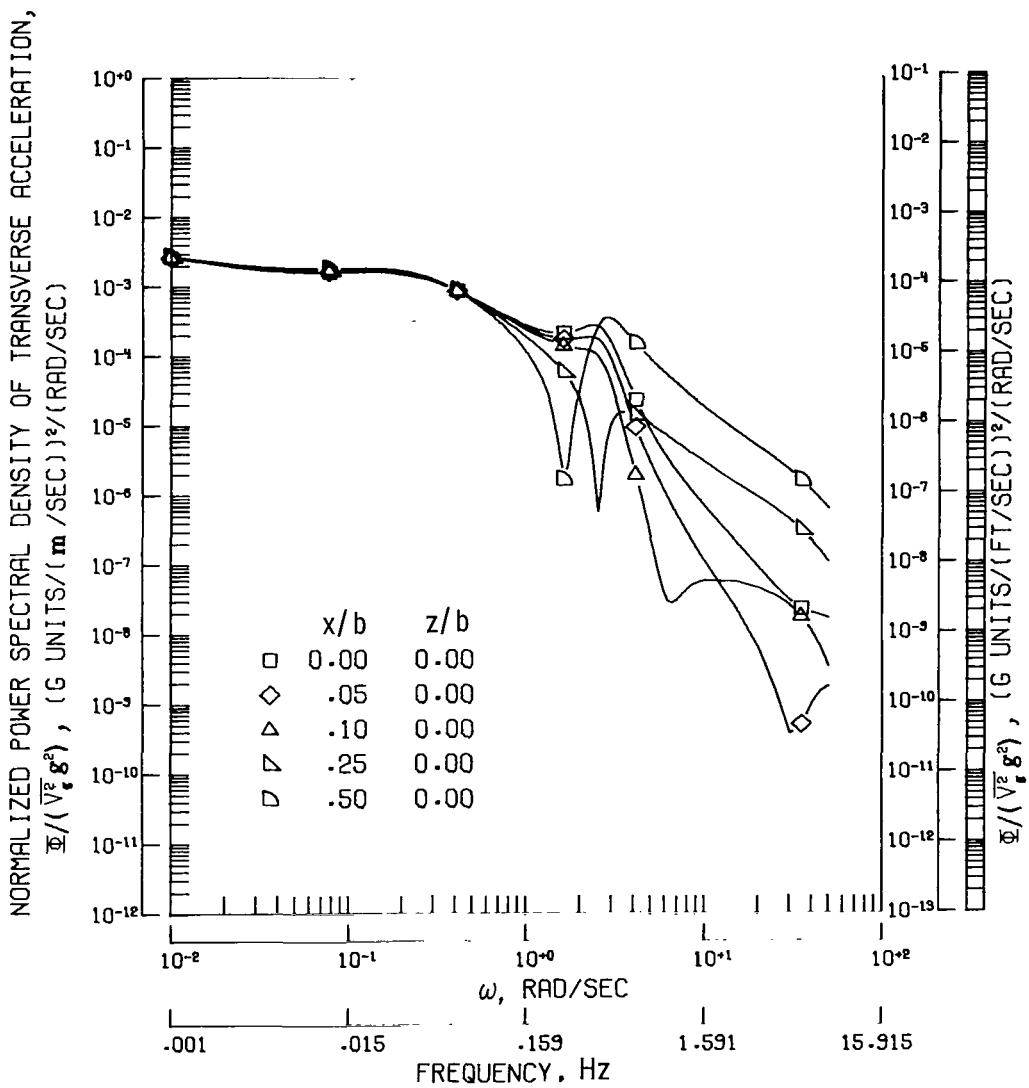


(d) Normalized power spectral density of transverse acceleration for locations forward of center of gravity.

Figure 10.- Continued.

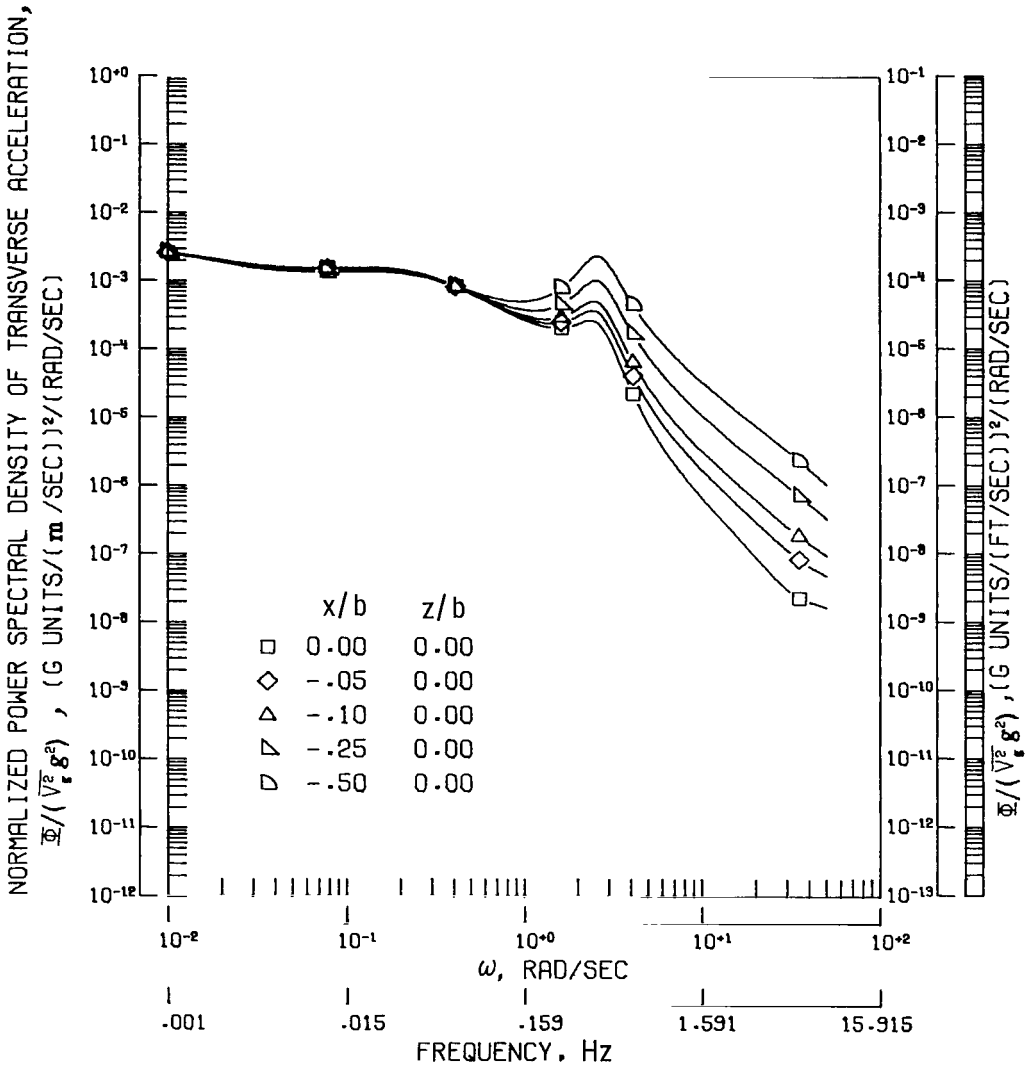


(e) Normalized power spectral density of transverse acceleration for locations rearward of center of gravity.

Figure 10.- Continued.

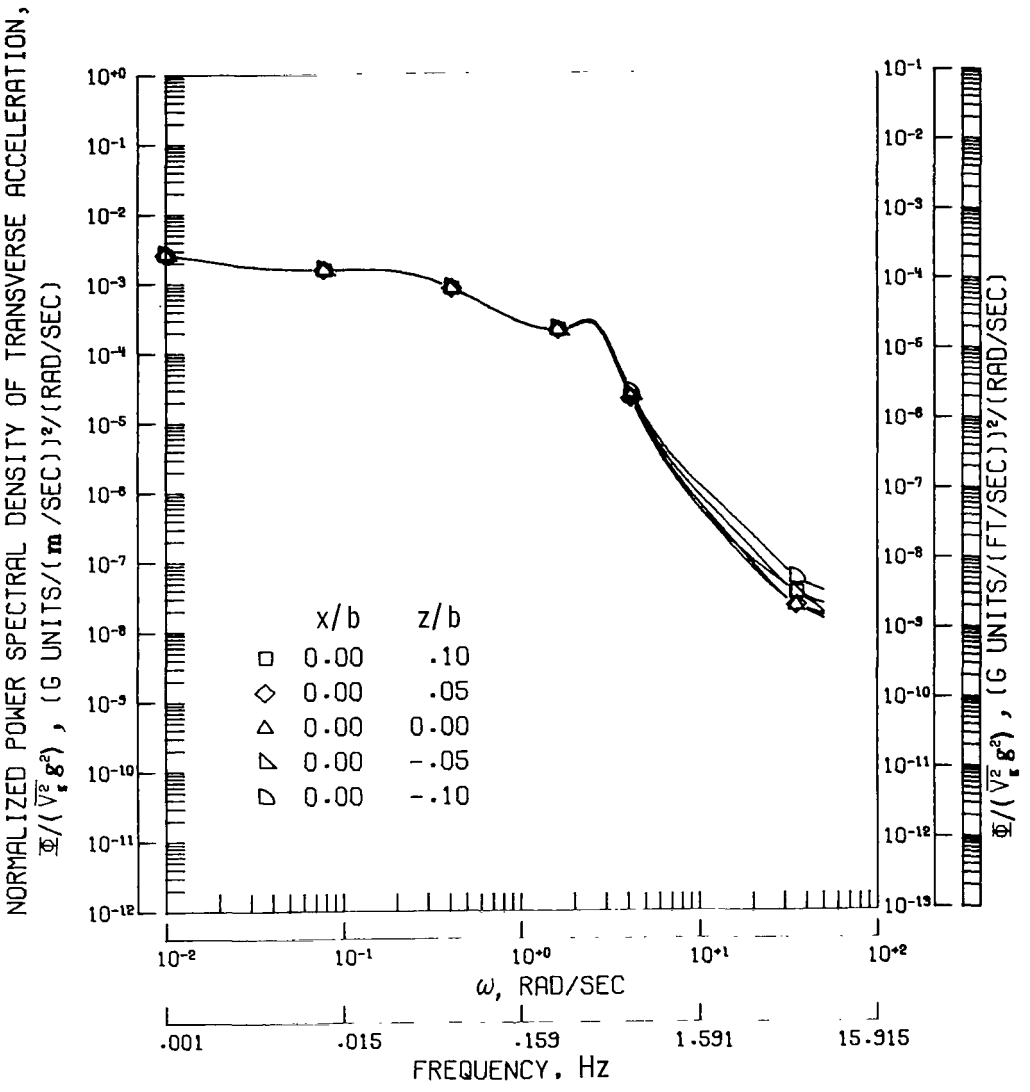


(f) Normalized power spectral density of transverse acceleration for several locations above and below center of gravity.

Figure 10.- Concluded.

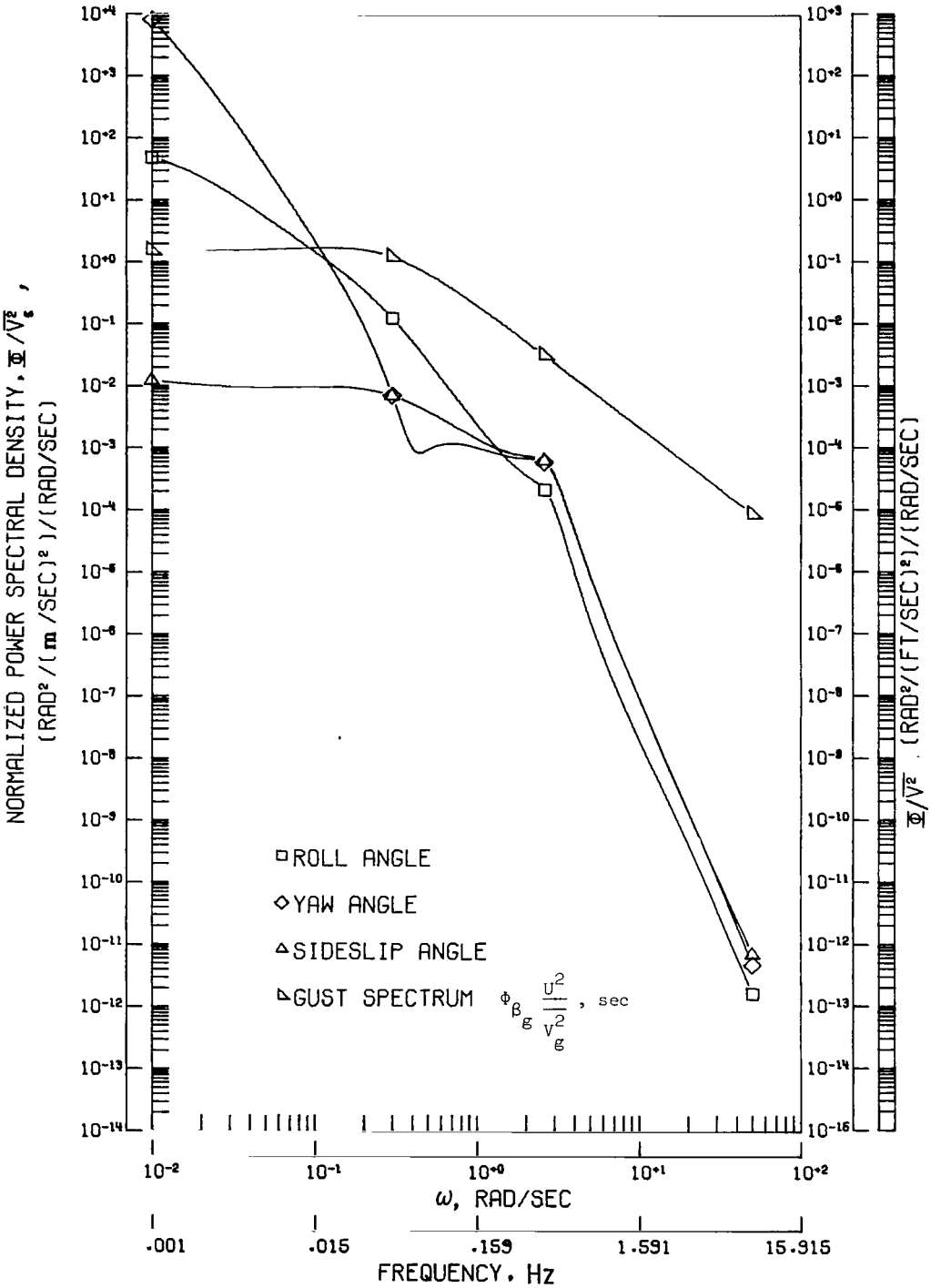


(a) Normalized power spectral density response for each lateral angular displacement.

Figure 11.- Response of airplane SS-C to random gusts for assumed scale length of 335.28 m (1100 ft). Note that units for gust spectrum are different from those for response spectra.

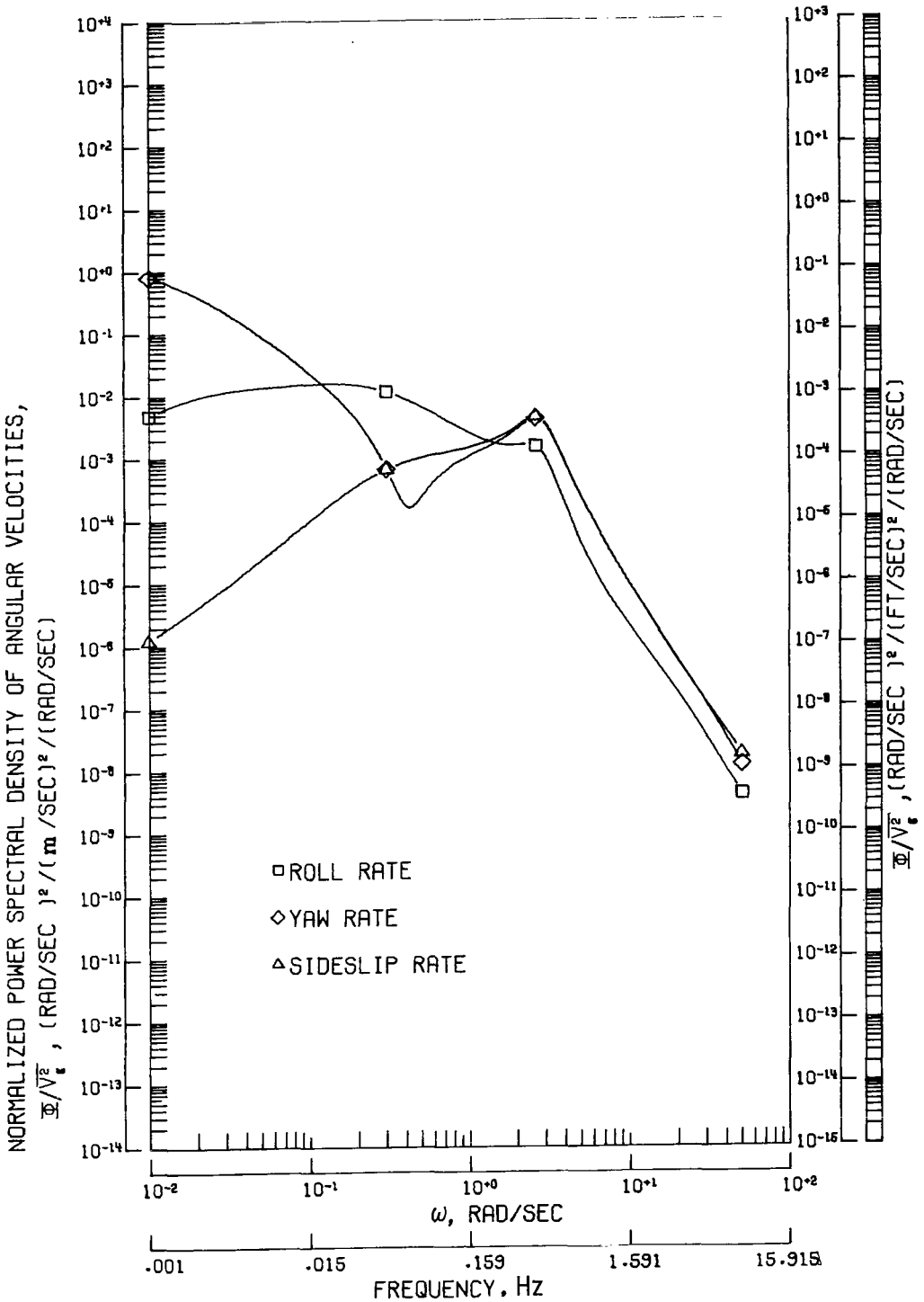


(b) Normalized power spectral density response for each lateral angular rate.

Figure 11.- Continued.

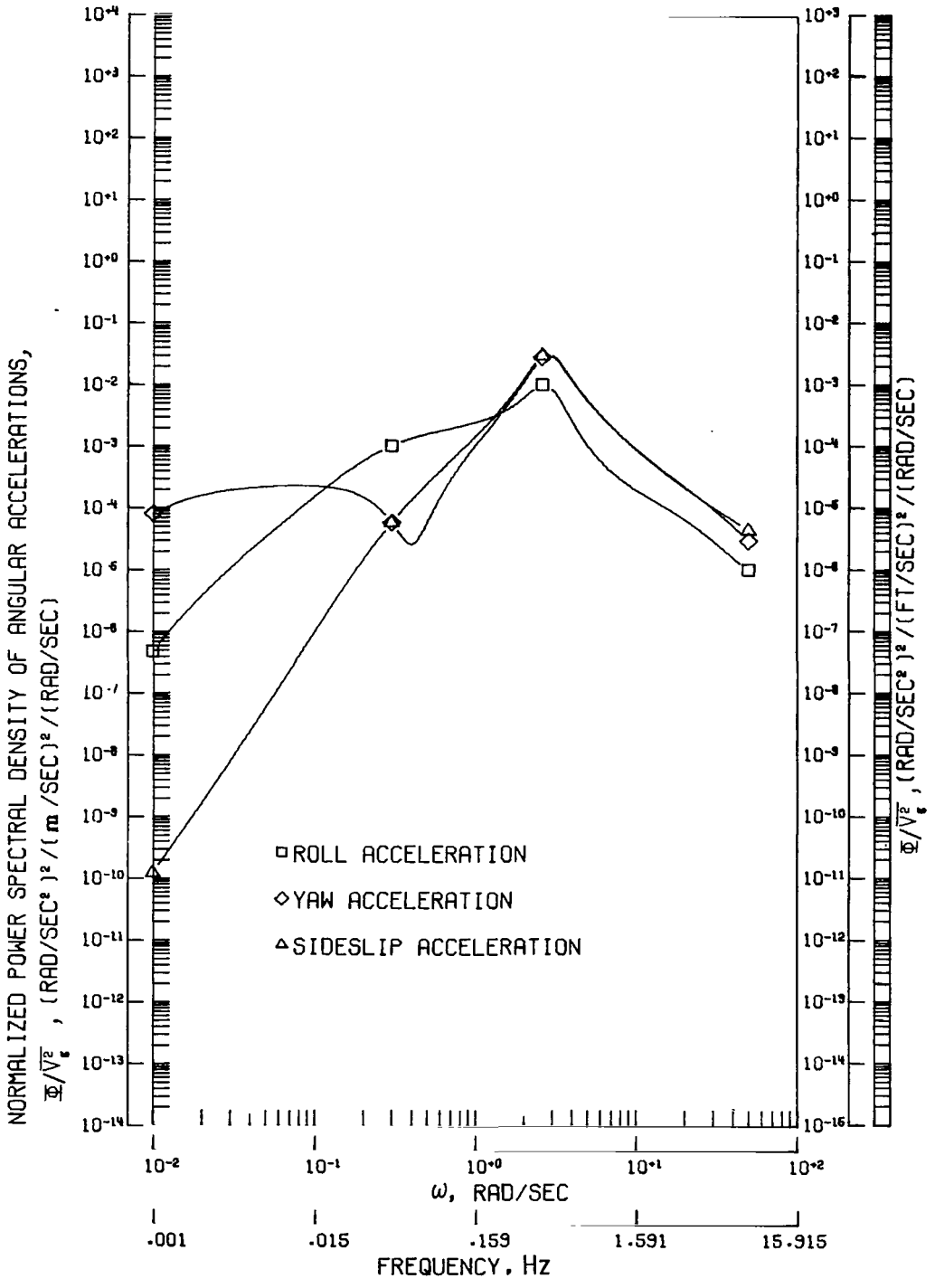


(c) Normalized power spectral density response for each lateral angular acceleration.

Figure 11.- Continued.

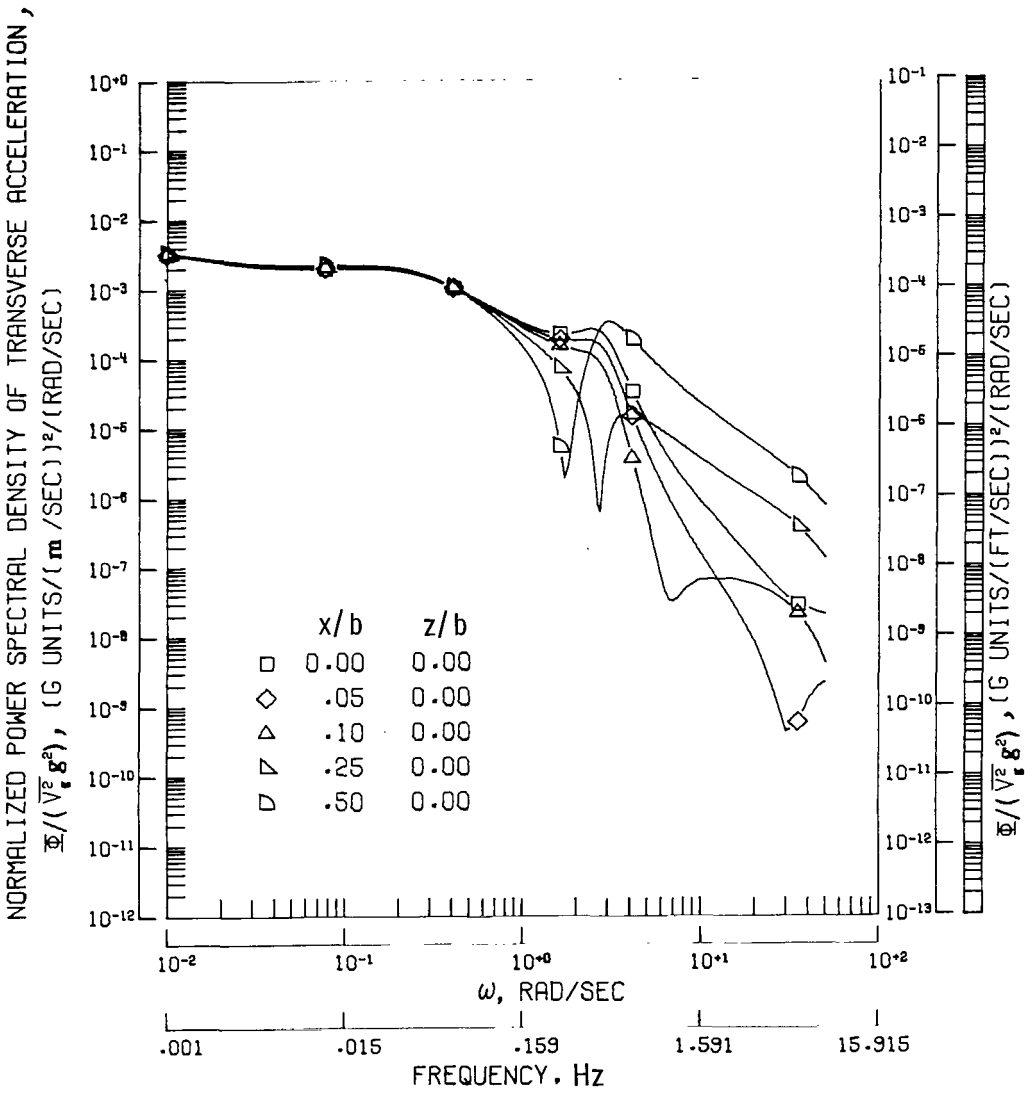


(d) Normalized power spectral density of transverse acceleration for locations forward of center of gravity.

Figure 11.- Continued.

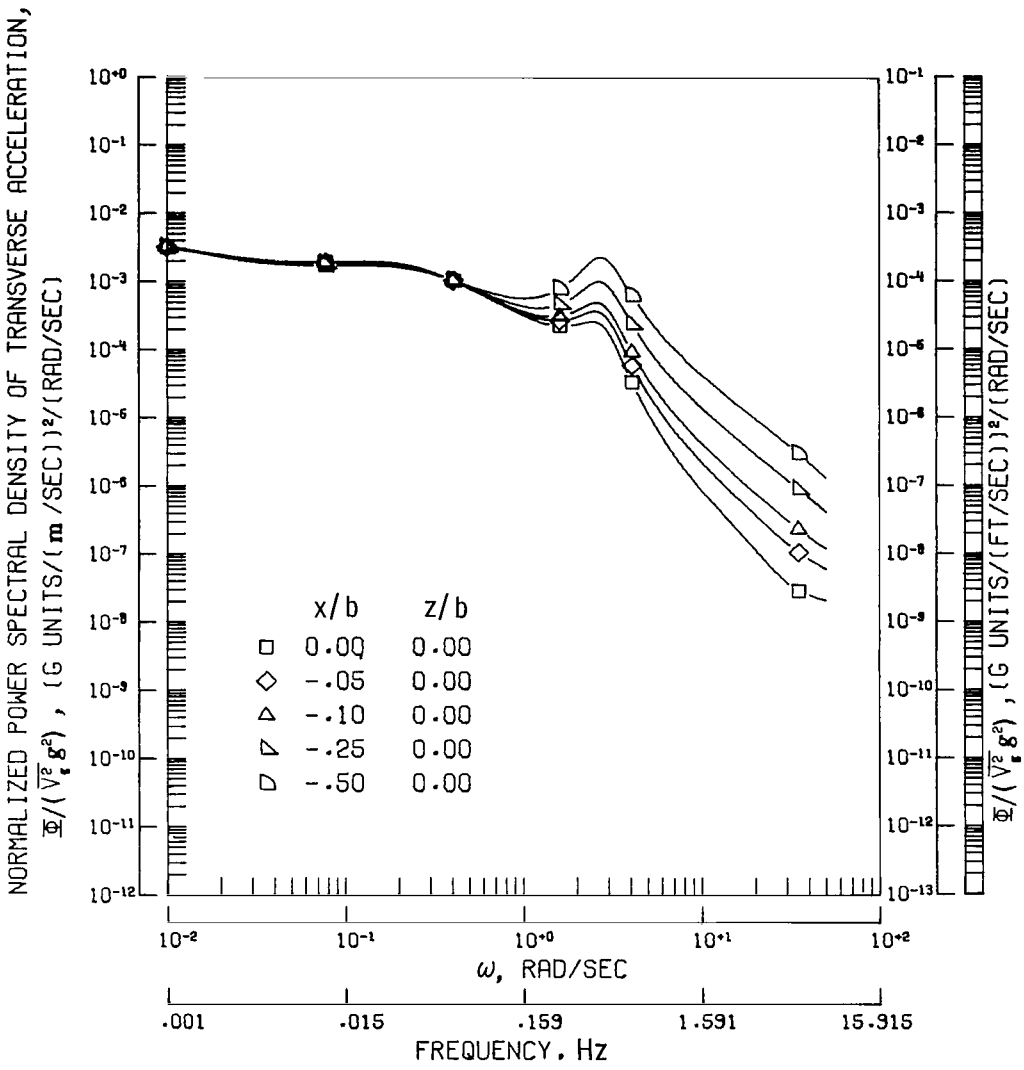


(e) Normalized power spectral density of transverse acceleration for locations rearward of center of gravity.

Figure 11.- Continued.

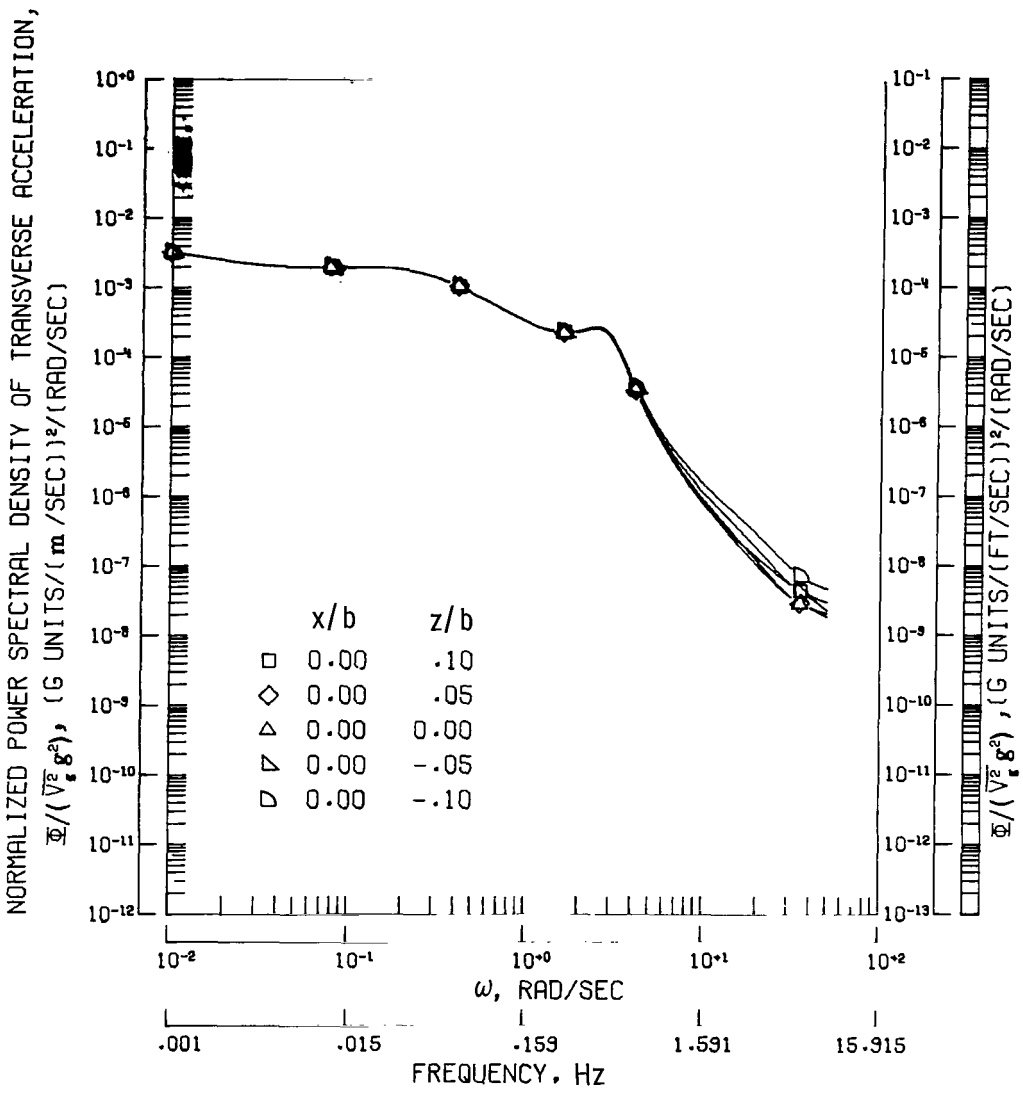


(f) Normalized power spectral density of transverse acceleration for several locations above and below center of gravity.

Figure 11.- Concluded.

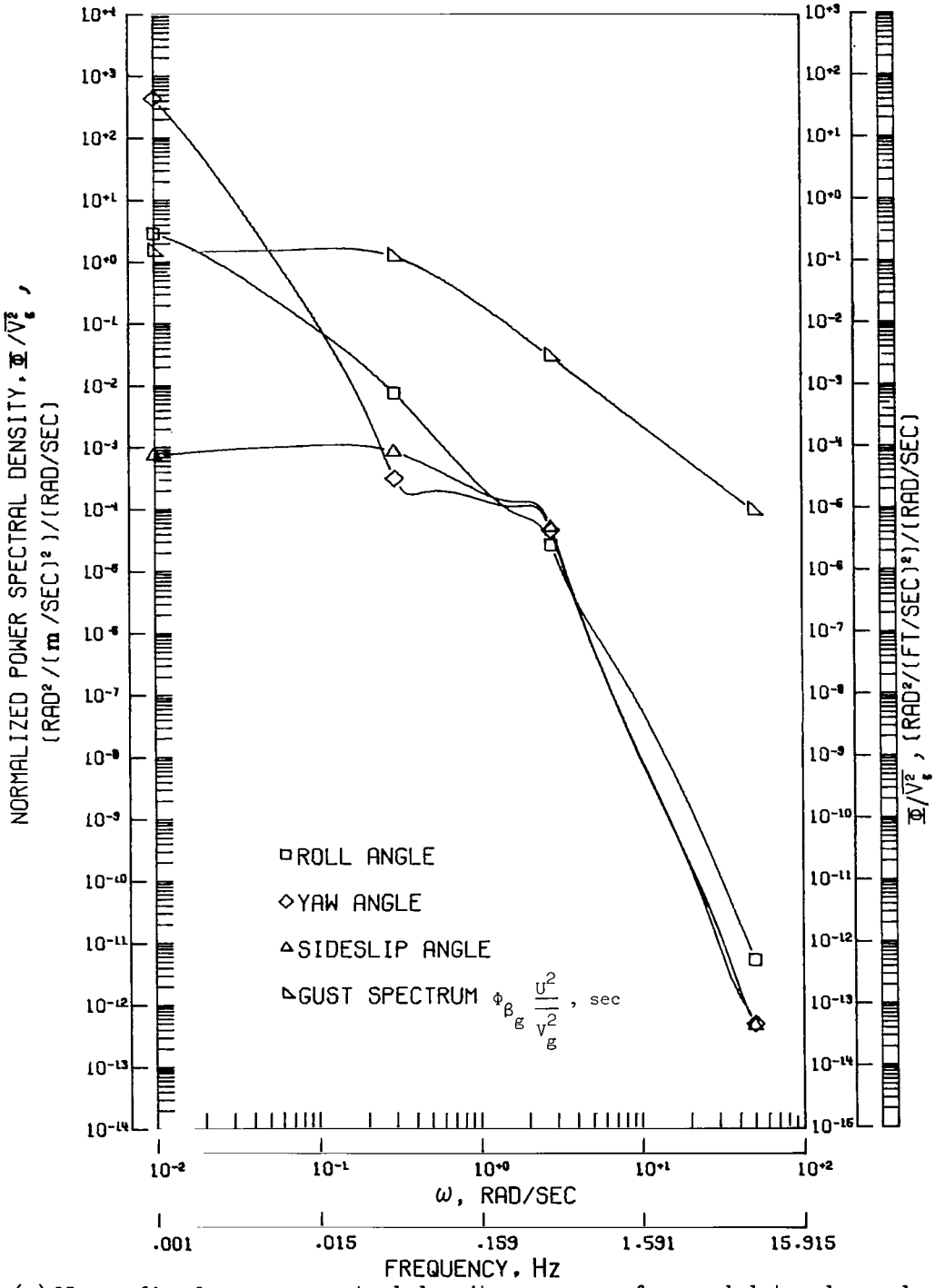


(a) Normalized power spectral density response for each lateral angular displacement.

Figure 12.- Response of airplane SS-D to random gusts for assumed scale length of 335.28 m (1100 ft). Note that units for gust spectrum are different from those for response spectra.

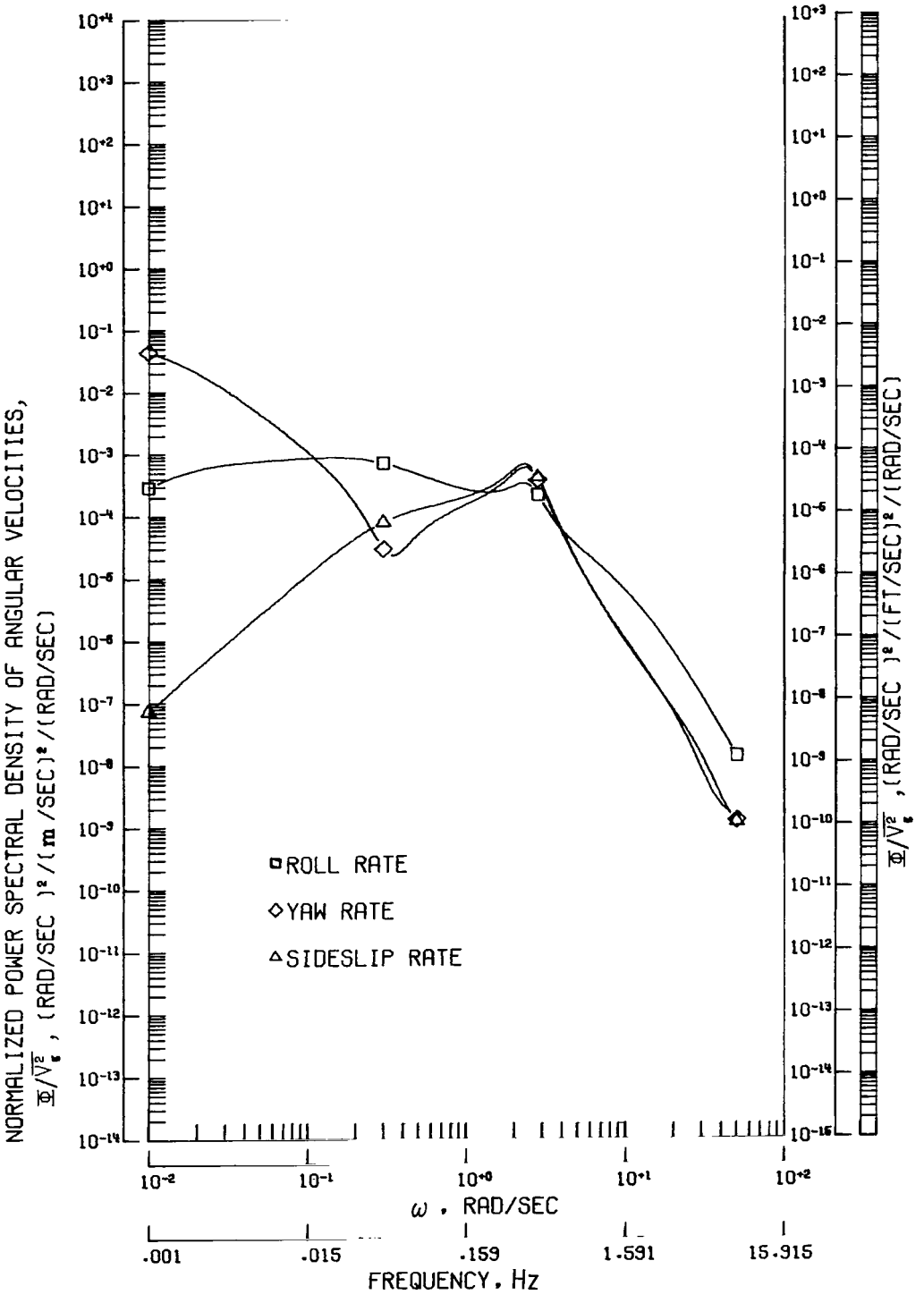


(b) Normalized power spectral density response for each lateral angular rate.

Figure 12.- Continued.

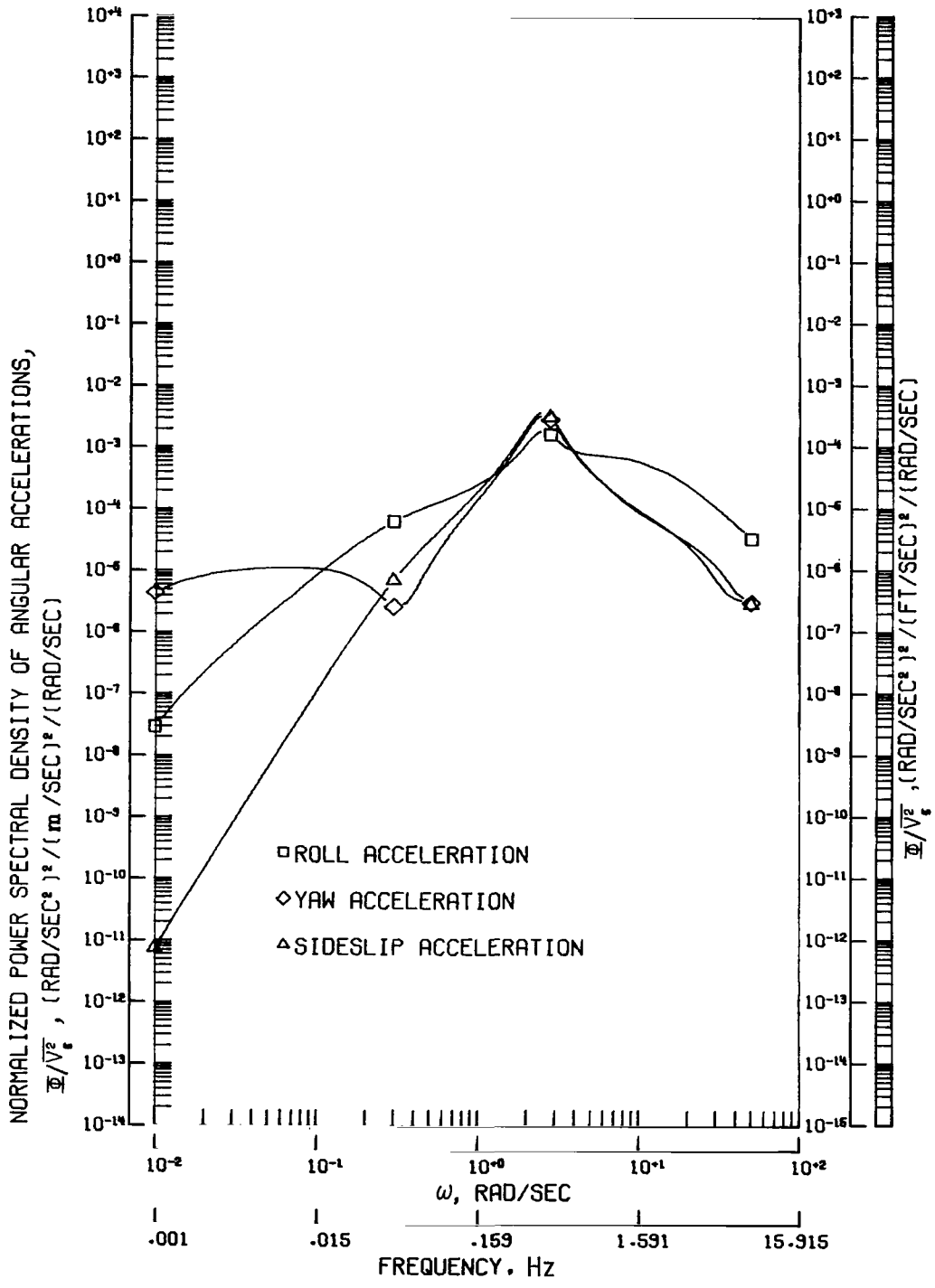


(c) Normalized power spectral density response for each lateral angular acceleration.

Figure 12.- Continued.

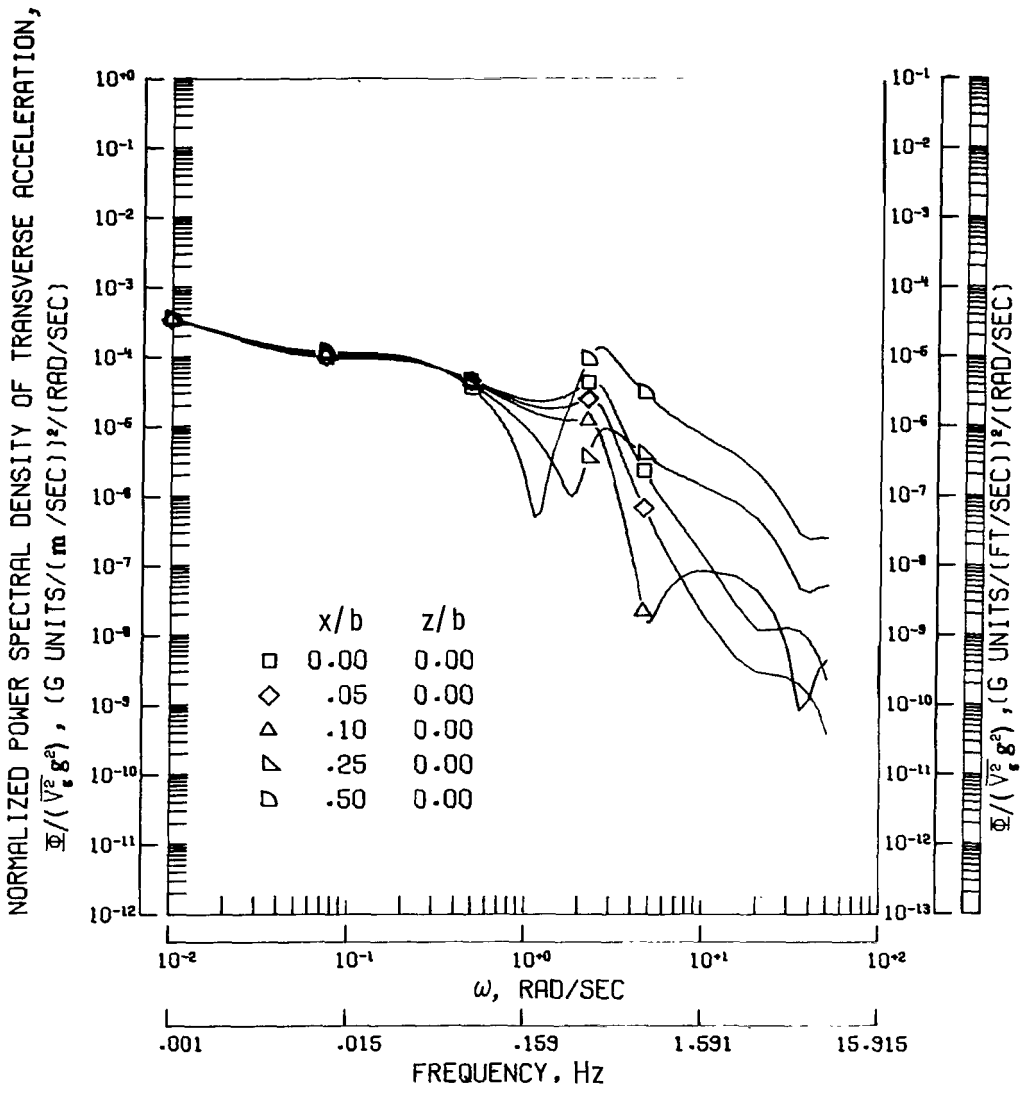


(d) Normalized power spectral density of transverse acceleration for locations forward of center of gravity.

Figure 12.- Continued.

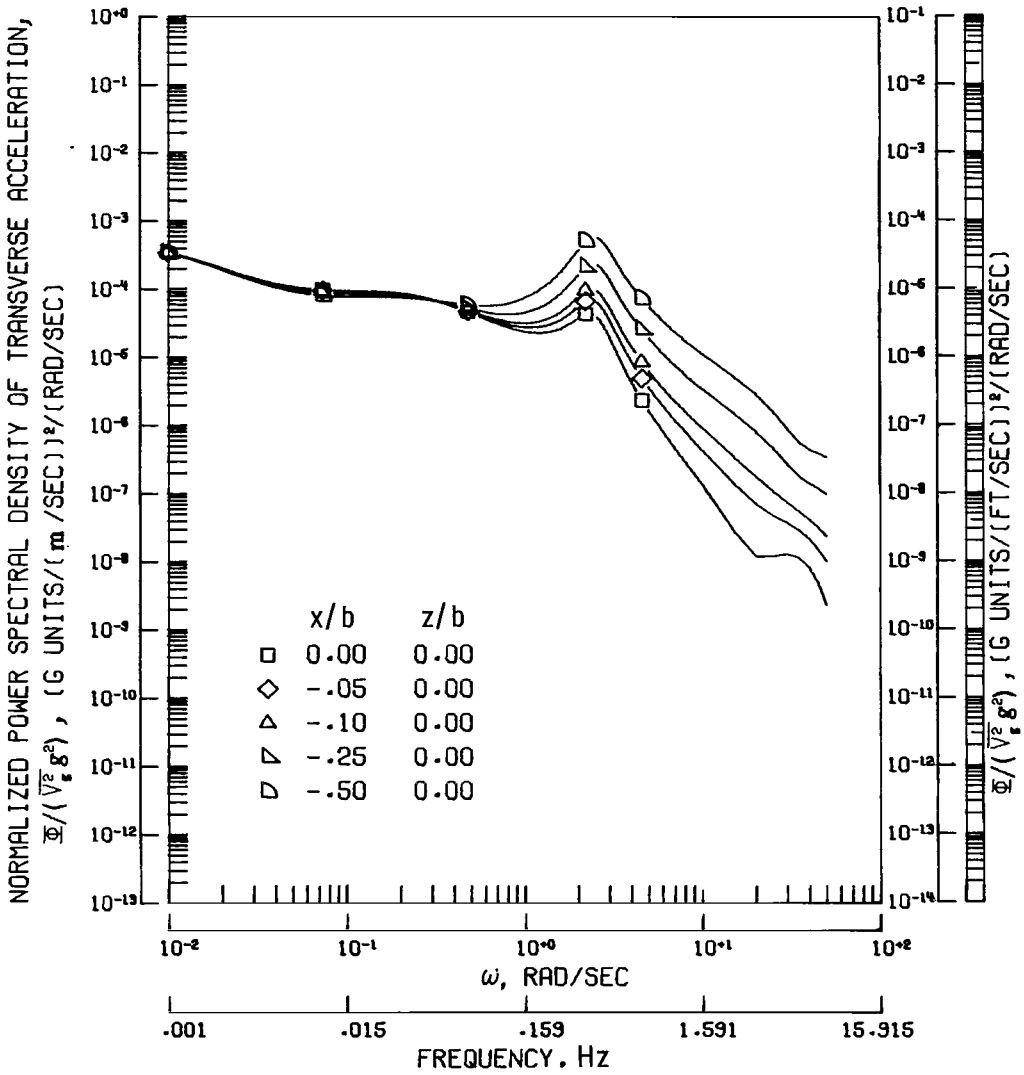


(e) Normalized power spectral density of transverse acceleration for locations rearward of center of gravity.

Figure 12.- Continued.

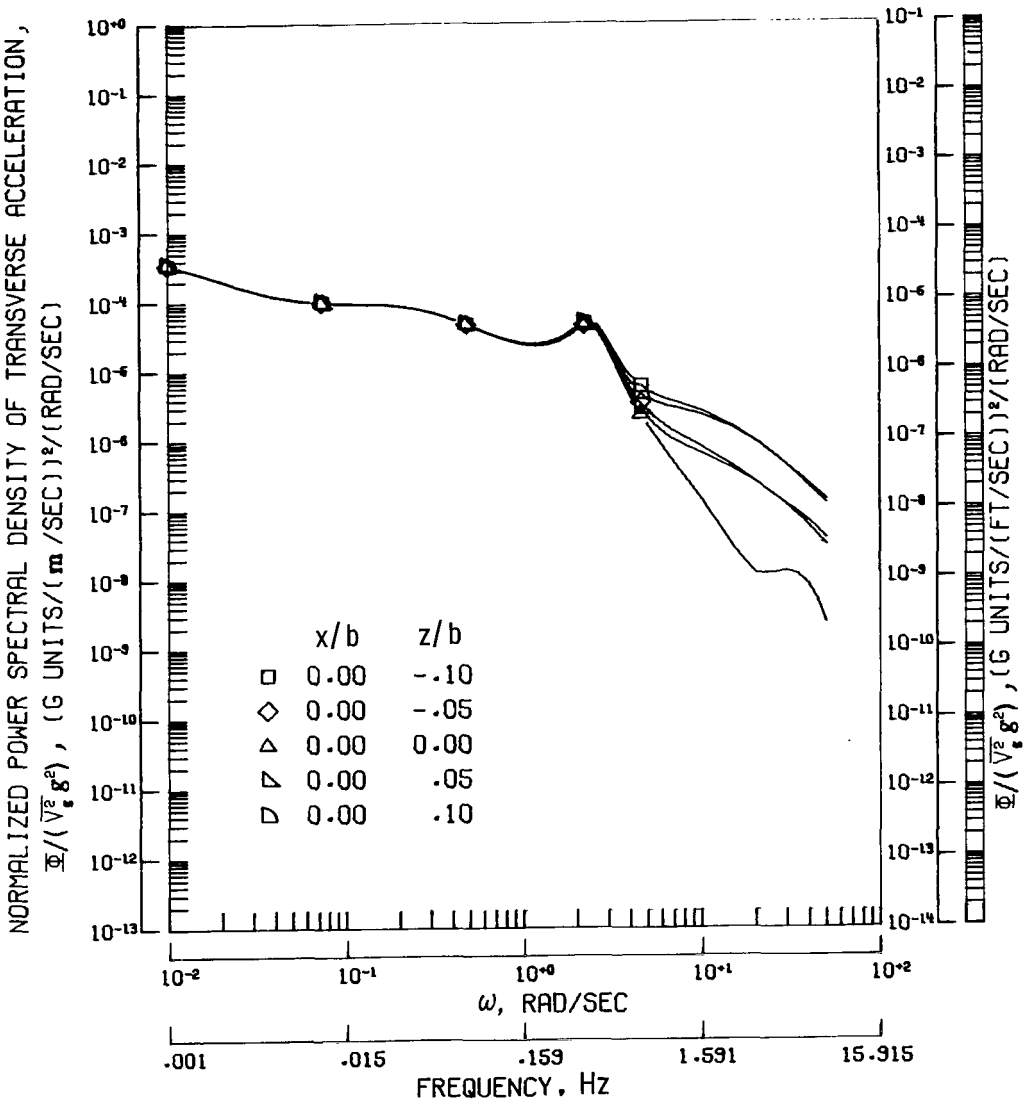


(f) Normalized power spectral density of transverse acceleration for several locations above and below center of gravity.

Figure 12.- Concluded.

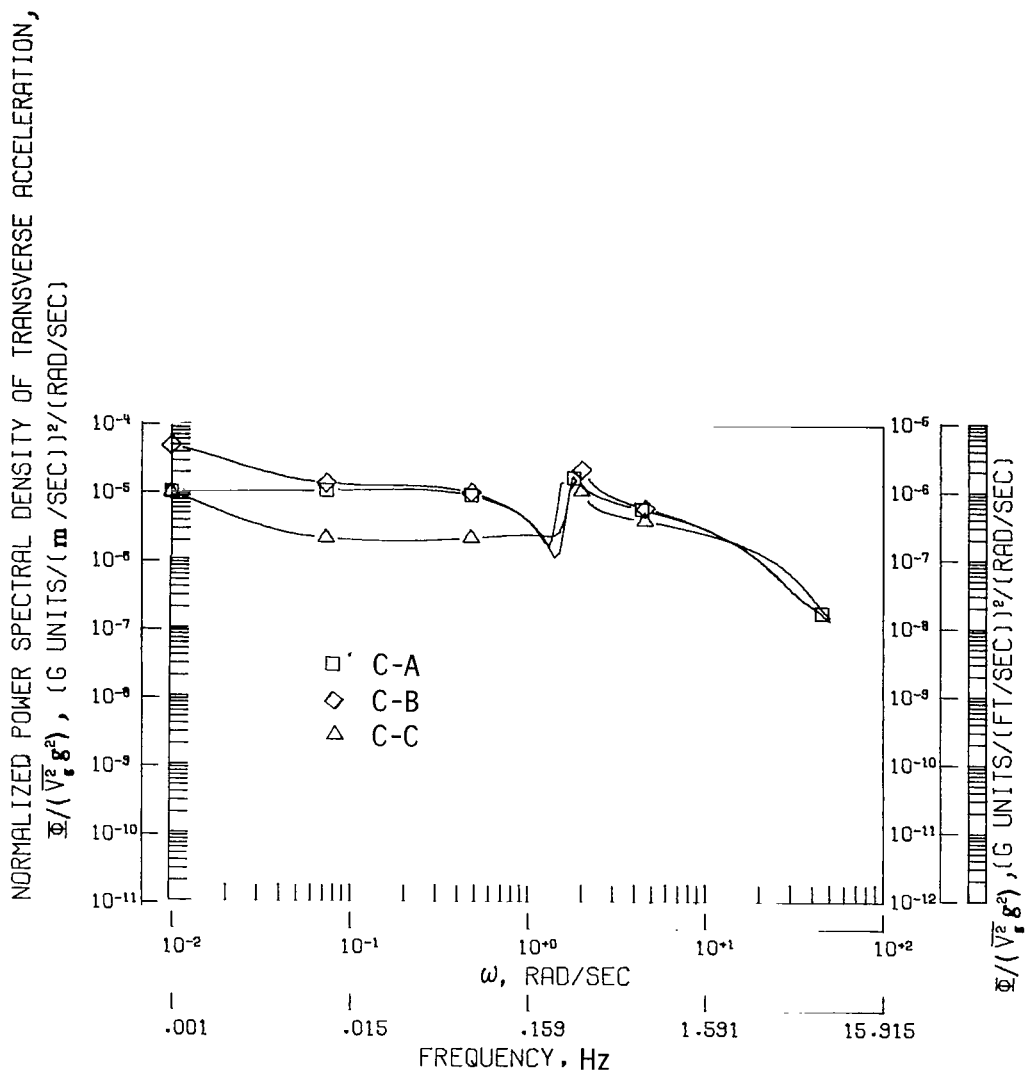


(a) Pilot position.

Figure 13.- Comparison of power spectra of transverse acceleration for conventional airplanes at three locations.

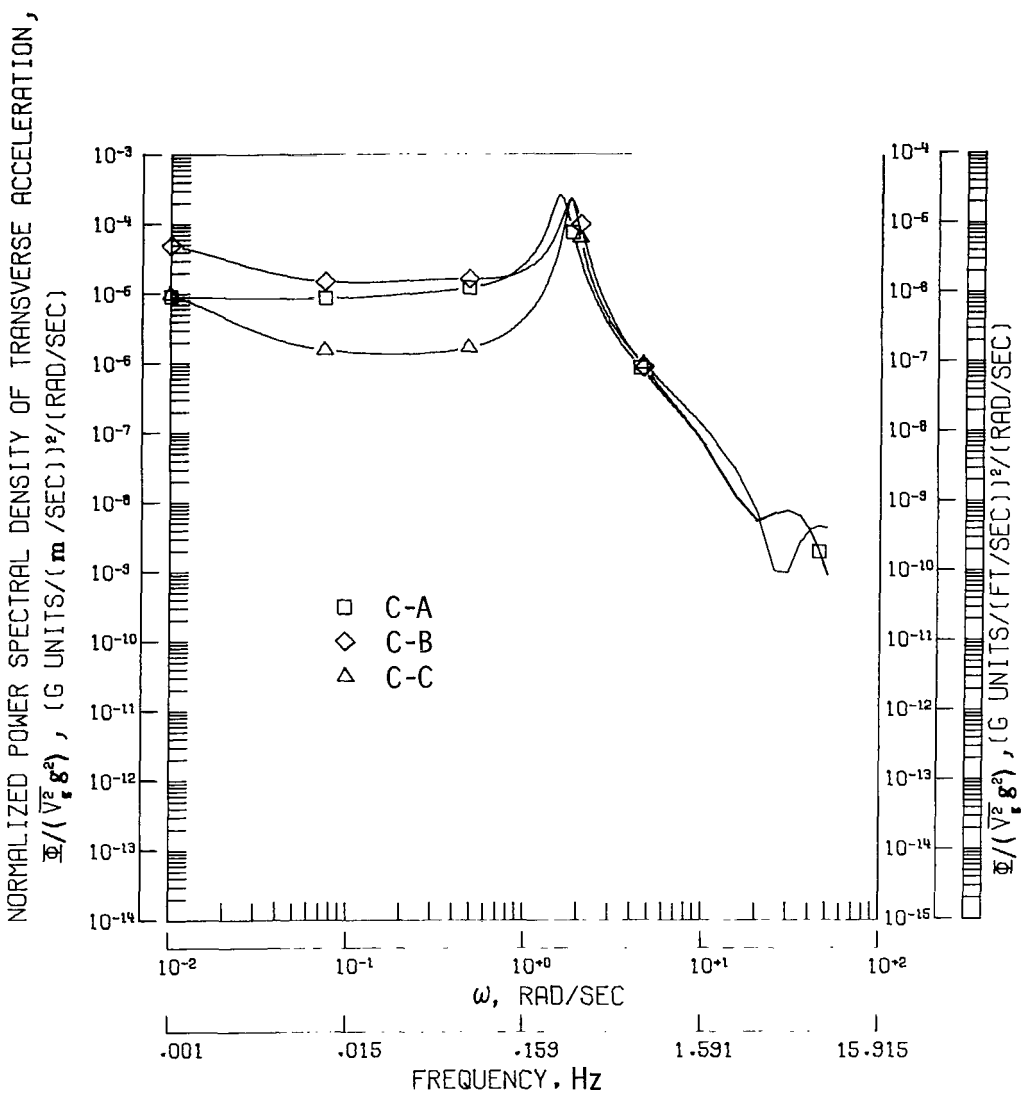


(b) Center of gravity.

Figure 13.- Continued.

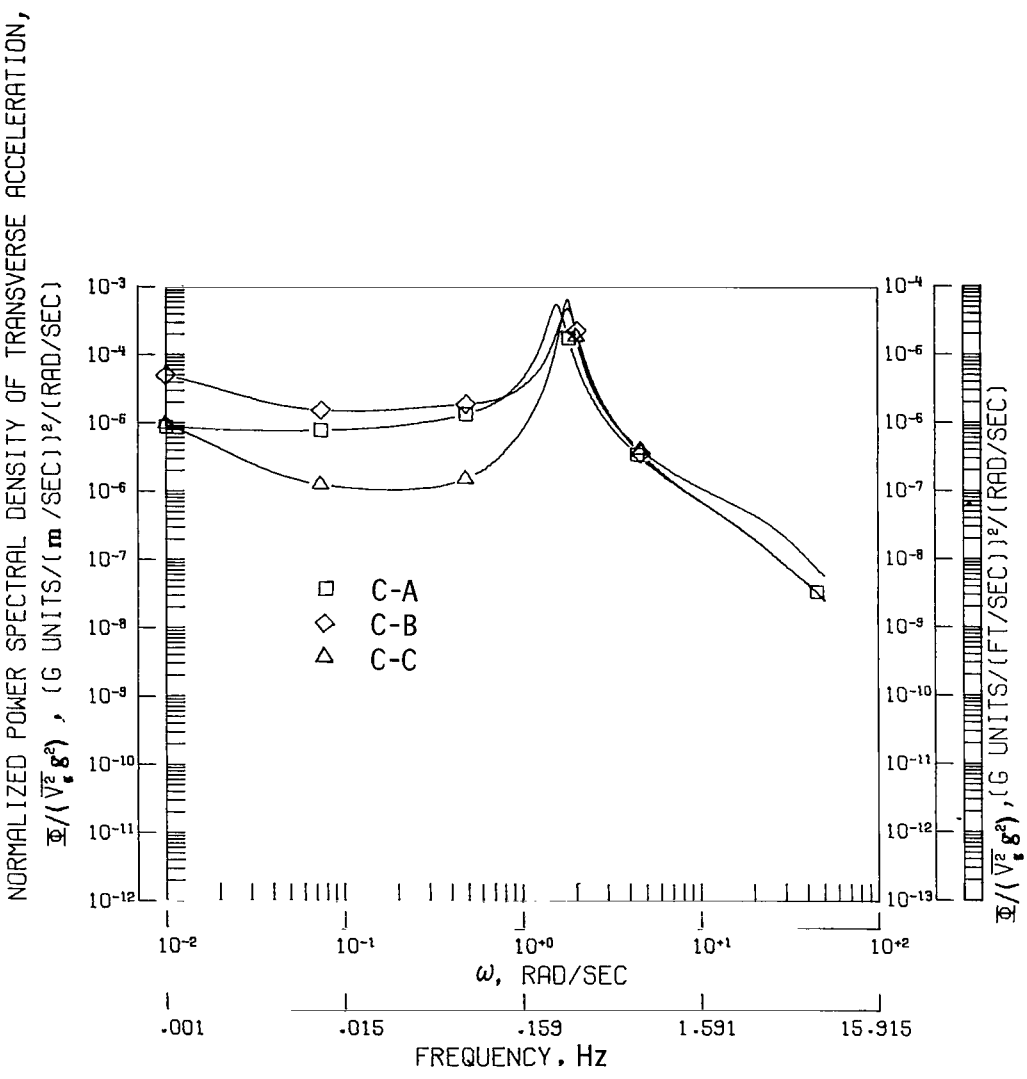


(c) Rear passenger position.

Figure 13.- Concluded.

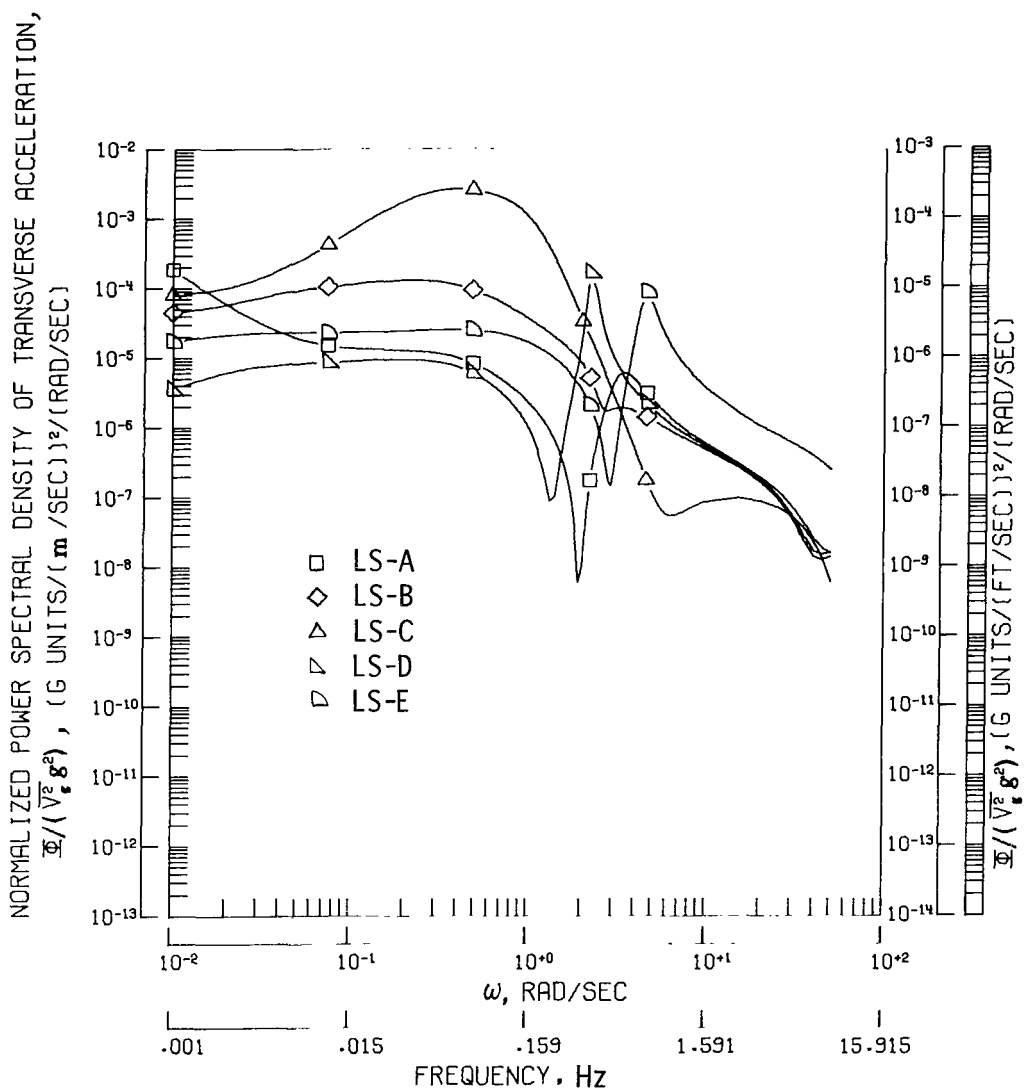


(a) Pilot position.

Figure 14.- Comparison of power spectra of transverse acceleration for large STOL airplanes at three locations.

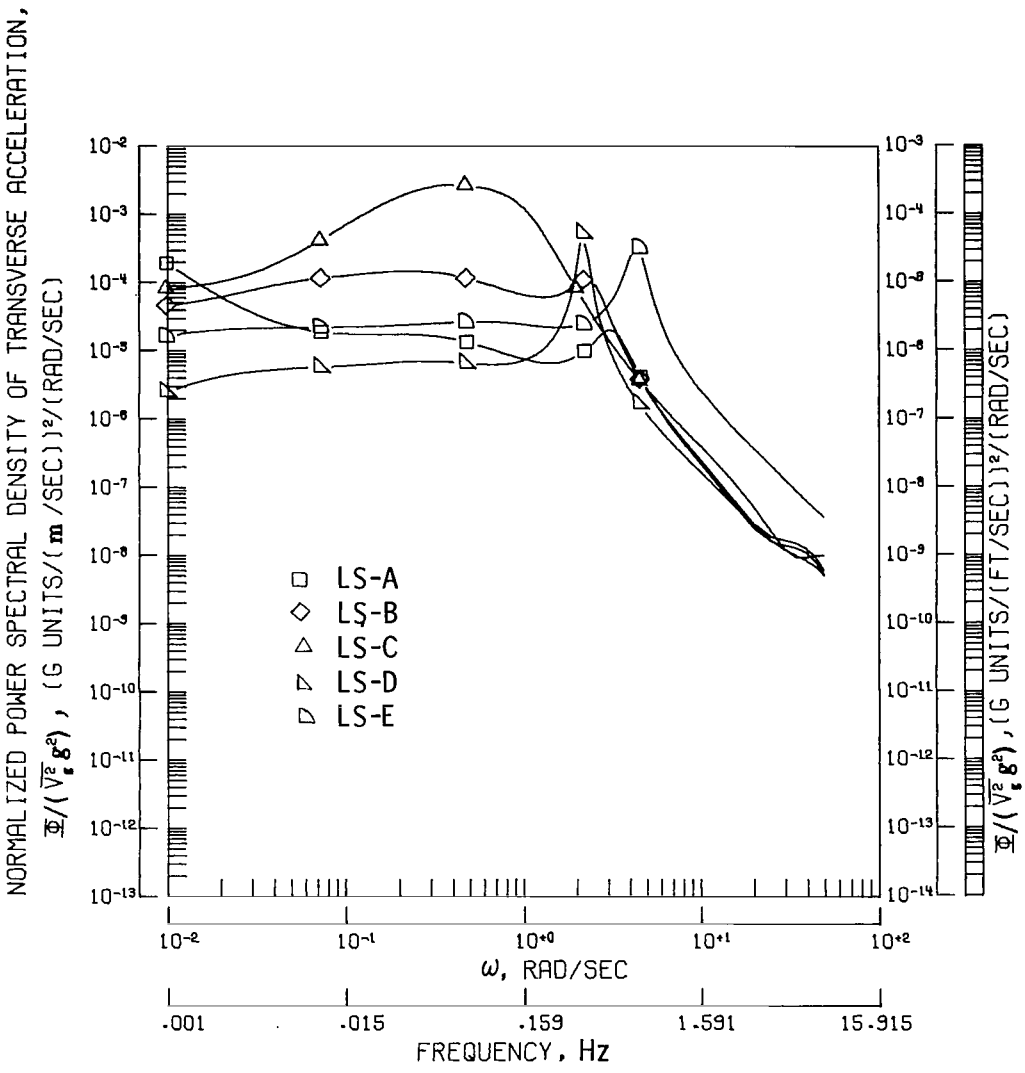


(b) Center of gravity.

Figure 14.- Continued.

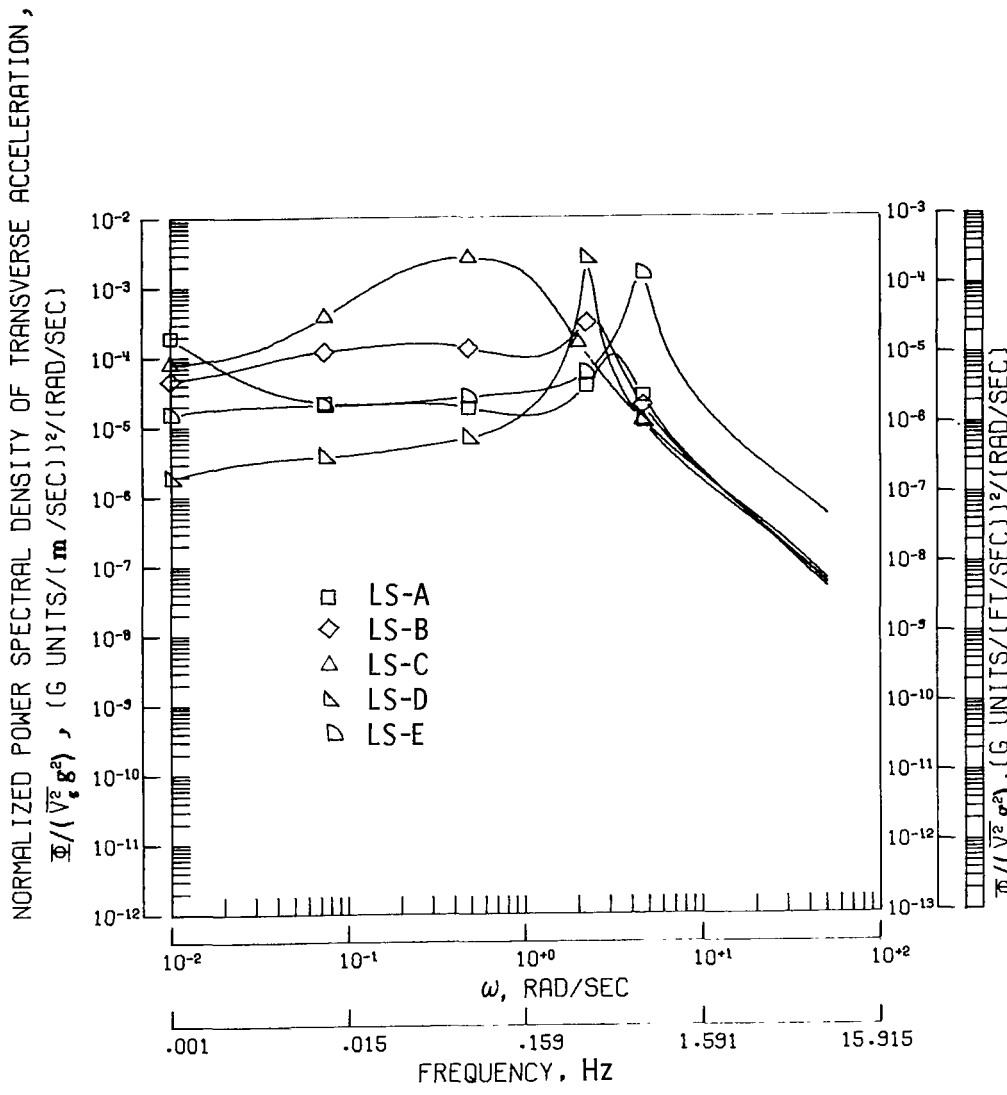


(c) Rear passenger position.

Figure 14.- Concluded.

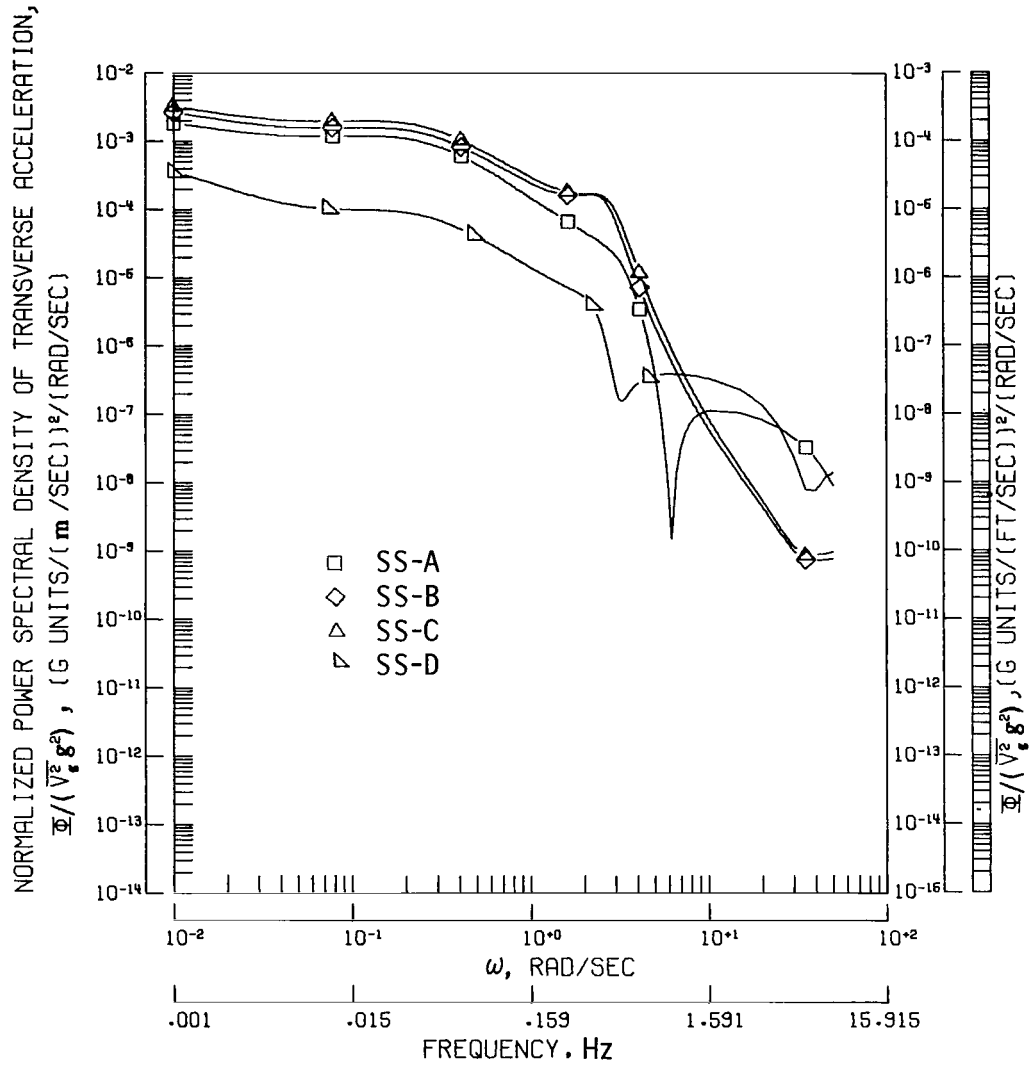


(a) Pilot position.

Figure 15.- Comparison of power spectra of transverse acceleration for small STOL airplanes at three locations.

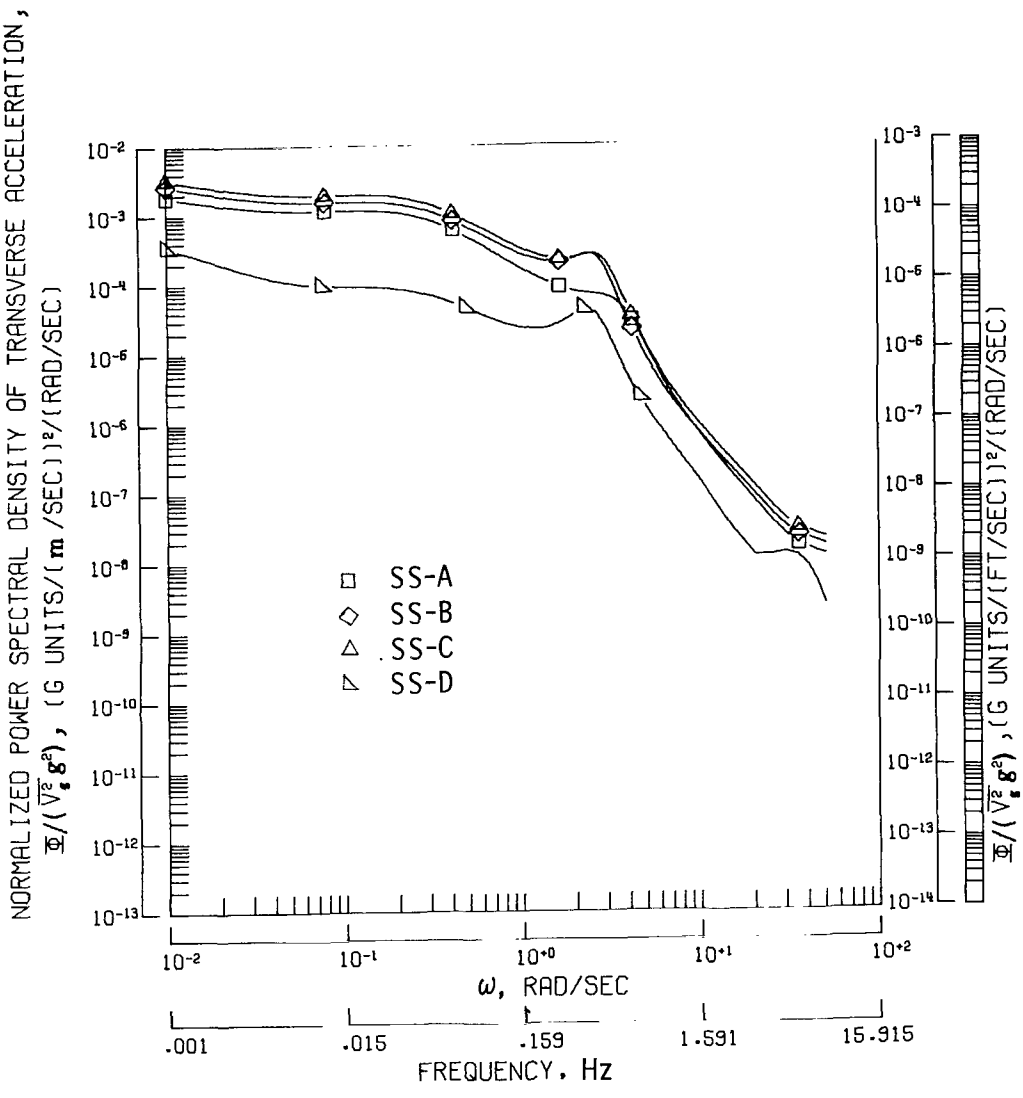


(b) Center of gravity.

Figure 15.- Continued.

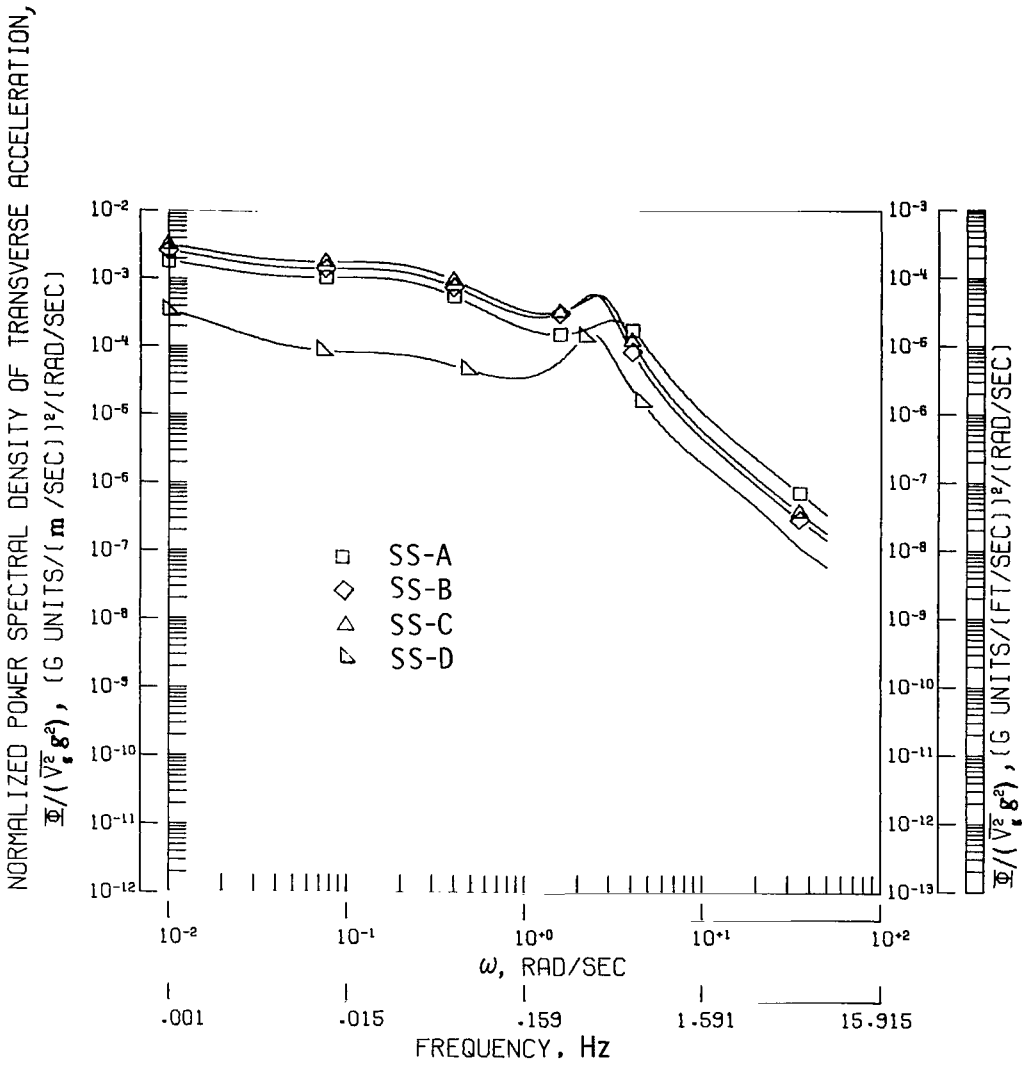


(c) Rear passenger position.

Figure 15.- Concluded.

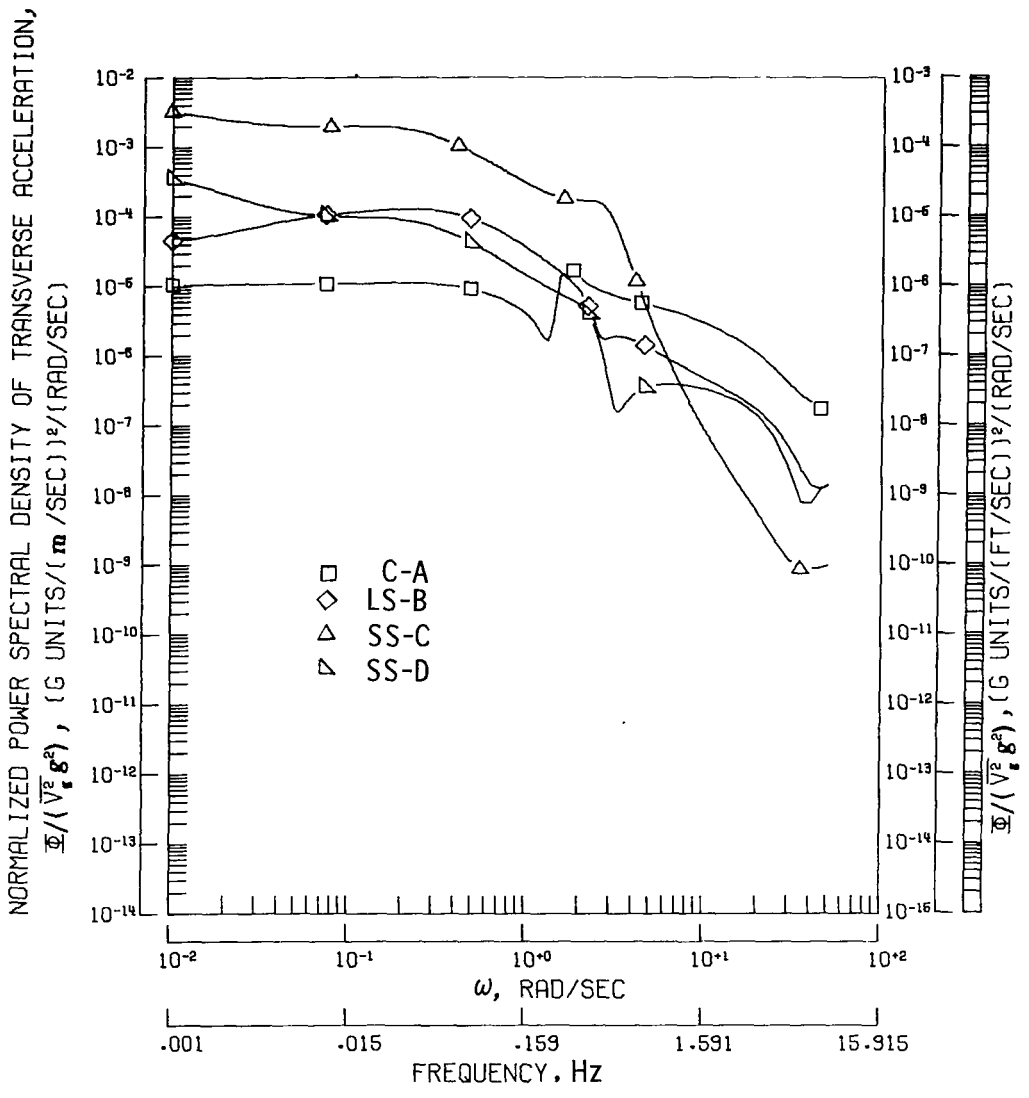


(a) Pilot position.

Figure 16.- Comparison of power spectra of transverse acceleration for several representative airplanes at three locations.

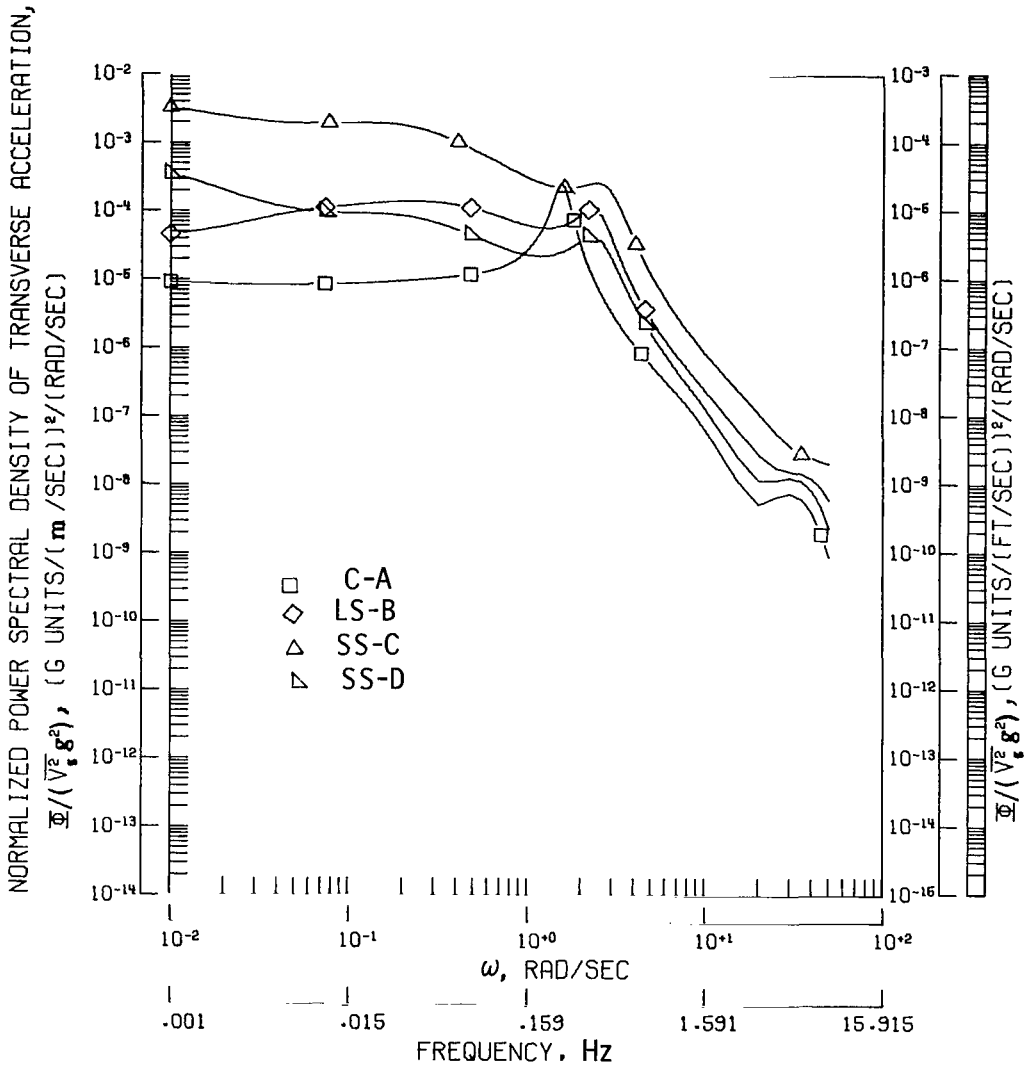


(b) Center of gravity.

Figure 16.- Continued.

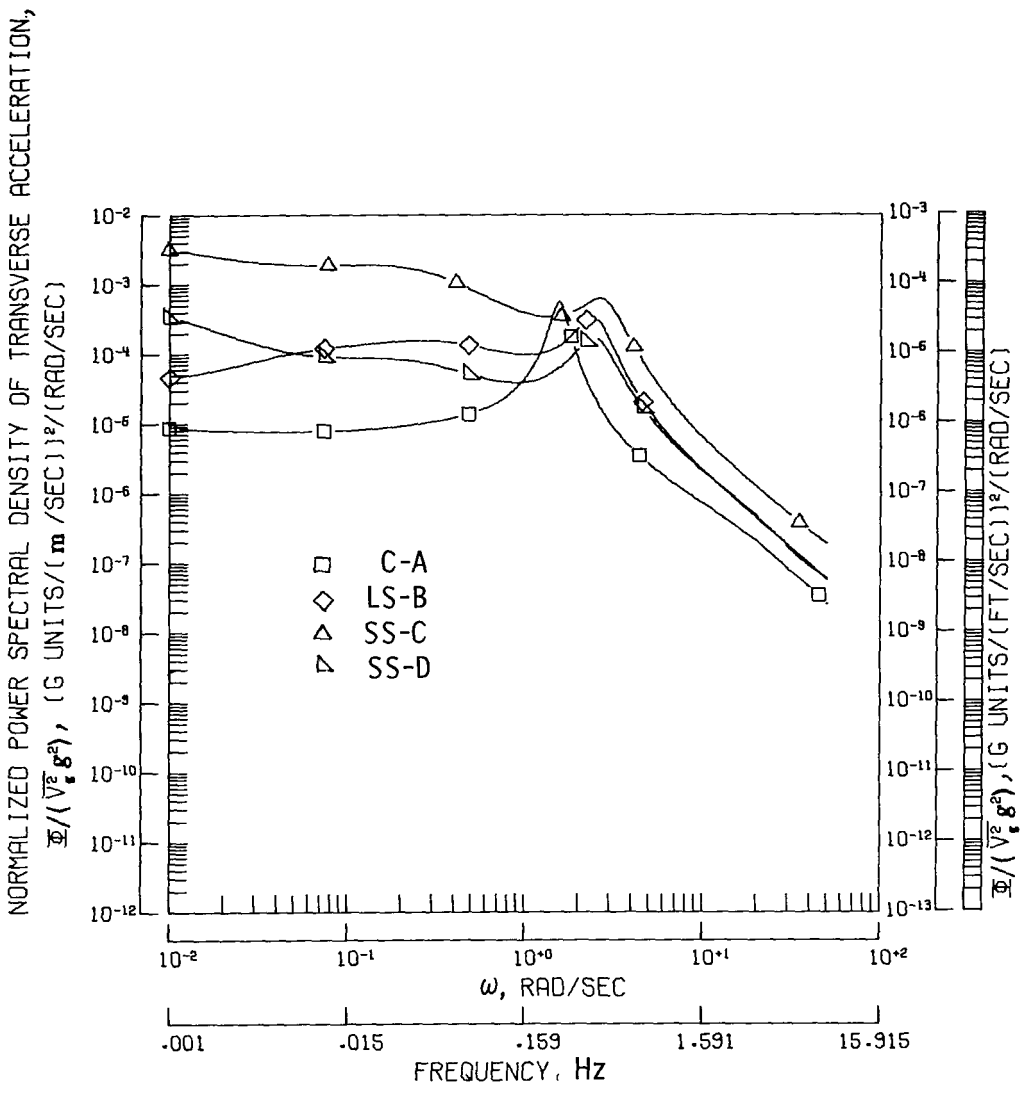


(c) Rear passenger position.

Figure 16.- Concluded.

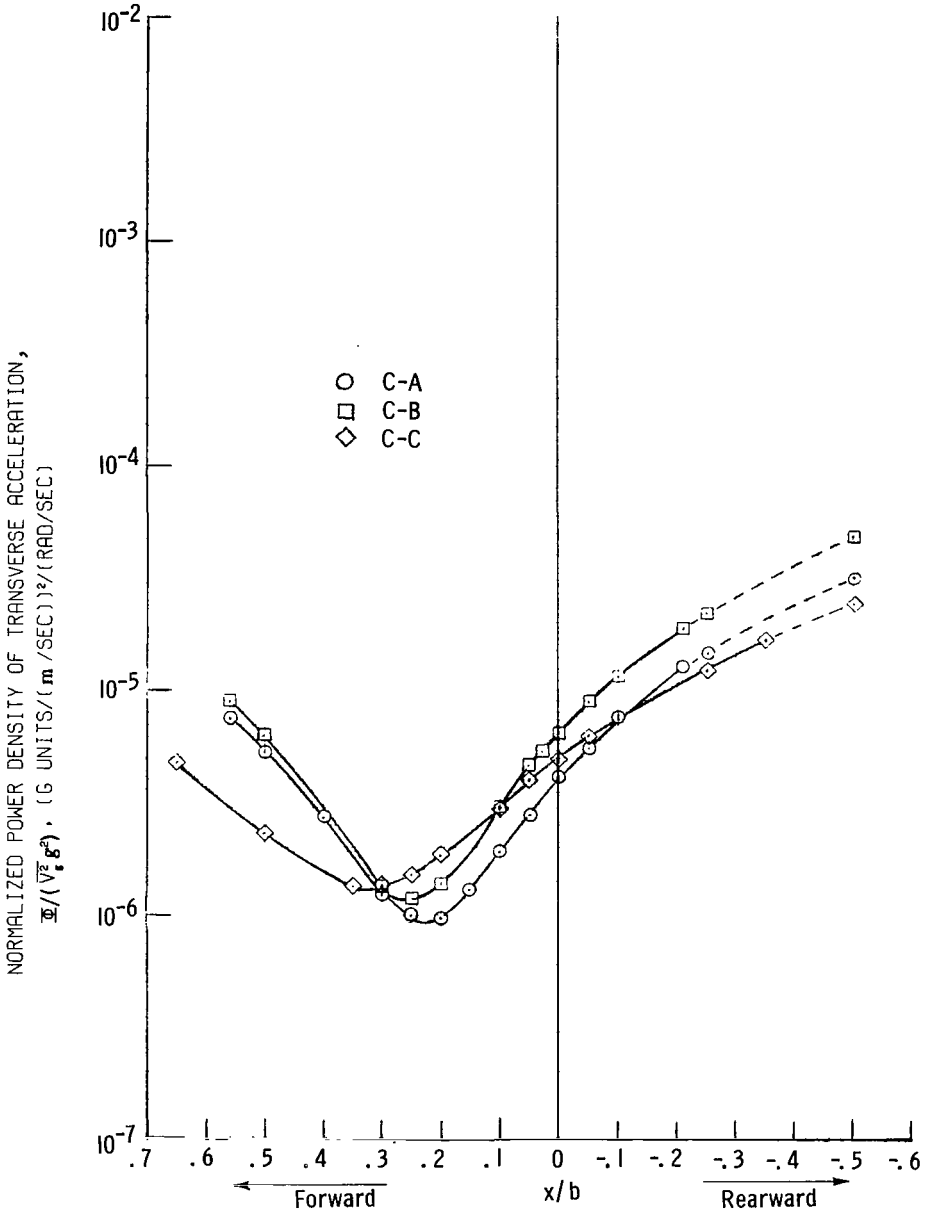


(a) Conventional airplanes.

Figure 17.- Variation of power spectrum of transverse acceleration with longitudinal location for various airplanes at 0.45 Hz. Solid-line curve represents spread in possible seating locations on airplane. Dash-line curve represents extrapolation to arbitrary limit 0.5x/b.

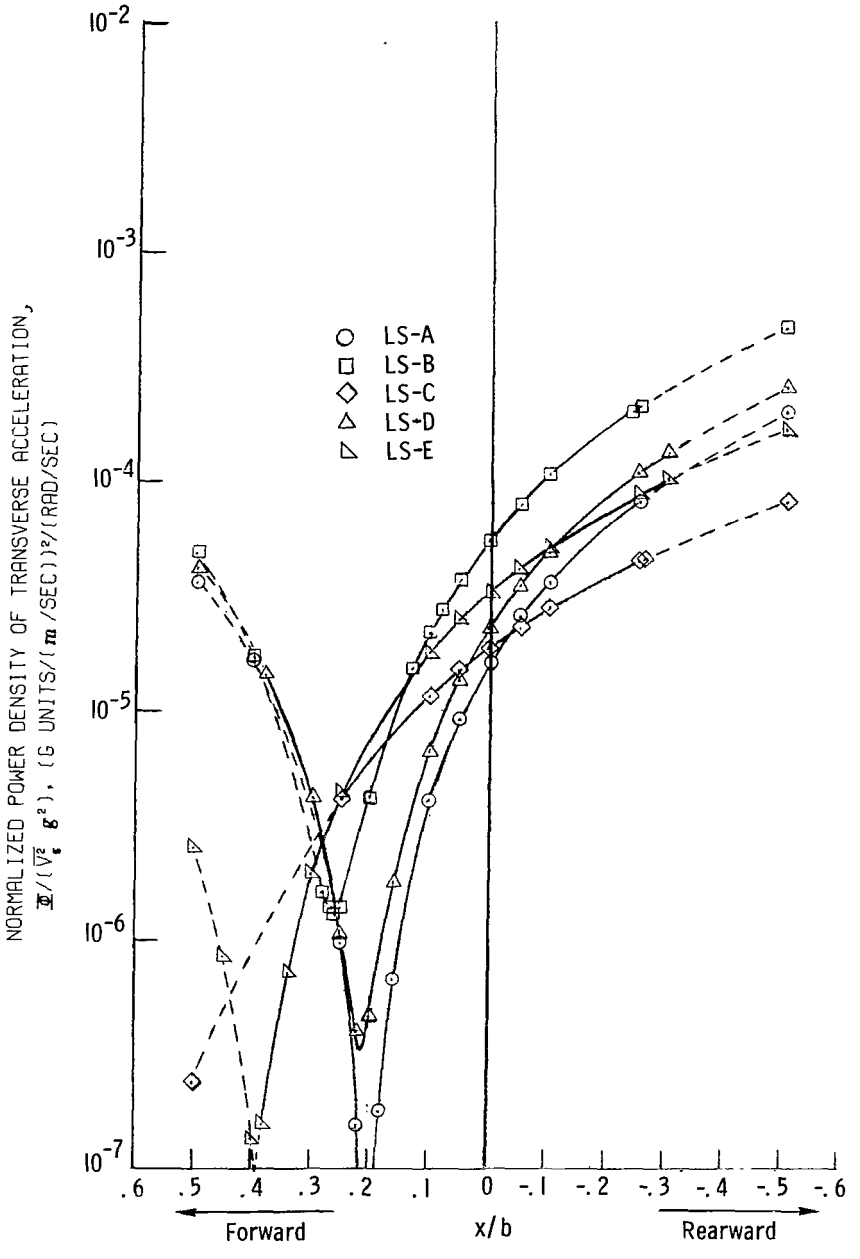


(b) Large STOL airplanes.

Figure 17.- Continued.

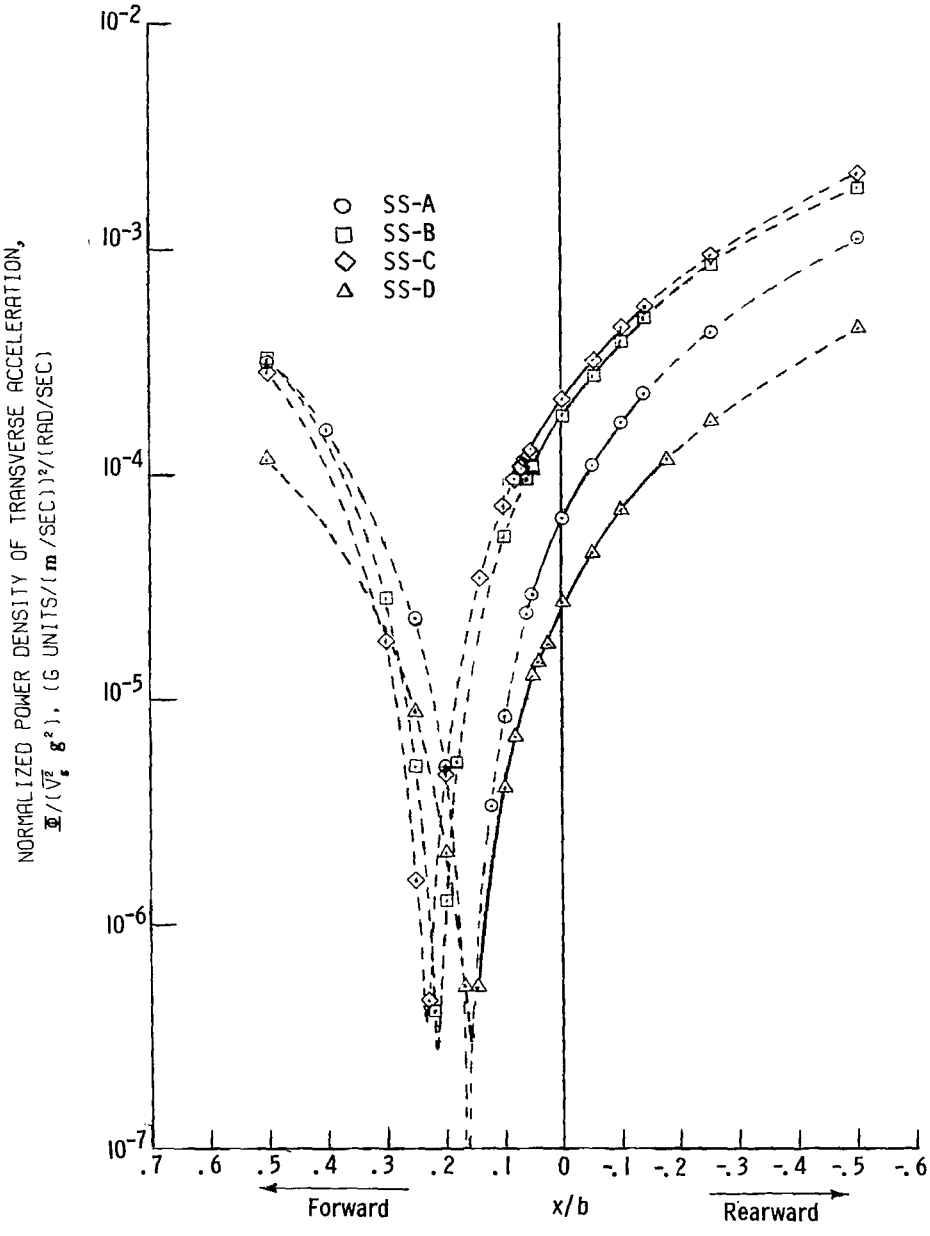


(c) Small STOL airplanes.

Figure 17.- Concluded.

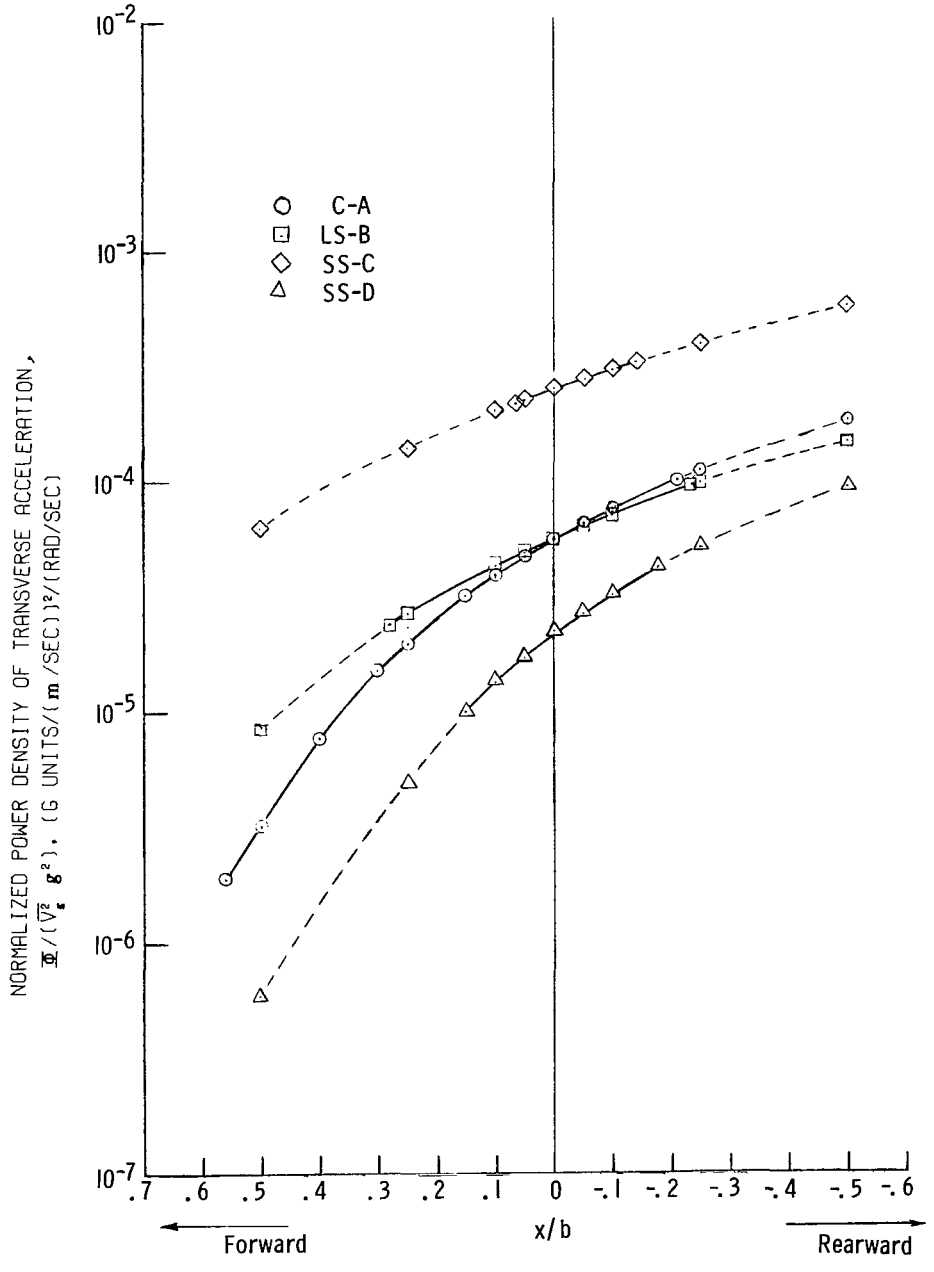


(a) 0.2 Hz.

Figure 18.- Variation of power spectrum of transverse acceleration with longitudinal location for several representative airplanes at four frequencies. Solid-line curve represents spread in possible seating locations on airplane. Dash-line curve represents extrapolation to arbitrary limit 0.5x/b.

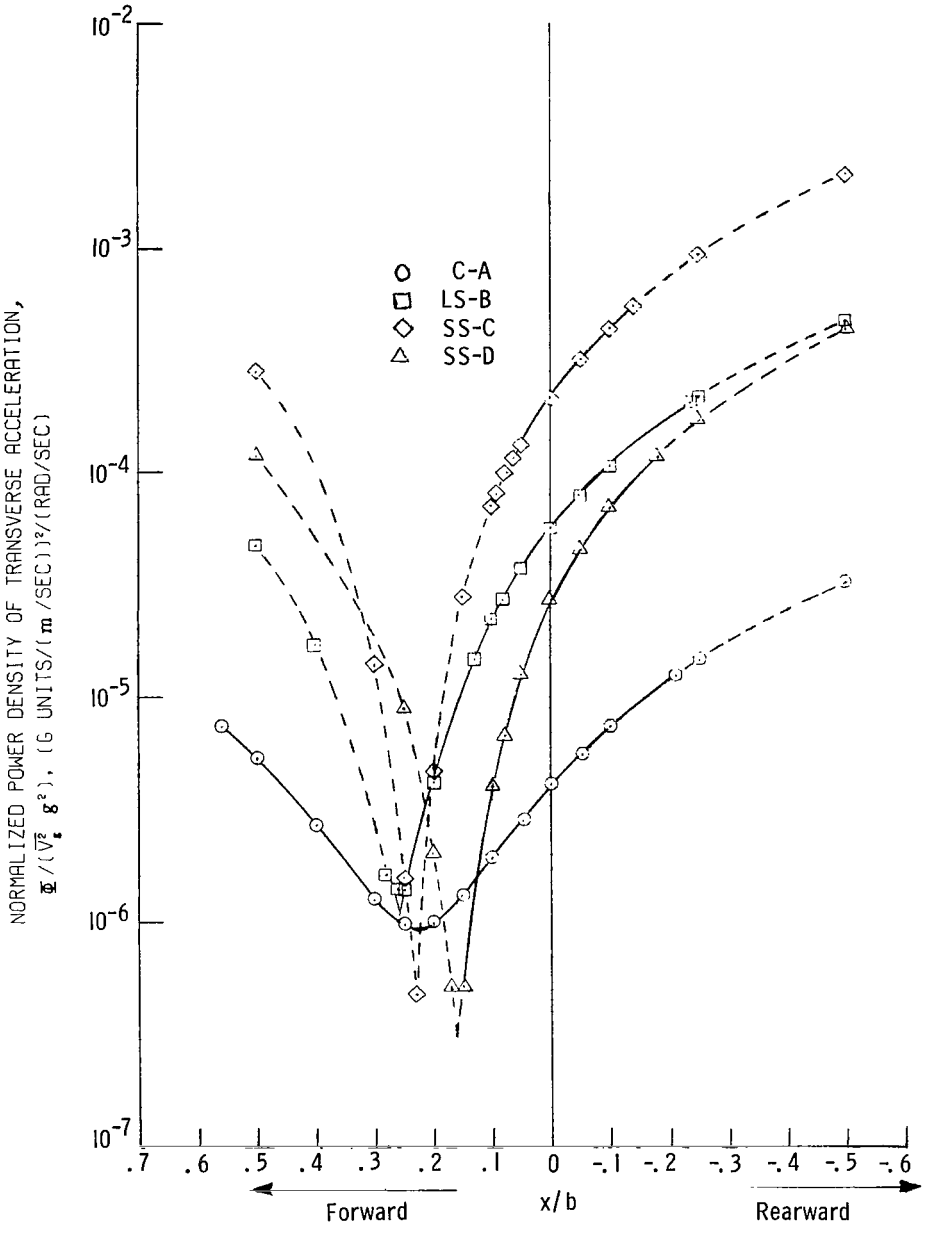


(b) 0.45 Hz.

Figure 18.- Continued.

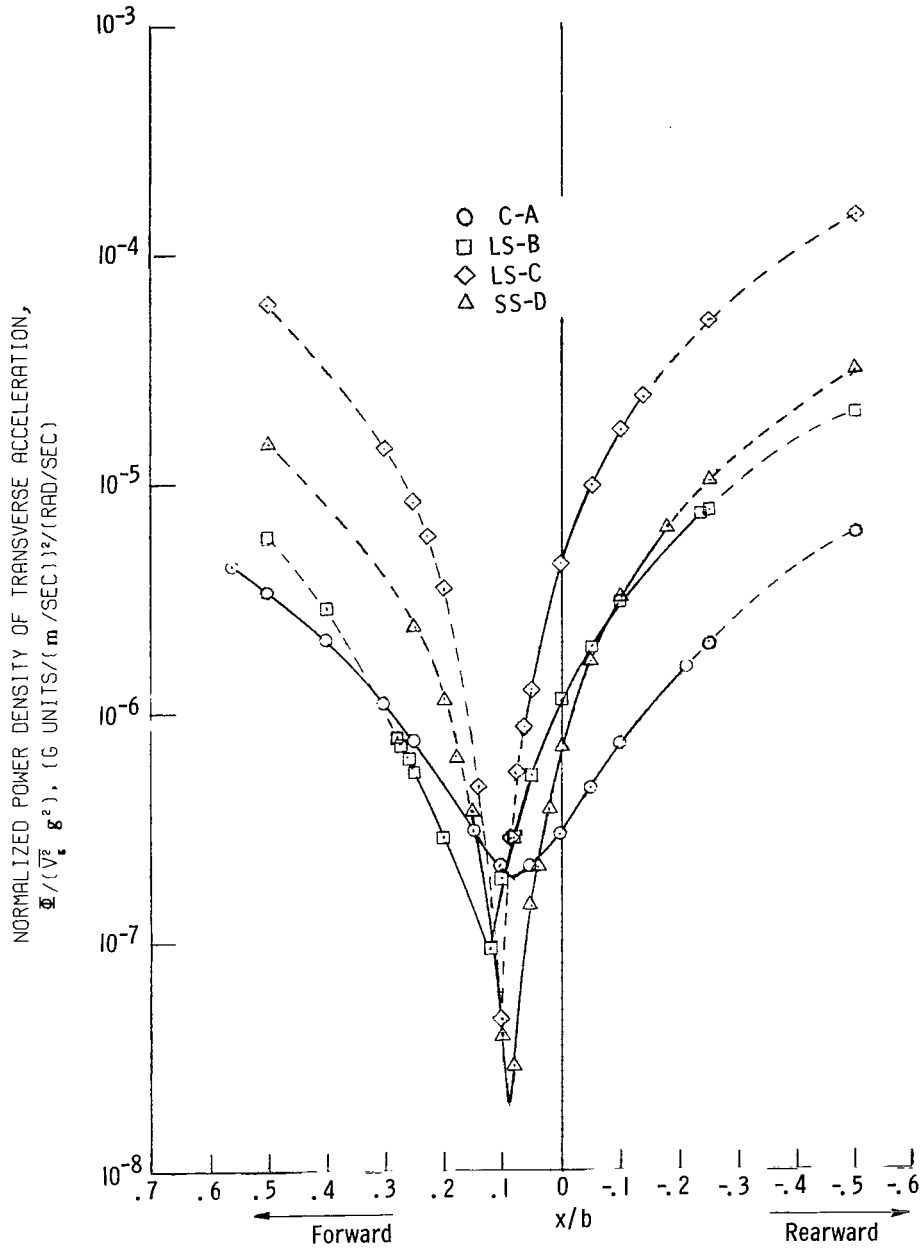


(c) 1.00 Hz.

Figure 18.- Continued.

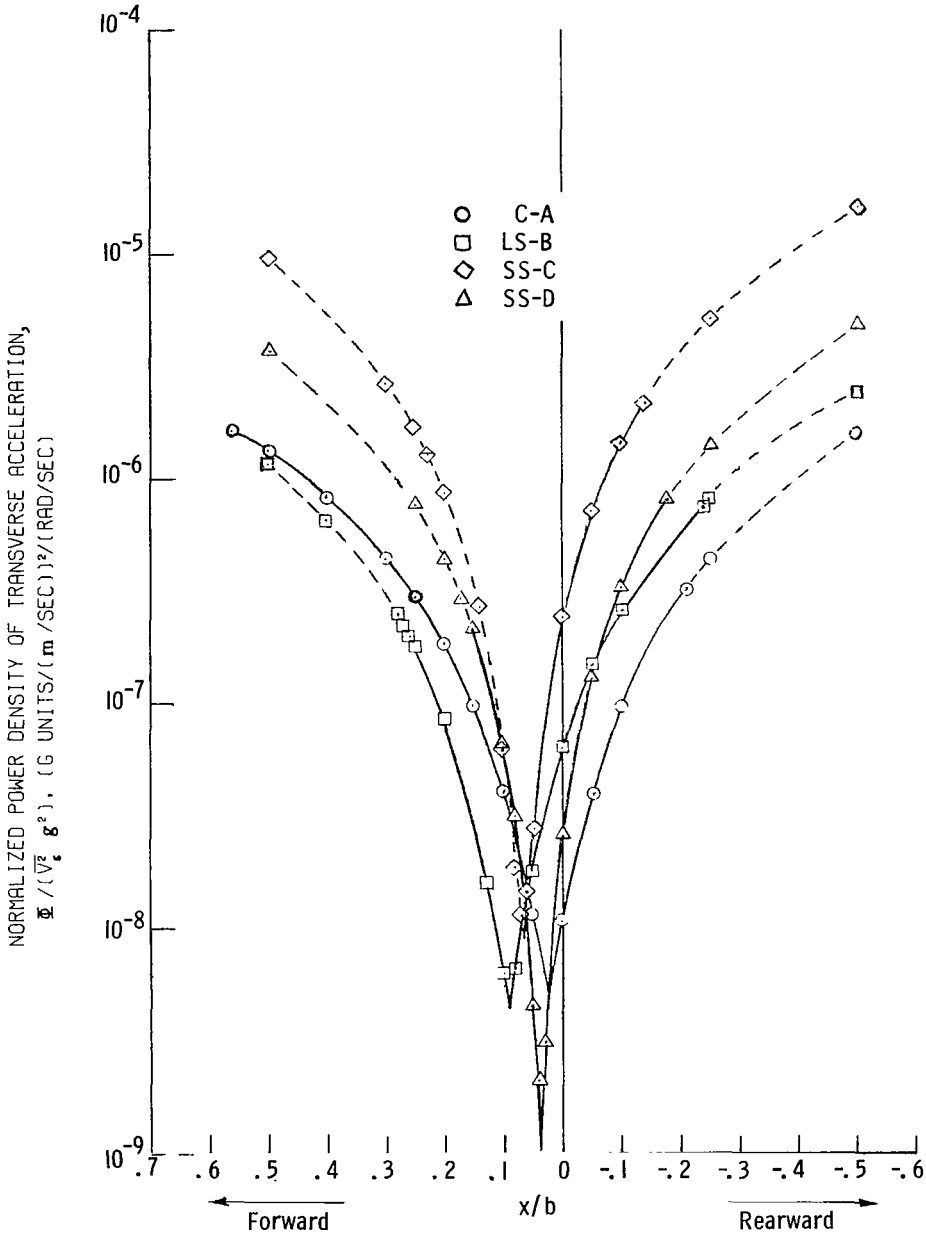


(d) 2.42 Hz.

Figure 18.- Concluded.

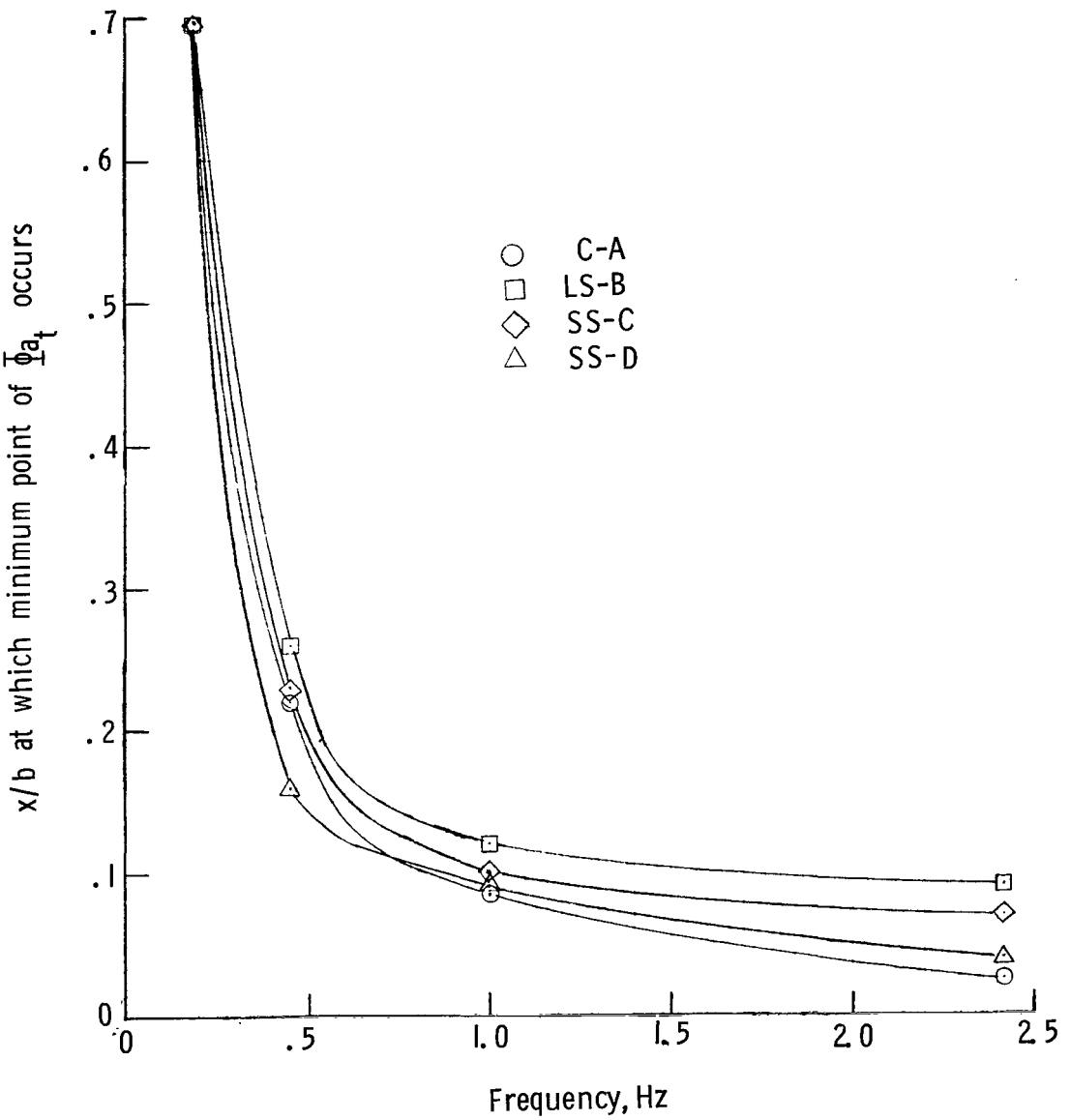


Figure 19.- Variation of location of minimum point of "variation of $\Phi_{a_t}$ with location" with frequency.

111 001 C1 U A 751204 S00903DS
DEPT OF THE AIR FORCE
AF WEAPONS LABORATORY
ATTN: TECHNICAL LIBRARY (SUL)
KIRTLAND AFB NM 87117



*"The aeronautical and space activities of the United States shall be conducted so as to contribute . . . to the expansion of human knowledge of phenomena in the atmosphere and space. The Administration shall provide for the widest practicable and appropriate dissemination of information concerning its activities and the results thereof."*

—NATIONAL AERONAUTICS AND SPACE ACT OF 1958

# NASA SCIENTIFIC AND TECHNICAL PUBLICATIONS

TECHNICAL REPORTS: Scientific and technical information considered important, complete, and a lasting contribution to existing knowledge.

TECHNICAL NOTES: Information less broad in scope but nevertheless of importance as a contribution to existing knowledge.

TECHNICAL MEMORANDUMS: Information receiving limited distribution because of preliminary data, security classification, or other reasons. Also includes conference proceedings with either limited or unlimited distribution.

CONTRACTOR REPORTS: Scientific and technical information generated under a NASA contract or grant and considered an important contribution to existing knowledge.

TECHNICAL TRANSLATIONS: Information published in a foreign language considered to merit NASA distribution in English.

SPECIAL PUBLICATIONS: Information derived from or of value to NASA activities. Publications include final reports of major projects, monographs, data compilations, handbooks, sourcebooks, and special bibliographies.

TECHNOLOGY UTILIZATION PUBLICATIONS: Information on technology used by NASA that may be of particular interest in commercial and other non-aerospace applications. Publications include Tech Briefs, Technology Utilization Reports and Technology Surveys.

***Details on the availability of these publications may be obtained from:***

**SCIENTIFIC AND TECHNICAL INFORMATION OFFICE**

**NATIONAL AERONAUTICS AND SPACE ADMINISTRATION**

**Washington, D.C. 20546**